Feary, D.A., Hine, A.C., Malone, M.J., et al., 2000
Proceedings of the Ocean Drilling Program, Initial Reports Volume 182

12. Site 1134[1]

Shipboard Scientific Party[2]

BACKGROUND AND OBJECTIVES

Site 1134 is located on the Eyre Terrace upper slope in 701.0 m of water (Fig. F1). This site was designed to intersect Cenozoic seismic Sequences 2, 3, and 4 and Lobes 2 and 3 of Sequence 6A (Feary and James, 1998, reprinted as Chap. 2; Fig. F2) and to intersect as much of the upper part of the Cretaceous section as time permitted. The target depth at this site was just below a high-amplitude reflector of probable Cenomanian age, estimated before drilling (on the basis of stacking velocities) to be at 520 meters below seafloor (mbsf).

The principal objectives at this site were to collect a detailed record of Paleogene–lower Neogene temperate to subtropical midlatitude sedimentation in an upper slope environment, and to recover a record of marine flooding of the evolving rift basin in the Cenomanian. Seismic interpretation (Feary and James, 1998, reprinted as Chap. 2) indicated that the lowermost Cenozoic sequence at this site (Sequence 6A) should be broadly contemporaneous with the Eocene?–middle? Miocene carbonate platform exposed on land and underlying the modern mid-inner shelf. Although seismic data show that a significant portion of this time interval (Sequence 6A, Lobe 1) is missing at this location, Site 1134 represents an ideal opportunity to sample the upper (Lobe 3) and the middle (Lobe 2) portions of this deep-water sequence, deposited apparently contemporaneous with this platform. Despite the absence of Lobe 1 at this location, it was likely that these deeper-water deposits should contain a more complete sequence than coeval shallow-water sediments, without lowstand hiatuses.

This site also constituted an upper slope component of the overall Leg 182 shelf-to-basin transect, designed to address a number of paleoceanographic problems: (1) the relationship between circulation patterns in the deep ocean and on the shelf during times of warm vs. cold oceanic conditions, (2) the precise timing and nature of the opening of

F1. Map showing Site 1134 in relation to other Leg 182 sites and the AGSO169 seismic lines, p. 31.

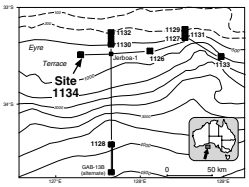

F2. Portion of seismic Line AGSO169/01e showing seismic stratigraphic sequences at Site 1134, p. 32.

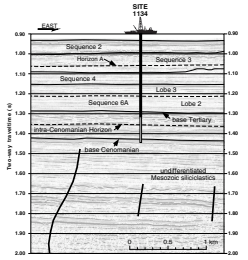

[1] Examples of how to reference the whole or part of this volume.
[2] Shipboard Scientific Party addresses.

Ms 182IR-112

the Tasman Gateway, (3) the evolution and effect of the Leeuwin Current, and (4) the relationship between primary productivity and cool-water carbonate development.

The relatively thin Cenozoic sequence at this location offered an opportunity to recover the uppermost part of the Mesozoic section, shown to be of Cenomanian age in the nearby Jerboa-1 exploration well. Although Jerboa-1 yielded a record of this interval in the form of ditch-cutting fragments, a fully cored section through this succession was sought to clarify facies relationships and the biostratigraphy of this near-shore marine interval.

Summary of Objectives for Site 1134

The drilling objectives at Site 1134 were to

1. Collect a detailed record of Paleogene–lower Neogene temperate to subtropical midlatitude sediments deposited as lowstand sediment lobes in an upper slope environment;
2. Contribute an upper slope component to the shelf-to-basin paleoceanographic transect;
3. Evaluate sea-level control on Neogene facies within an upper slope setting; in particular, to evaluate stratigraphic response to eustatic oscillations by comparison with equivalent time intervals in shelf and deep oceanic settings;
4. Determine diagenetic history and processes within Neogene upper slope facies; and
5. Collect a record of marine flooding of the evolving rift basin between Australia and Antarctica from the Cenomanian.

OPERATIONS

Transit to Site 1134

The 63-nmi transit required 6.25 hr at 10.1 kt. A beacon was dropped at 0430 hr on 1 December, initiating operations at Site 1134.

Hole 1134A

The ship was stabilized on position and the bit was positioned at 708 meters below rig floor (mbrf). Hole 1134A was spudded at 0840 hr on 1 December, recovering 4.50 m in Core 1H, which indicated a water depth of 701.0 meters below sea level (mbsl). Advanced hydraulic piston (APC) coring advanced to 126.0 mbsf, ceasing after a liner shattered and the regular APC cutting shoe was damaged upon striking a presumed chert interval on Core 14H. Cores 3H–14H were oriented and an Adara temperature tool heat-flow measurement was performed on Core 4H. The nonmagnetic cutting shoe and flapper core catcher, with a steel 10-finger core catcher, were deployed on Cores 3H, 5H, 7H, 9H, 11H, and 13H. Extended core barrel (XCB) coring deepened the hole from 126.0 to 397.1 mbsf, with 25.0% recovery (Table T1). A short wiper trip was made to 348 mbsf to check hole conditions, and 13 m of fill was noted on bottom. Consequently, a hole-conditioning trip was made to 105 mbsf; however, 20 m of fill was noted when bottom was tagged again. Thus, coring was terminated because of the unstable hole conditions. The hole was cleaned out to bottom, filled with mud, and then

T1. Site 1134 coring summary, p. 59.

the bit was pulled up to 105 mbsf in preparation for logging. The following logs were run from 388 mbsf: (1) triple combination logging tool (triple combo), (2) Formation MicroScanner (FMS)/sonic, and (3) well seismic tool (WST), recording seven check-shot stations. The pipe was retrieved, clearing the seafloor at 1335 hr on 3 December, ending Hole 1134A.

Hole 1134B

The ship was moved 20 m north, and the bit was positioned at 711 mbrf. Hole 1134B was spudded at 1455 hr on 3 December, recovering 8.60 m in Core 1H, which indicated a water depth of 699.9 mbsl. Advanced piston coring advanced to 122.6 mbsf and Cores 3H–13H were oriented. The nonmagnetic cutting shoe, flapper core catcher with a steel 10-finger core catcher, and nonmagnetic core barrels were run on Cores 3H, 5H, 7H, 9H, 11H, and 13H. Extended core barrel coring deepened the hole from 122.6 to 234.8 mbsf (Table T1), after which coring was terminated because available operational time had expired. The drill string was retrieved, the rig was secured for transit, and the vessel was under way at 1130 hr on 4 December.

Transit to Fremantle

The 820-nmi sea voyage to Fremantle, Australia, required 79.9 hr at an average speed of 10.3 kt. The first line was ashore at Fremantle Harbor Dock at 1925 hr on 7 December, ending Leg 182.

LITHOSTRATIGRAPHY

Introduction

Site 1134 is located at a water depth of 701 m. It provides a 397.1-m-thick record of Eocene–Pleistocene sedimentation in a middle to upper slope depositional setting. The sedimentary succession is similar in a general way to the succession at Site 1126 and comprises two sedimentary packages.

The lower package is a sandstone unit of uncertain, probable middle Eocene age (see "Seismic Stratigraphy," p. 26) (Fig. F3). The presence of bioclasts and planktonic foraminifers points to a marine origin for these sediments. The upper package at Site 1134 consists of upper? Eocene–Pleistocene pelagic marine carbonates, wackestone to floatstone, and minor chert and porcellanite. Some of these deposits are slumped (Fig. F3).

Based on major sediment types, compositional changes, and sediment deformation structures, six lithostratigraphic units are differentiated. Because core recovery at Site 1134 was good within the uppermost 180 m, the level of confidence for the placement of the boundaries in this part of the succession is high. Core recovery was low below Cores 182-1134A-17X and 182-1134B-20X; therefore information from the downhole logs (see "Downhole Measurements," p. 23) was used to refine depth assignments of individual boundaries.

F3. Site 1134 of summary of sediments and lithostratigraphy, p. 33.

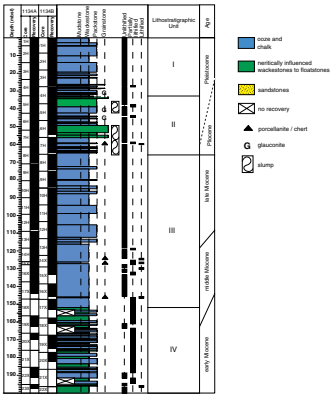

Lithostratigraphic Units

Unit I

Intervals: Cores 182-1134A-1H through 4H; Sections 182-1134B-1H through 4H-5, 100 cm
Depth: 0–33.00 mbsf (Hole 1134A); 0–34.60 mbsf (Hole 1134B)
Age: Pleistocene

Unit I consists of calcareous nannofossil ooze with varying amounts of planktonic foraminifers. The base of the unit is placed between Cores 4H and 5H in Hole 1134A at the contact between an unlithified wackestone and a calcareous nannofossil ooze. In general, whitish matrix-supported intervals alternate with darker, light gray intervals that are grainier and have a wackestone to packstone texture. In the light intervals, the major sedimentary components in the >63-µm fraction are planktonic foraminifers, sponge spicules, bioclasts, benthic foraminifers, radiolarians, and minor tunicate spicules. The darker sediments also contain echinoid spines as well as rare glauconite, pyrite, and black grains. The glauconite and pyrite content of the sediments is highest in light gray layers in the lower part of the Unit (Core 182-1134A-4H) (Fig. F3).

In general, the boundaries between lighter and darker sediments are gradual because of intense bioturbation, but some of the contacts are sharp. These sharp contacts occur at the base of the grainier layers. Bioturbation of the deposits appears as faint white to gray mottling but also as well-defined burrows which are conspicuously present at the transition between light and dark sediments.

Unit II

Intervals: Sections 182-1134A-5H through 8H-3, 150 cm; Sections 182-1134B-4H-5, 100 cm, through 7H-6
Depth: 33.00–66.00 mbsf (Hole 1134A); 34.60–64.50 (Hole 1134B)
Age: Pliocene?–Pleistocene

Unit II is characterized by soft-sediment deformation that is interpreted as slumping. Two slump intervals occur (Fig. F3): the upper one in Core 182-1134A-5H and the lower one in Cores 182-1134A-6H through 8H. The base of the lower slump interval defines the lower boundary of Unit II.

Unit II contains calcareous nannofossil ooze, calcareous nannofossil foraminifer ooze, as well as unlithified wackestones, packstones, floatstones, and rudstones. The ooze is white to light gray. Components in the >63-µm fraction are planktonic foraminifers, echinoid spines, bioclasts, sponge spicules, and minor bryozoans. In the lower part of the unit (Core 182-1134A-8H), some of the planktonic foraminifers are infilled with glauconite; glauconite also occurs as isolated grains. The light gray wackestones to rudstones contain a wide variety of coarse components such as different types of bryozoans (robust and delicate branching, arborescent, and fenestrate growth forms), bioclasts, sponge and tunicate spicules, as well as pellets. Pebble-sized lumps of calcareous nannofossil ooze, which are interpreted to be reworked clasts, are present in packstones and floatstones of Sections 182-1134A-5H-3 through 5H-CC and 6H-5 through 6H-CC. Soft-sediment deformation affects both the ooze and the deposits dominated by neritic compo-

nents. Sediment between the slump packages is calcareous nannofossil ooze and calcareous nannofossil foraminifer ooze rich in glauconite.

Unit III

Intervals: Section 182-1134A-8H-3 through Core 17X; Sections 182-1134B-7H-6 through 17X-2
Depth: 66.00–152.00 mbsf (Hole 1134A); 64.50–151.20 mbsf (Hole 1134B)
Age: middle Miocene–late Miocene

Unit III consists of calcareous nannofossil ooze and calcareous nannofossil foraminifer ooze. The lower limit of the unit is indicated by a change from dominantly pelagic sediments of this unit to partially lithified wackestones in Unit IV. At this point, carbonate content drops from values of ~90% in Unit III to values <80% in Unit IV (see **"Inorganic Geochemistry,"** p. 20). The boundary between the units was not recovered in Hole 1134A, but was observed between Sections 17X-2 and 17X-3 in Hole 1134B. The gamma-ray log shows a downhole increase at 152 mbsf (see **"Downhole Measurements,"** p. 23) that probably reflects the corresponding lithologic change. Although the deposits of Unit III are not uniform throughout, it was decided not to subdivide them further because such lithologic changes are minor.

In general, the matrix of the ooze in Unit III is clearly dominated by calcareous nannofossils with only minor amounts of clay (see **"Site 1134 Smear Slides,"** p. 64). In addition to the planktonic foraminifers, the >63-µm fraction contains benthic foraminifers, bioclasts, sponge spicules, minor silicoflagellates, and traces of glauconite. The first lithologic variation in Unit III occurs in Core 182-1134A-12H, where the matrix of the deposit contains minor amounts of silt-sized rock fragments and clay (see **"Site 1134 Smear Slides,"** p. 64). This interval correlates well with a minor hiatus as detected in the same core by the calcareous nannofossil associations (see **"Biostratigraphy,"** p. 8).

The second lithologic variation is in Cores 182-1134A-14H through 16X, where the degree of lithification alternates between unlithified and lithified over short intervals. These short-term variations imply processes other than simple depth-related sediment compaction. This lower limit of the interval with alternating lithification corresponds to the base of Sequence 3 (see **"Seismic Stratigraphy,"** p. 26); therefore, the lithification pattern may reflect condensed sedimentation related to this sequence boundary.

Unit IV

Intervals: Cores 182-1134A-18X through 24X; Sections 182-1134B-17X-2 through 24X-12, 12 cm
Depth: 152.00–214.30 mbsf (Hole 1134A); 151.20–217.20 mbsf (Hole 1134B)
Age: early Miocene

Unit IV consists of unlithified to partially lithified wackestone/packstone, foraminifer chalk, and very minor packstone. The lower boundary of the unit is at the top of a white foraminifer chalk in Core 182-1134A-25X and also occurs in Section 182-1134B-24X-2. This boundary is also well defined on the sonic velocity log, where an abrupt downhole in-

crease of the sonic velocity occurs at 217 mbsf (see "Downhole Measurements," p. 23).

The style of deposition is uniform throughout the unit and characterized by a metric alternation of light gray foraminifer chalk and light gray to gray wackestone/packstone. The chalk contains planktonic foraminifers, bioclasts, and sponge spicules, as well as minor quartz grains, glauconite, benthic foraminifers, and echinoid spines. The unlithified to partially lithified wackestone/packstone—although richer in glauconite and having more abundant bioclasts—contains the same components. Some of these layers (e.g., in Core 182-1134A-17X) have a sharp base and are normally graded. Such beds may represent turbidites.

Composition of the packstones can be seen in the "Site 1134 Thin Sections," p. 65. The components are very fine sand sized and rich in glauconite and quartz. Biogenic components are planktonic and benthic foraminifers, bryozoans and ostracode fragments. Dolomite makes up ~10% of the sediment. Deposits of Unit IV are intensely bioturbated; thus, in general, boundaries between the different lithologies are transitional. Centimeter-scale dark green reduction laminae are scattered throughout the succession.

Unit V

Intervals: Cores 182-1134A-25X through 40X; Section 182-1134B-24X-2, 12 cm, through Core 182-1134B-25X
Depth: 214.30–368.20 mbsf (Hole 1134A); 217.20–234.80 (Hole 1134B)
Age: late Eocene–early? Miocene

Two main lithologies were recovered between 214.3 and 368.2 mbsf: (1) calcareous nannofossil chalk and (2) fragments of porcellanite and chert. The matrix of the white chalk is dominated by calcareous nannofossils, with common sponge spicules as well as trace amounts of bioclasts and dolomite. The coarse fraction consists of planktonic and benthic foraminifers. The chalks are strongly bioturbated. Burrows appear as faint color mottling (gray-white) but also as well-defined traces, such as *Zoophycos*. (e.g., Core 182-1134A-39X). Green and dark gray to black reduction laminae are present throughout the unit. The gray and green porcellanite lithologies are silicified chalk.

Although the core recovery was very poor in the interval corresponding to Unit V and no subunits were defined, there appears to be a division into three major sedimentary packages. This differentiation relies on textural trends of the deposits. The uppermost package, which is dominated by a wackestone texture, is from Cores 182-1134A-25X through 28X (214.3–252.9 mbsf). The lower limit of this interval matches with a strong excursion of the gamma-ray log to higher values at 252 mbsf (see "Downhole Measurements," p. 23). The base of the middle package is at the top of Core 182-1134A-34X at a depth of 300.8 mbsf. This limit probably corresponds to a peak of the gamma-ray log, followed by a general decrease of the values at 305 mbsf (see "Downhole Measurements," p. 23). This middle package shows an uphole change from a packstone to a mudstone texture. The lower sedimentary package of Unit V is dominated by a mudstone texture with wackestone and packstone texture intervals.

Unit VI

Intervals: Cores 182-1134A-41X through 43X
Depth: 368.20–397.10 mbsf
Age: early?–middle Eocene

Only 30 cm of the lowermost deposits at Site 1134 were recovered. The sediments are brown limonitic sandstone with quartz, limonite, glauconite, mica, and abundant skeletal grains, as well as minor planktonic foraminifers. Siliciclastic components are as large as coarse sand sized.

Discussion

The basal sandstones at Site 1134 (Unit VI) were so poorly recovered that no information can be provided as to the development of the succession. The deposits are probably marine, as indicated by the occurrence of planktonic foraminifers and bioclasts. The seismic tie with the succession drilled in the borehole Jerboa-1 (see **"Seismic Stratigraphy,"** p. 26) indicates that the sandstones form a ~40- to 50-m-thick cap of probable Eocene age that overlies Cretaceous sandstone.

The nature of the contact between the basal siliciclastics and the chalks could not be assessed at Site 1134 because of poor core recovery. The overlying sediments of Unit V roughly coincide with the seismically defined Sequence 6A (see **"Seismic Stratigraphy,"** p. 26). These sediments are pelagic carbonates that formed under well-oxygenated bottom-water conditions, as indicated by the intense burrowing. The limits of the sedimentary bundles within this unit correspond roughly to the Eocene/Oligocene and the Oligocene/Miocene boundaries, respectively.

In contrast to Site 1126, where pelagic sedimentation was uniform throughout the early Miocene, Site 1134 records a subtle early Miocene change of the sedimentary regime toward an increased input of shelf and shallower water particles at the base of Unit IV. This turnover roughly corresponds to the base of the outer slope part of the "Little Barrier Reef" Sequence 6B as defined by Feary and James (1998, reprinted as **Chap. 2**) (see **"Seismic Stratigraphy,"** p. 26). The discrepancy between the record at Site 1126 and 1134 is best explained by the lateral variability of Sequence 6B, which is characterized by a lobate geometry north of Site 1134 (fig. **10** in Feary and James, 1998, reprinted as Chap. 2). Site 1134 records the most distal part of this lobe, whereas Site 1126 records the pure pelagic equivalent, as the limit of the distal part of Sequence 6B at this locality is situated further to the north.

Pure pelagic conditions at Site 1134 returned during middle Miocene time with the formation of calcareous ooze. An interruption in uniform pelagic sedimentation is represented by the slumps of Unit II. In contrast to Site 1126, where slumping occurs in an equivalent stratigraphic position, slumps at Site 1134 contain a mixture of pelagic and neritic sediments. Porcellanite fragments in the slumped deposits at Site 1134 show that sediment as old as middle Miocene age may have been affected by the slumping, as the first in situ porcellanite occurrence at Site 1134 is in the middle Miocene sequence. Relatively monotonous pelagic sedimentation at Site 1134 resumed during the Pliocene (Unit I) and persisted throughout the Pleistocene. Similar to Site 1126, sediments of Unit I alternate between layers rich in planktonic foraminifers and layers dominated by calcareous nannofossils. How this alternation

correlates with the Pleistocene depositional cycles recorded in the Leg 182 shallower water drill sites will be addressed during additional post-cruise research.

BIOSTRATIGRAPHY

Introduction

Calcareous nannofossils and planktonic foraminifers indicate that sediments recovered at Site 1134 range from Quaternary to middle Eocene in age. Several hiatuses were indicated. The first was in the Pliocene (nannofossil Zones NN18–NN13 missing at ~57 mbsf) and the second in the middle–upper Miocene (nannofossil Zones NN9–NN7 missing at ~114 mbsf). Several datum levels occurred together at the Oligocene/Miocene boundary, indicating a hiatus of ~1 m.y. In the Eocene section, the absence of nannofossil Zone NP17 suggests that a time interval of ~3 m.y. is not represented at the middle/upper Eocene boundary. Planktonic foraminifers indicate hiatuses at approximately the same depths as the calcareous nannofossils. However, poor core recovery in critical intervals within the Oligocene–Eocene makes determination of smaller scale hiatuses impossible.

Calcareous nannofossils are moderately well preserved above ~200 mbsf and become poorly preserved below this level. Planktonic foraminifers are moderately well preserved throughout most of Hole 1134A, with only the lowermost 30 m of the hole containing poorly preserved specimens. Benthic foraminifers are generally rare in comparison to the planktonic foraminifers and decrease in abundance significantly in the lowermost 130 m of Hole 1134A. The preservation of the benthic foraminifers is comparable to that of the planktonic foraminifers. The five main assemblages of benthic foraminifers recognized all indicate middle bathyal paleodepths and can be correlated with coevel assemblages at Site 1126.

The sedimentary successions at Site 1134 bear many similarities to those at Site 1126. Not only was a similar succession of zones recognized, but the hiatus positions are strikingly similar between the two sites. The uppermost hiatus in Site 1134 (~57 mbsf) appears to correlate with the first two hiatuses encountered in Site 1126 (~57 and ~67 mbsf), where most of the Pliocene is missing. The second hiatus encountered in Site 1134 (~114 mbsf) correlates well with the third hiatus in Site 1126 (~118 mbsf), with most of the middle–upper Miocene missing.

Calcareous Nannofossils

Calcareous nannofossils indicate that drilling at Site 1134 recovered a Pleistocene–middle Eocene succession. Two main disconformities occur and a third is suspected. The entire Pliocene is either missing or condensed between two successive core catchers. Similarly, the upper–middle Miocene Zones NN9–NN7 seem to be missing from the record. Poor recovery in the Eocene, between a chalk section containing Zone NP18 indicators and a limonitic sandstone containing rare nannofossils suggestive of Zone NP16, makes it difficult to ascertain whether the middle Eocene Zone NP17 is missing. The nature of the transition from the Neogene to the Paleogene (whether abrupt or gradational) could not be determined. The zones within a lower Miocene interval, ~61 m thick, between Zones NN3 and NP25, could not be determined during

our shipboard study. Nannofossil preservation is moderate in the Quaternary and Neogene and poor in the Paleogene.

Pleistocene

Sample 182-1132A-1H-CC contains *Calcidiscus leptoporus, Gephyrocapsa caribbeanica,* and small *Gephyrocapsa* spp., without *Pseudoemiliania lacunosa,* indicating the combined Zones NN21–NN20. The key species *P. lacunosa* occurs in Samples 182-1132A-2H-CC (14.21 mbsf) to 6H-CC (52.01 mbsf), together with *Braarudosphaera bigelowii, C. leptoporus, Coccolithus pelagicus,* small *Gephyrocapsa* spp., *Syracosphaera pulchra,* and *Rhabdosphaera clavigera.* In the absence of species of *Discoaster,* this association indicates Zone NN19. *Gephyrocapsa* spp. (small) have their highest abundance acme in the uppermost part of Zone NN19. *Calcidiscus macintyrei* has its highest occurrence at 33.12 mbsf in the lower part of the zone.

Braarudosphaera bigelowii reached its acme abundance in Sample 182-1134A-5H-CC. Below this peak abundance of *B. bigelowii,* the assemblage from Sample 182-1134A-6H-CC (52.01 mbsf) is indicative of the lowermost part of Zone NN19, with rare small *Gephyrocapsa* spp. and no larger *Gephyrocapsa.* Other species in this assemblage include *C. leptoporus, C. macintyrei, C. pelagicus, Dictyococcites productus, Helicosphaera carteri, P. lacunosa,* and *Reticulofenestra minuta.* However, intervals from ~36 to 42.5 mbsf, 49.5 to 56.2 mbsf, and 57.8 to 66.0 mbsf are clearly slumped (see **"Lithostratigraphy,"** p. 3), so biostratigraphic relationships are in question.

Miocene

A well-diversified assemblage is recorded from Samples 182-1134A-7H-CC (61.89 mbsf) and 8H-CC (70.83 mbsf), indicative of the lower part of Zone NN12 (Subzone CN10a) of latest Miocene age. This assemblage includes *Amaurolithus ninae, Amaurolithus tricorniculatus, C. leptoporus, C. macintyrei, Discoaster pentaradiatus, Discoaster surculus, Discoaster variabilis, Scyphosphaera* spp., *Reticulofenestra gelida, Reticulofenestra pseudoumbilicus,* and *Triquetrorhabdulus rugosus.* Zones NN18–NN13 and the younger part of NN12, representing the entire Pliocene, are either missing or contained in a condensed section between Samples 182-1134A-8H-CC and 182-1134A-7H-CC (at ~57 mbsf).

An upper Zone NN11 (Subzone CN9b) assemblage occurs in Samples 182-1134A-9H-CC (80.73 mbsf) to 11H-CC (108.35 mbsf). This assemblage is characterized by the co-occurrence of *Discoaster quinqueramus* (rare), and both *A. ninae* and *A. tricorniculatus* (few). These key taxa are absent from Sample 182-1134A-12H-CC (108.35 mbsf), although *Minylitha convallis* and *Discoaster neohamatus* are present instead, suggesting the upper Miocene Zone NN10. The assemblage from Sample 182-1134A-13H-CC (118.54 mbsf) indicates the middle Miocene Zone NN6. The upper–middle Miocene Zones NN9–NN7 are either missing or condensed in the 9.5-m interval between Samples 182-1134A-12H-CC and 13H-CC (at ~114 mbsf).

The association of *Calcidiscus premacintyrei, Cyclicargolithus floridanus, Dictyococcites antarcticus, Discoaster exilis, D. variabilis, Helicosphaera rhomba, Reticulofenestra gelida, R. pseudoumbilicus,* and *T. rugosus* characterizes Zone NN6 in Samples 182-1134A-13H-CC (118.54 mbsf) to 16X-CC (137.71 mbsf). Heavily calcified *Discoaster deflandrei* "group," *B. big-*

elowii, and *Micrantholithus entaster* are present in the lower part of Zone NN6.

The stratigraphic range of *Sphenolithus heteromorphus,* the key species for the combined Zones NN5–NN4, is present between 147.10 and 144.17 mbsf (Samples 182-1134A-17X-CC and 18X-CC). This is a very thin interval for the combined Zones NN5–NN4 compared to other Leg 182 sites in which these zones occur. The thickness of the combined Zones NN5–NN4 ranges from ~85 m at the shallow-water Site 1132 to >100 m at the deeper water Site 1133 (where it was not totally penetrated). In addition to *S. heteromorphus, C. leptoporus, C. premacintyrei, C. floridanus, D. variabilis, H. carteri,* and *R. pseudoumbilicus* are present in Samples 182-1134A-17X-CC and 18X-CC.

Nannofossils in Sample 182-1134A-19X-CC (162.84 mbsf) are few and moderately preserved. These include *Sphenolithus belemnos,* the key species for Zone NN3 of early Miocene age, as well as *C. floridanus, Helicosphaera euphratis, Sphenolithus conicus,* and *Sphenolithus moriformis.* This is the only record of undeniable Zone NN3 from Leg 182 sites.

Below Zone NN3, a thick interval (between 162.84 and 224.05 mbsf, ~61 m thick) contains associations with an early Miocene aspect, although the interval lacks specific age-diagnostic taxa. At most levels, nannofossil preservation is moderate where the abundance is low, and poor where the abundance and diversity are relatively high. The taxa list from this interval (Samples 182-1134A-20X-CC to 26X-CC) includes *B. bigelowii, D. antarcticus, Cyclicargolithus abisectus, C. floridanus,* heavily calcified specimens of the *D. deflandrei* "group," *H. carteri, H. euphratis, Helicosphaera obliqua, Micrantholithus* sp., and *S. moriformis.*

Oligocene

Sample 182-1134A-27X-CC (238.64 mbsf) contains the key taxa *Dictyococcites bisectus, Sphenolithus capricornutus,* and *S. delphix,* which indicates the uppermost Oligocene NP25. Other species in this sample include *B. bigelowii, Coccolithus miopelagicus, C. abisectus, C. floridanus, Micrantholithus* sp., and *S. conicus.* Sample 182-1134A-32X-CC (281.96 mbsf) contains the highest occurrence of the key species, *Reticulofenestra umbilicus,* and no *Coccolithus formosus,* indicating Zone NP22 of early Oligocene age. The interval between Zone NP25 at 238.64 mbsf and Zone NP22 at 281.96 mbsf could not be assigned to a zone because of the lack of the low-latitude taxa *Sphenolithus distentus* and *Sphenolithus ciperoensis* in the core-catcher samples examined. This interval is tentatively assigned to the combined Zones NP23–NP25. The highest occurrence of *Chiasmolithus altus* is within this NP23–NP25 zonal interval, at 262.72 mbsf (Sample 182-1134A-30X-CC).

Shafik (1990) indicated that the presence of *S. distentus* and *S. ciperoensis* in southern Australia was probably caused by warm waters being brought from the Indian Ocean by an intermittent surface-water current, the proto-Leeuwin Current. The implications are that both the stratigraphic and geographic ranges of these taxa in southern Australia are probably sporadic. Detailed postcruise examination will be performed to document the distribution pattern of *S. distentus* and *S. ciperoensis* at this site and at Site 1132, for which biostratigraphic refinement is needed for the Zone NP23 or younger interval (see **"Biostratigraphy,"** p. 13, in the "Site 1132" chapter).

Zone NP21 assemblages are recorded from Samples 182-1134A-33X-CC (291.4 mbsf) to 35X-CC (310.93 mbsf). These include *Chiasmolithus*

altus, Chiasmolithus oamaruensis, D. bisectus, Discoaster nodifer, Reticulofenestra hillae, R. umbilicus, and *Zygrhablithus bijugatus*.

Eocene

The association *Isthmolithus recurvus, Discoaster saipanensis,* and *C. oamaruensis* in the assemblage from Sample 182-1134A-36X-CC (322.09 mbsf) indicates Zones NP19–NP20, of late Eocene age. Both *D. saipanensis* and *C. oamaruensis* occur downhole to 361.91 mbsf in Sample 182-1134A-40X-CC, although without the association of *I. recurvus*. This indicates Zone NP18 of late Eocene age. Other species present in Zone NP18 include *Coccolithus eopelagicus, C. formosus, Cribrocentrum reticulatum, D. bisectus, D. nodifer,* and *Z. bijugatus*.

Rare, poorly preserved nannofossils in the limonitic sandstone underlying the upper Eocene chalk in Sample 182-1134A-40X-CC indicate a middle Eocene age. The taxa identified from Sample 182-1134A-41X-CC (368.4 mbsf) include *Chiasmolithus grandis, Chiasmolithus solitus, C. formosus,* and *R. umbilicus,* suggesting Zone NP16. A disconformity may exist between the upper Eocene chalk in Sample 182-1134A-40X-CC and the middle Eocene sandstone in Sample 182-1134A-41X-CC, as Zone NP17 appears to be missing. This uncertainty mainly results from the poor core recovery in this interval (see **"Operations,"** p. 2). The duration of this suspected hiatus is ~3 m.y.

Planktonic Foraminifers

Planktonic foraminifers in all core-catcher samples were studied from Hole 1134A. Selected samples from Hole 1134B were also examined, mainly for correlation purposes. The preservation of planktonic foraminifers is good to moderate throughout the Quaternary to Eocene sections, and poor only at levels with cherts or where the lithologies are lithified. All samples studied were assigned to the relevant planktonic foraminifer zones of Berggren et al. (1995) and Jenkins (1993). Preliminary results indicate that the sediment sequence recovered at Site 1134, which is similar to that at Site 1126, contains Pleistocene, Miocene, Oligocene, and upper Eocene intervals (Fig. **F4**). Slumping between ~36 to 66 mbsf makes stratigraphic relationships unclear in the lower Pleistocene–lower Pliocene section. A large part of the Pliocene is missing, representing a hiatus of at least 2 m.y. The upper/middle Miocene contact is also disconformable, and a hiatus of ~4 m.y. was estimated. Zonal resolution declines in lower Miocene–Eocene sediments partly because of the temperate planktonic foraminiferal assemblages, which contain few age-diagnostic species and datum levels.

F4. Calcareous nannofossil and planktonic foraminiferal zones, and benthic foraminiferal assemblages, **p. 35.**

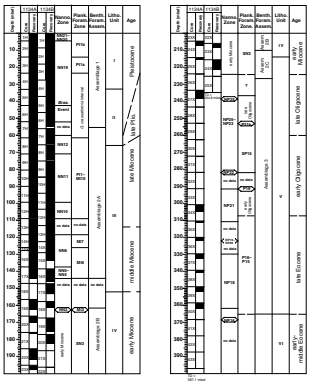

Pleistocene–Late Pliocene

Two planktonic foraminiferal assemblages are present. The younger assemblage is mainly composed of *Globorotalia inflata, Globigerinoides ruber, Globorotalia truncatulinoides, Globigerina falconensis, Globigerina bulloides, Globigerina quinqueloba, Neogloboquadrina pachyderma, Orbulina universa,* and *Globigerinita glutinata*. With the index species *G. truncatulinoides,* it belongs to Zone Pt1 of Berggren et al. (1995), and encompasses the interval of Cores 182-1134A-1H through 3H. The first occurrence (FO) of *G. truncatulinoides* coincides with the last occurrence (LO) of the Subzone Pt1a marker species *Globorotalia tosaensis* at 33.41 mbsf (Sample 1134A- 3H-CC, 15–18 cm), indicating that much of Sub-

zone Pt1a is probably missing or condensed above the slumps between ~36 to 66 mbsf (see "Lithostratigraphy," p. 3).

Cores 182-1134A-4H and 7H contain an assemblage characterized by numerous globorotaliid forms, but lacking *G. truncatulinoides*. Common species are *Globorotalia crassaformis, Globorotalia puncticulata, Globorotalia crassula,* and many species that are also common in cores above (such as *Globorotalia inflata, N. pachyderma, Globigerina bulloides, G. falconensis,* and *G. ruber*). Chronostratigraphically, this "*G. crassaformis*" interval appears to straddle the Pleistocene/Pliocene boundary (see "Biostratigraphy," p. 12, in the "Site 1129" chapter), although further studies are needed to clarify its exact age. Interpretation of this interval is further complicated by slumping.

Early Pliocene–Late Miocene

The early Pliocene–late Miocene in Cores 182-1134A-7H through 12H is characterized by a relatively diverse planktonic foraminifer assemblage. Species restricted to this interval include *Globorotalia menardii, Globorotalia margaritae, Globorotalia cibaoensis, Globorotalia conomiozea, Zeaglobigerina woodi,* and *Zeaglobigerina nepenthes*. The occurrence of *Globoconella sphericomiozea* in Samples 182-1134A-7H-CC, 13–16 cm, and 8H-CC, 19–23 cm (61.89–70.83 mbsf), indicates Zone Pl1 across the lower Pliocene/upper Miocene boundary (Berggren et al., 1995). Zone Mt10 is assigned to Samples 182-1134A-9H-CC through 12H-CC with the consistent presence of *Globorotalia conomiozea*. However, the planktonic foraminiferal assemblages in all samples appear to be more or less homogeneous, probably as a result of slump accumulation during these periods (see "Lithostratigraphy," p. 3)

Middle Miocene

Sediments underlying the late Miocene at 118.54 mbsf (Sample 182-1134A-13H-CC, 10–13 cm) are lower middle Miocene Zone Mt7, indicating a hiatus of ~4 m.y. across the middle/upper Miocene boundary. This boundary occurs at ~113 mbsf within lithostratigraphic Unit III (see "Lithostratigraphy," p. 3) and correlates with the contact between dominantly dark gray packstones to light-colored foraminifer-nannofossil oozes and wackestones with cherts. The middle Miocene planktonic foraminifer assemblage is characterized by *Globoquadrina dehiscens, Globorotalia conoidea, Sphaeroidinellopsis kochi, O. universa, Z. woodi, Zeaglobigerina druryi,* and *Zeaglobigerina apertura,* although without *Z. nepenthes*. Further downhole, Samples 182-1134A-14H-CC through 17X-CC contain Zone Mt6 planktonic foraminiferal assemblages that include most of the species found in Zone Mt7 plus *Fohsella peripheroronda*. Some advanced forms of this species, resembling *Fohsella peripheroacuta,* were also recorded.

Early Miocene

The first chert interval in Core 182-1134A-18X not only marks a lithologic change, but also the lower/middle Miocene boundary. The core-catcher sample at 162.84 mbsf (Sample 182-1134A-19X-CC, 29–32 cm) contains poorly preserved planktonic foraminifers indicating the lower Miocene Zone Mt3. They include few *Globoquadrina venezuelana, Globoconella incognita,* and *Globorotalia praescitula.* The absence of Zones Mt4 and Mt5 suggests either a hiatus of ~1 m.y. or a highly condensed

section across the lower/middle Miocene boundary. Further downhole, the planktonic foraminifer assemblage is mainly composed of southern temperate-water species. Cores 182-1134A-20X through 26X contain *Z. woodi, Zeaglobigerina connecta, Paragloborotalia* cf. *semivera,* and *Globorotaloides suteri*. The absence of *Globigerinoides trilobus* from this association indicates Zone SN3 in the early part of the early Miocene. It is not known, however, whether the transition from Zone SN3 to Mt3 is continuous, as suggested by Jenkins (1993), because no paleomagnetic constraint has ever been applied to the SN zonal scheme.

Oligocene

The late Oligocene is represented by three core-catcher samples. Sample 182-1134A-27X-CC, 34–37 cm (238.64 mbsf), contains an impoverished assemblage with common *G. suteri, Catapsydrax* spp., and *Globigerina euapertura*. The absence of the Miocene index species *G. dehiscens* indicates that this assemblage is of Oligocene age. Berggren (1992) used the LO of *G. euapertura* as a proxy of the Oligocene/Miocene boundary. This species, however, appears to range into the early part of the Miocene in southern Australia. At Site 1134, *G. euapertura* was found together with *G. dehiscens* at 215.19 and 224.05 mbsf (Sample 182-1134A-25X-CC, 34–37 cm, and 26X-CC, 15–18 cm), indicating that the LO of *G. euapertura* is probably diachronous. Although the chert sample at 243.42 mbsf was barren of planktonic foraminifers, a late Oligocene age is indicated by nannofossils (see **"Calcareous Nannofossils,"** p. 8). The assemblage from 253.08 mbsf (Sample 182-1134A-29X-CC, 18–21 cm) is similar in composition to that observed above at 238.64 mbsf. With the presence of *Paragloborotalia opima,* the assemblage indicates upper Oligocene Zone P21b (Berggren et al., 1995).

The consistent occurrence of *Chiloguembelina cubensis* in the interval 262.72–304.51 mbsf (Cores 182-1134A-30X through 34X) suggests an early Oligocene age or older. It is associated with *Globigerina ciperoensis, Globigerina officinalis, G. suteri, Globorotaloides testarugosa,* and numerous *Tenuitella* spp. in Samples 182-1134A-30X-CC, 22–25 cm; 31X-CC, 0–4 cm; and 32X-CC, 16–19 cm. In the southern Australian region, the assemblage is probably equivalent to Zones P20–P21a (McGowran et al., 1997). The addition of *Subbotina angiporoides* and *Subbotina praeturritilina* to this assemblage in the interval of 291.4–304.51 mbsf (Samples 182-1134A-33X-CC, 0–2 cm, and 34X-CC, 31–34 cm) suggests Zone SP13 of Jenkins (1993), equivalent to Zones P18–P19 (Chaproniere et al., 1995).

Eocene

An upper Eocene planktonic foraminifer assemblage was recorded in samples from 310.93 to 361.91 mbsf. It mainly includes *Globigerinatheka index, S. angiporoides, Subbotina eocaena, Subbotina linaperta,* and *C. cubensis*. Lacking typical middle Eocene taxa such as *Acarinina,* this association was correlated to the combined Zone P15–16 in Samples 182-1134A-35X-CC, 0–2 cm, through 40X-CC, 31–34 cm. Further downhole, dark brown, Fe-stained sands were found in Core 182-1134A-41X toward the base of Hole 1134A. Sample 182-1134A-41X-CC, 20–22 cm, the only core-catcher sample available from this interval, contains a rare, poorly preserved *S. angiporoides–S. linaperta* complex, indicating a middle–late Eocene age.

Benthic Foraminifers

Benthic foraminifers were studied from every fourth core-catcher sample from Hole 1134A. Additional samples were also analyzed in intervals in which rapid lithologic or faunal change occurred. Abundant sponge spicules in many samples from that interval indicate an extended episode of increased biosiliceous sedimentation. A major lithologic change from light carbonate rocks to brown limonitic sandstones with skeletal fragments and quartz occurs in Core 182-1133A-41X. These Eocene sandstones contain an impoverished, poorly preserved, benthic foraminiferal assemblage.

Between 100 and 300 specimens were picked from the >63-µm fraction, except in samples in which benthic foraminifer abundance was low. Benthic foraminifers are generally rare in comparison with planktonic foraminifers, and abundance drops significantly in the lower part of Hole 1134A (Cores 27X to 40X). Preservation is good to moderate except in Core 182-1133A-41H, which contains a significant proportion of abraded and corroded specimens. The benthic foraminiferal assemblages studied include mainly calcareous taxa and only a few species and specimens of agglutinated taxa. Most species have a cosmopolitan bathyal distribution. However, further work is needed to determine more precisely the ranges of stratigraphically important taxa in the Great Australian Bight in comparison with published data. Postcruise studies will also allow integration of these ranges within regional and global biostratigraphic schemes. The following benthic foraminiferal assemblages are recognized in the Cenozoic succession of Hole 1134A.

Assemblage 1 (Holocene–Late Early Pliocene)

Cores 182-1134A-1H through 6H

This is a relatively diverse assemblage, characterized by the rare or few occurrences of *Planulina wuellerstorfi, Martinottiella communis, Sigmoilina obesa, Anomalinoides globulosus, Sigmoilopsis schlumbergeri, Hoeglundina elegans, Cibicidoides mundulus, Bulimina aculeata, Cibicidoides* spp., *Textularia* spp., *Pleurostomella* spp., *Lenticulina* spp., and *Pullenia* spp. Middle bathyal paleodepths are indicated by the presence of *H. elegans, C. mundulus, A. globulosus, S. schlumbergeri,* and *P. wuellerstorfi,* generally found in water depths exceeding 500 m, and by the lack of deeper water indicators. Fluctuations in the relative abundance of some taxa may relate to carbon flux fluctuations, changes in sea level, or circulation. A high-resolution study is needed to analyze benthic foraminiferal distribution patterns in relation to paleoceanographic changes during the deposition of the sedimentary succession.

Slumped packages in Cores 5H through 6H (see **"Lithostratigraphy," p. 3**) contain displaced benthic foraminiferal assemblages. For instance, Sample 182-1134A-6H-CC contains a relatively well-preserved upper bathyal assemblage including *Bigenerina nodosaria, Heterolepa dutemplei, S. obesa, Sphaeroidina bulloides, Textularia* spp., *Loxostomum* spp., *Tritaxia* spp., and *Elphidium* spp., together with numerous, diverse, well-preserved bryozoans. This assemblage is similar to the Pleistocene assemblages found in bryozoan-rich accumulations at Sites 1129, 1131, and 1132.

Assemblage 2A (Late Early Pliocene–Middle Miocene)

Cores 182-1134A-7H to17X

This assemblage occurs in a lithostratigraphic unit consisting of nannofossil ooze and calcareous foraminifer ooze (see "Lithostratigraphy," p. 3). It is characterized by the rare to few occurrences of *P. wuellerstorfi, Rectuvigerina striata, Siphonina tenuicarinata, B. aculeata, Globocassidulina subglobosa, S. schlumbergeri, Karreriella bradyi* and *Laticarinina pauperata, C. mundulus, S. bulloides, Lagena sulcata, Uvigerina hispidocostata, Vulvulina spinosa, Stilostomella* spp., *Uvigerina* spp., *Lenticulina* spp., *Cibicidoides* spp, *Anomalinoides* spp., *Pullenia* spp., and various nodosariids. Middle bathyal paleodepths are indicated by the presence of *P. wuellerstorfi, R. striata, A. globulosus,* and *S. schlumbergeri*. The FO of the stratigraphically significant species *B. aculeata* is observed in Sample 182-1134A-8H-CC, corresponding to combined Zones Pl1–Mt10 (late Pliocene–upper Miocene), which is in agreement with the published stratigraphic range of this taxon in the late Miocene (FO in Zone N16, according to van Morkhoven et al., 1986).

Assemblage 2B (Early Miocene)

Cores 182-1134A-19X to 24X

Assemblage 2B is found in a discrete lithostratigraphic unit (lithostratigraphic Unit IV) consisting of alternating dark wackestones/packstones and light gray chalk (see "Lithostratigraphy," p. 3). The benthic foraminifer assemblage in the core-catcher samples examined includes many species also found in Assemblage 2A, but additionally contains *Stilostomella subspinosa, Patellina corrugata, Elphidium* spp., and *Palliolatella* spp. The presence of typically shallow-water species such as *P. corrugata, Elphidium* spp., and *Palliolatella* spp. within a typically middle bathyal assemblage suggests that sediments from shallower depths were redeposited into deeper water. A corresponding assemblage was recorded at Site 1126, which was drilled farther east in approximately the same water depth (see "Biostratigraphy," p. 12, in the "Site 1126" chapter). The FO of the stratigraphically important species *P. wuellerstorfi* is noted in Sample 182-1134A-17-CC, within Zone Mt6, which agrees with the recorded FO for this species in Zone N9 (van Morkhoven et al., 1986). The LO of *V. spinosa,* with a stratigraphic range extending to Zone N12, is also recorded in the same sample. *R. striata,* which has a FO in the early middle Miocene (Zone N9), is also a stratigraphically significant species within the assemblage.

Assemblage 2C (Early Miocene)

Cores 182-1134A-25X to 26X

A major lithologic change occurs in Core 25X from the cyclic succession of dark wackestones and light packstones (lithostratigraphic Unit IV) to a uniform light nannofossil ooze (lithostratigraphic Unit V) containing abundant sponge spicules (see "Lithostratigraphy," p. 3). The impoverished benthic foraminifer assemblage in Cores 25X and 26X is dominated by small specimens of *Bolivina* spp., *Cibicidoides* spp., and *Trifarina* spp. Also present are a few *Patellina* spp. A similar assemblage occurs in coeval sediments at Site 1126 (Cores 24X through 25X). Upper to middle bathyal paleodepths are tentatively suggested from the

overall composition of the assemblage, as no distinctive paleobathymetric indicator was found.

Assemblage 3 (Late Oligocene–Late Eocene)

Cores 182-1134AS-27X to 40X

This is a diversified, generally well-preserved assemblage, which is characterized by the rare to few occurrences of *Oridorsalis umbonatus, Cibicidoides praemundulus, S. tenuicarinata, G. subglobosa, V. spinosa, Hanzawaia ammophila, L. pauperata, Gyroidinoides soldanii, Stilostomella* spp., *Uvigerina* spp., *Cibicidoides* spp., *Pullenia* spp., and various nodosariids. Middle bathyal paleodepths are suggested for the assemblage by the presence of *L. pauperata, C. praemundulus, S. tenuicarinata, G. subglobosa,* and *V. spinosa*. Stratigraphically significant species within Assemblage 3 are *C. praemundulus* with a stratigraphic range from the early Eocene (P6b) to early Oligocene (P22) and *S. tenuicarinata* with FO in the late Eocene (P16) and LO in the early middle Miocene (N9).

Comparison of Assemblages at Sites 1126 and 1134

Site 1134 is located ~60 km west of Site 1126, which was drilled in comparable water depths. There is a strong similarity in the composition of the benthic assemblages at the two sites: Assemblages 1, 2A, 2B, 2C, and 3 can be recognized at both sites, although there are differences in the relative abundances of some species within these assemblages. For instance, *Uvigerina* spp. is present in higher numbers in Assemblage 1 at Site 1126. Assemblage 2B at Site 1134 contains *Elphidium* spp., whereas *Patellina* spp. are more common in the corresponding assemblage at Site 1126.

Assemblage boundaries between Assemblages 2B, 2C, and 3 appear to be coeval. This suggests that changes in benthic foraminifer distribution were controlled by major environmental changes during the late Oligocene and early Miocene. Some discrepancies are observed between the boundaries of Assemblages 1, 2A, and 2B. These may relate to stratigraphic or lithologic differences caused by distinct depositional regimes at these two sites during the middle and late Miocene. The overall faunal changes and the variability within each of the assemblages need to be better defined, and the timings of the faunal changes need to be related to carbon and oxygen isotopic events during postcruise studies. The benthic foraminifer record at Sites 1126 and 1134, however, appears excellent for evaluating changes in deep-water circulation in the Great Australian Bight during the Oligocene and Miocene.

Sedimentation Rates

Sediment accumulation rates, shown in Fig. **F5,** were calculated from preliminary biostratigraphic and paleomagnetic results at Site 1134 (see **"Paleomagnetism,"** p. 17). The biostratigraphic datum levels and relevant paleomagnetic data used to calculate sedimentation rates are listed in Table **T2.**

Figure **F5** shows three hiatuses: one at the upper/lower Pliocene boundary, one at the upper/middle Miocene boundary, and one possible hiatus within the Eocene. The two in the Neogene are more confidently delineated by the biostratigraphy than the Eocene hiatus.

The Pleistocene section registered a sedimentation rate of 28–30 m/m.y., whereas the late Miocene recorded a rate of ~17 m/m.y. A hiatus

F5. Sedimentation rate curve from datum levels for Site 1134, **p. 36.**

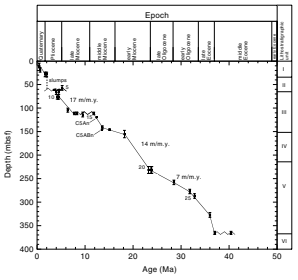

T2. Datum levels used to calculate sedimentation rates, **p. 61.**

associated with slumps occurred during much of the Pliocene (2–4 Ma). Preliminary biostratigraphic data suggest that nannofossil Zones NN18–NN13 and planktonic foraminifer Zones Pl2–Pl5 are missing.

The second hiatus occurred during the early late and late middle Mio-cene, coincident with the nannofossil Zones NN9–NN7 and the planktonic foraminifer Zones Mt9 (part)–Mt8. The duration of this hiatus is ~4 m.y. The sedimentation rate during the middle–early Miocene fluctuated. The middle Miocene registered a rate of 15–16 m/m.y., and the early Miocene recorded an average rate of 10–14 m/m.y.

The sedimentation rate was only 7 m/m.y. in the Oligocene and was as fast as 38 m/m.y. in the Eocene. The oldest hiatus occurred between the upper Eocene chalk and the middle Eocene limonitic sandstone. The nannofossil Zone NP17, which spans ~3.2 m.y, is missing.

PALEOMAGNETISM

At Site 1134, archive halves of all APC and XCB cores were measured using the 2-G 760-R magnetometer, except for those core sections obviously disturbed by drilling, or with inadequate recovery for meaningful measurements. The cores were routinely measured at 5- to 10-cm intervals at natural remanent magnetization (NRM) and after 20-mT demagnetization. These analyses were performed using the methods described in **"Paleomagnetism,"** p. 12, in the "Explanatory Notes" chapter. Four whole-core sections were measured to compare with standard archive half-core measurements, in connection with the experimental coring using nonmagnetic cutting shoes and APC assemblies. In addition, a comparison between the effects of the cutting shoe (Hole 1134A) and the complete core-barrel assembly (Hole 1134B) was made. Discrete samples were taken to compare the orientation they yield with that of the Tensor tool and to establish the rock magnetic characteristics of the core. Discrete sample analysis will be largely shorebased.

Long-Core Measurements

The results of long-core measurements of the nannofossil ooze cores from Holes 1134A and 1134B were only partially successful. The NRM is dominated by a vertically downward coring contamination that was largely removed by 20-mT demagnetization. After this, the signal was almost uniformly reduced to near the noise level of the instrument (Fig. **F6**). The long-core measurements did give an interval between 0 and 30 mbsf of negative inclination. However, the signal was very weak, with intensities falling from on the order of 10^{-4} A/m near the top of the core to on the order of 10^{-5} A/m near 120 mbsf. The intensity then increased substantially, which appeared to coincide with the first appearance of chert in the hole. At 160 mbsf, the intensity again decreased. A continuous interval from ~120 to ~145 mbsf gave a sequence of reversals that could be correlated within the Miocene segment of the geomagnetic polarity time scale (GPTS).

Discrete Samples

Analysis of Sample 182-1134A-10H-CC showed that there is a stable normal moment in the upper weakly magnetized section. (Fig. **F7**). Further work with these samples will be performed postcruise.

F6. Intensity of magnetization in Hole 1134A, **p. 37.**

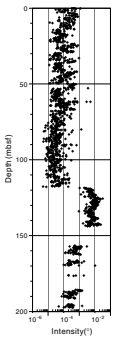

F7. AF demagnetization of Sample 182-1134A-10H-CC, **p. 38.**

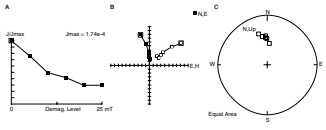

Magnetostratigraphy

In Core 1134A, the late Pleistocene magnetostratigraphy is defined to ~40 mbsf, with the Brunhes/Matuyama boundary at 32 mbsf, although the data quality in this interval is only marginal (Fig. F8). In Core 1134B the Brunhes/Matuyama boundary is at 38 mbsf. Poor data precluded further long-core interpretations in the interval from ~50 to 90 mbsf. However, below this interval, although the intensity remains low, reversals were again apparent. The availability of an estimate of age and sedimentation rate from biostratigraphic data permitted a possible correlation with the GPTS in Cores 182-1134A-13H through 17X, which corresponds to an interval of high remanence intensities that are nearly two orders of magnitude higher than in the shallower cores. The sequence of reversals is not long enough to give unequivocal magnetostratigraphic data, but a possible correlation is given in Figure F8.

F8. Inclination data and interpreted magnetostratigraphy for Holes 1134A and 1134B, p. 39.

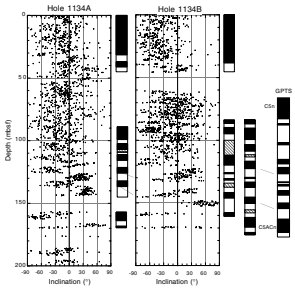

COMPOSITE DEPTHS

Introduction

Construction of the composite and spliced section from Holes 1134A and 1134B followed the methods outlined in "Composite Depths," p. 14, in the "Explanatory Notes" chapter. Table T3 (also in ASCII format) relates meters below seafloor (mbsf) depth to meters composite depth (mcd) for each core and section at Holes 1134A and 1134B and provides offset values for the conversion of mbsf depths to mcd. The composite section was constructed to a depth of 151.7 mcd and indicates complete recovery of the cored Holocene–middle Miocene sedimentary section at Site 1134.

T3. Site 1134 core and section depths in mcd and mbsf, p. 62.

Data Input

The primary lithologic parameters used to create the composite section were the 400-nm color reflectance data, a ratio of the 700- to 400-nm color reflectance data measured on split cores, and gamma-ray attenuation (GRA) bulk density data collected by the multisensor track (MST) on whole-round cores (Fig. F9). Natural gamma radiation (NGR) emissions measured by the MST exhibited low values with little variation and were, therefore, not used for composite section construction. For specifics regarding data collection procedures and parameters, see "Physical Properties," p. 21.

F9. Composite depth section produced using Splicer software, p. 40.

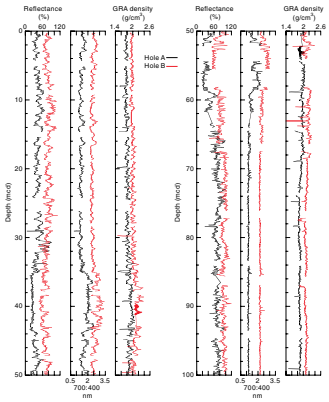

Composite Section Construction

The composite section for Site 1134 is presented in Figure F9. The primary difficulty encountered in the construction of this composite section was the presence of several thick slumped intervals within the upper Miocene and Pliocene section.

The sediments comprising the composite section are of Holocene–early Miocene age, based upon biostratigraphic data (see "Biostratigraphy," p. 8). The stratigraphic record within the range of the composite section is divided into three primary lithostratigraphic units (Fig. F9; see "Lithostratigraphy," p. 3). The upper unit, lithostratigraphic Unit I (0–33 mbsf, 0–34.7 mcd), is defined by the presence of calcareous nannofossil ooze that alternates between a wackestone and packstone tex-

ture. The color reflectance data record the lithologic variations as well-defined, high-amplitude (20%–40%) oscillations with a wavelength of 1–2 m that are easily correlated between holes. The lithologic variations are not as clearly defined in the GRA density data.

Lithostratigraphic Unit II is late Miocene–Pliocene in age and occurs from 33–66 mbsf (34.7–68.9 mcd). This unit is characterized by two slumped intervals at 35–43.3 mcd and 51.2–67.4 mcd (Fig. F9). The top of each slump is easily correlated between holes based upon a dramatic excursion to low color reflectance values and high 700:400 nm reflectance values. The slumps are also characterized by a slight plateau and a more constant signal in GRA density data. The base of each slump is easily recognized and correlated, based upon an abrupt return to the more typical, high-amplitude oscillations in the record.

Lithostratigraphic Unit III is middle–late Miocene in age and occurs from 66 to 152 mbsf (68.9–158.3 mcd). This unit is defined by the presence of calcareous nannofossil ooze, alternating between wackestone and packstone texture and exhibiting variable degrees of lithification. This unit exhibits relatively high reflectance values (60%–80%), with oscillations over very short wavelengths (<0.5 m) and fewer long wavelength features. The 700:400 nm data show a nearly constant record within this unit. Overall, the record within lithostratigraphic Unit III is relatively dissimilar between holes, making correlations more difficult. This may be the result of differential lithification and diagenesis.

The composite and spliced sections indicate that the entire section from 0 to 151.7 mcd was recovered at Site 1134 (Figs. F9, F10). However, correlations between ~100 and 130 mcd are difficult and yield poor correlation coefficients. As a result, Cores 182-1134A-13H and 14H were appended to the splice rather than tied (Table T4, also in ASCII format). Below 152 mcd, core recovery was greatly diminished because of the presence of chert horizons, and core overlap was negligible.

F10. Spliced section of smoothed color reflectance and NGR data produced using Splicer software, p. 42.

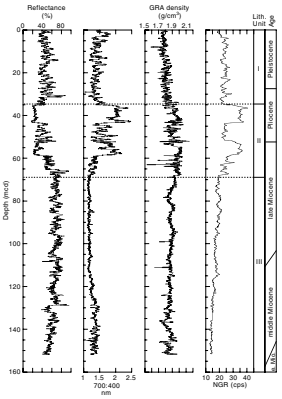

T4. Site 1134 splice tie points, p. 66.

T5. Headspace gas composition, Hole 1134A, p. 67.

T6. $CaCO_3$ content, Hole 1134A, p. 68.

F11. $CaCO_3$ content in samples from Hole 1134A, p. 43.

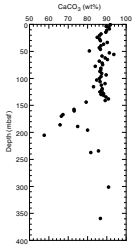

ORGANIC GEOCHEMISTRY

At Site 1134, in addition to routine monitoring of hydrocarbon gases for safety, inorganic carbon analyses were performed. The analytical procedures are described in "Organic Geochemistry," p. 16, in the "Explanatory Notes" chapter.

Volatile Hydrocarbons

Concentrations of volatile hydrocarbons were routinely determined in every core from Hole 1134A using standard ODP headspace sampling procedures. Only low concentrations of methane were detected; the maximum concentration was 8 ppm, with most samples having <5 ppm (Table T5). No heavier hydrocarbon gases (C_{2+}) were detected.

Inorganic and Organic Carbon, Sulfur, and Nitrogen

Calcium carbonate content in Hole 1134A ranges from 57.6 to 93.6 wt%, and most samples have 80 to 92 wt% (Table T6; Fig. F11).

Methane concentrations in the headspace samples in Hole 1134A were only slightly above background. No samples were analyzed for total carbon, sulfur, or nitrogen.

INORGANIC GEOCHEMISTRY

Interstitial Waters

Samples were taken from Hole 1134A at a rate of one sample per core over the upper 15 cores, and every other core thereafter (recovery permitting). Samples were analyzed according to the procedures outlined in "Inorganic Geochemistry," p. 18, in the "Explanatory Notes" chapter. These data are presented in Table T7 and Figures F12, F13, and F14.

T7. Interstitial water geochemistry, p. 69.

Salinity, Chlorinity, Potassium, and Sodium

Salinity shows a rapid increase at Site 1134, rising to 97 at a depth of 65.9 mbsf (Fig. F12). The rate of increase in salinity is significantly greater than at the shallow-water sites and is similar to Sites 1126 and 1130. Concentrations of Na^+ and K^+ are conservative with respect to Cl^-, and Na^+/Cl^- values are relatively constant throughout the cored interval. Between 304.5 and 352 mbsf, the concentrations of Cl^-, Na^+, and K^+ decline slightly. Whether this decrease is real and may therefore indicate the limits of the saline brine observed at this and other sites, or whether it is the result of contamination by seawater, is not known.

F12. Interstitial water trends, p. 44.

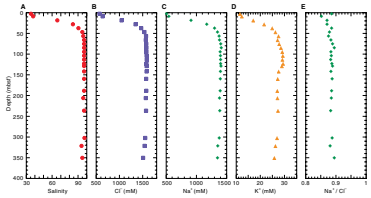

Calcium, Magnesium, Lithium, Silica, and Strontium

The concentrations of Mg^{2+} and Ca^{2+} increase with depth associated with the change in salinity. The concentration of Mg^{2+} rises to ~120 mM between 46.9 and 206.1 mbsf (Fig. F13). Toward the bottom of the cored interval, the concentration of Mg^{2+} decreases slightly to 110.3 mM. Although Mg^{2+} concentration increases with depth, the concentration normalized to Cl^- actually decreases, reaching a maximum depletion of 13 mM at 46.9 mbsf. The decrease in Mg^{2+} is possibly associated with the formation of dolomite, which is present throughout the upper 40 mbsf (Table T8, also in ASCII format). In contrast, the normalized concentration of Ca^{2+} increases by 6 mM over the same interval, indicating a net dissolution of carbonate. Recrystallization is also evident in the concentration of Sr^{2+} in the pore fluids, which rises rapidly to 364 µM at 37.4 mbsf. However, below this depth, the concentration decreases to 243 µM and subsequently declines more slowly to the bottom of the cored interval. The concentration of Li^+ increases slightly relative to Cl^-, associated with the recrystallization of calcium carbonate (Fig. F13).

F13. Concentration depth profiles, p. 45.

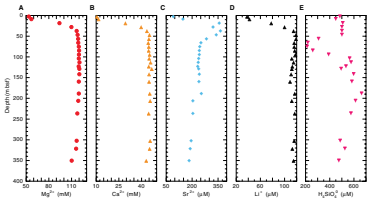

T8. XRD data, p. 70.

Sulfate, Alkalinity, Ammonium, Iron, and pH

The extent of organic reactions at Site 1134 are minimal compared to many of the other sites drilled during Leg 182. Alkalinity reached a maximum of 4.21 mM at 27.9 mbsf, slightly deeper than (1) the maximum in the concentration of dissolved Sr^{2+}, (2) the maximum depletion in the normalized concentration of SO_4^{2-} (4 mM), and (3) the highest concentration of NH_4^+ (Table T7; Fig. F14). The lack of sulfate depletion and the high alkalinity probably result from the relative absence of organic material caused both by oxidation of the organic material before burial and by the low rate of sedimentation at this site (see "Biostratigraphy," p. 8). The absence of H_2S, combined with a pH slightly lower than seawater, makes Fe^{2+} more soluble in interstitial wa-

F14. Variations in pH and interstitial water compositions, p. 46.

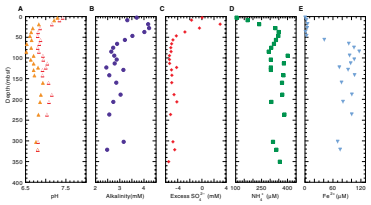

ters than in normal marine fluids. As a consequence, the concentration of Fe^{2+} is higher than that observed at other H_2S-rich sites cored during Leg 182, exceeding values of 80 µM (Fig. F14).

X-Ray Mineralogy

The sediments at Site 1134 are composed of low-Mg calcite (LMC), high-Mg calcite (HMC), quartz, aragonite, and dolomite (Table T8). In the uppermost portion of Site 1134, the sediments are composed of aragonite, HMC, LMC, quartz, and dolomite. However, HMC rapidly disappears with increasing depth, and aragonite vanishes coincident with the boundary between the middle and upper Miocene (see "Biostratigraphy," p. 8). Below 55.6 mbsf, the sediments appear to contain only LMC and a small amount of quartz, together with 5% and 10% insoluble material (see "Organic Geochemistry," p. 19). A small amount of aragonite accompanied by high concentrations of quartz was detected between 167.2 and 189.1 mbsf in sediments of middle Miocene age (see "Lithostratigraphy," p. 3).

PHYSICAL PROPERTIES

Introduction

Measurements of physical properties at Site 1134 followed the procedures outlined in "Physical Properties," p. 19, in the "Explanatory Notes" chapter. These included nondestructive measurements of *P*-wave velocity (every 4 cm; Table T9, also in ASCII format), GRA bulk density (every 4 cm; Table T10, also in ASCII format), magnetic susceptibility (MS) (every 8 cm; Table T11, also in ASCII format), and NGR (every 16 cm; Table T12, also in ASCII format) using the MST. The *P*-wave logger (PWL) was activated only on APC cores. Thermal conductivity was measured in unconsolidated sediment at a frequency of one per core (Table T13, also in ASCII format), with three samples analyzed on the core after the deployment of the Adara tool. A minimum of two discrete *P*-wave velocity measurements were made on the working half of the split cores (Table T14, also in ASCII format), and the measurement frequency was increased to five per section after the PWL was turned off. Standard index properties (Table T15, also in ASCII format) and undrained shear strength (only in unconsolidated sediments) (Table T16, also in ASCII format) were measured at a frequency of one per section. Difficulties occurred with the pycnometer used for determination of dry volume for index properties measurements (see "Index Properties," p. 21, in the "Explanatory Notes" chapters).

The following sections describe the variations in sediment physical properties and their relationships to lithology and downhole logging measurements. Variations in MS are described in "Paleomagnetism," p. 17.

Index Properties, *P*-wave Velocity, Natural Gamma Radiation, and GRA Densiometry

Sediment physical properties measurements at Site 1134 closely reflect lithologic variations observed in the recovered sediments and provide essential data for core-log correlation. (Fig. F15). An offset was seen between the discrete bulk density measurements and the GRA densiom-

T9. *P*-wave velocity measurements, p. 71.

T10. GRA densiometry measurements, p. 72.

T11. Magnetic susceptibility measurements, p. 73.

T12. Natural gamma-ray measurements, p. 74.

T13. Thermal conductivity measurements, p. 75.

T14. Discrete *P*-wave velocity measurements, p. 76.

T15. Index properties measurements, p. 77.

T16. Undrained shear strength measurements, p. 78.

F15. Discrete *P*-wave velocity, bulk densities, magnetic susceptibility, porosity, and NGR measurements, p. 47.

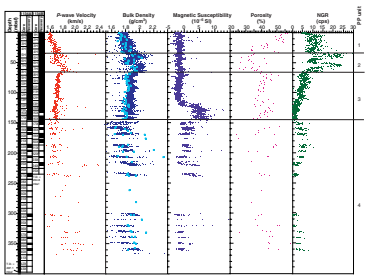

etry measurements of the MST in the upper 145 mbsf of the sedimentary section. This offset was corrected using the equation of Boyce (1976), as described in **"Index Properties,"** p. 21, in the "Explanatory Notes" chapter. Incomplete core recovery below 150 mbsf limited investigation of petrophysical properties within the lower parts of the sedimentary section (Fig. **F15**).

Physical properties data can be divided into four units on the basis of trends in measured parameters. Physical properties Unit (PP Unit) 1 (0–33 mbsf) is characterized by a decrease in porosity (50%–30%) and an increase in both bulk density (1.7–2.0 g/cm^3) and *P*-wave velocity (1.6–1.8 km/s) (Fig. **F15**). These trends are most likely caused by lithostatic compaction. The lower boundary of PP Unit 1 is identified by a spike in NGR (30 cps), bulk density (2.2 g/cm^3), and a decrease in *P*-wave velocity (Fig. **F15**). Physical properties Unit 1 correlates well to lithostratigraphic Unit I, which consists primarily of nannofossil ooze and changes abruptly to an unlithified wackestone at 33 mbsf (see **"Lithostratigraphy,"** p. 3).

Physical Properties Unit 2 (33–66 mbsf) is identified by high variability in *P*-wave velocity, bulk density, porosity, and NGR. There are two identifiable spikes in NGR and bulk density (33 and 52 mbsf) (Fig. **F15**) that correspond well to soft-sediment deformation interpreted as slumps (see **"Lithostratigraphy,"** p. 3). The lower boundary of PP Unit 2 is identified by an increase in porosity (30%–44%) and a decrease in *P*-wave velocity (1.75–1.7 km/s), bulk density (2.1–1.9 g/cm^3), and NGR (24.5 cps) (Fig. **F15**). This corresponds to the boundary between lithostratigraphic Units II and III (see **"Lithostratigraphy,"** p. 3).

Physical properties Unit 3 (66–145 mbsf) is characterized by low variability in *P*-wave velocity, bulk density, porosity, and NGR (Fig. **F15**). *P*-wave velocity, bulk density, and NGR trend to lower values. The decreased bulk density values and *P*-wave velocities are typical of the calcareous nannofossil ooze and calcareous nannofossil foraminiferal ooze found in this unit. The lower boundary for this unit is marked by an increase in NGR (2–7 cps) and an increase in the variability in bulk density and *P*-wave velocity and corresponds to the boundary between lithostratigraphic Units III and IV (see **"Lithostratigraphy,"** p. 3).

Physical properties Unit 4 (145–368 mbsf) is characterized by high variability in *P*-wave velocity, bulk density, and porosity, with generally low values of NGR resulting from the lithologic alternation of foraminiferal chalk and wackestones/packstones (see **"Lithostratigraphy,"** p. 3). Low recovery precludes recognition of further physical properties units lower in the sedimentary section.

Clear correlations appear between physical properties and downhole logging data, especially between bulk density measurements. Unfortunately, the length of pipe necessary for hole stability precludes analysis of the first 110 mbsf of downhole logging data. GRA density values are well correlated to downhole density logs, although with increasing depth in the sequence, GRA densities become less than in situ densities (Fig. **F16**). Discrete *P*-wave velocities are also generally lower than downhole sonic logs (Fig. **F16**). These differences are due to the fact that discrete *P*-wave velocities and GRA bulk densities were not measured under in situ pressure conditions. NGR data measured on cores show similar patterns to the downhole NGR log even within the interval logged in pipe (Fig. **F16**).

F16. Downhole logging data and physical properties measurements, **p. 48.**

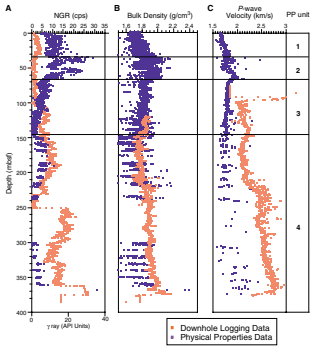

Shear Strength

Undrained peak and residual shear strength were measured on unconsolidated sediments from 0 to 66 mbsf (Fig. F17), and values varied between 4 and 75 kPa. Shear strength at Site 1134 is relatively constant from 0 to 33 mbsf and increases throughout the rest of the measured section.

F17. Shear strength measurements, p. 49.

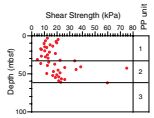

Thermal Conductivity

Thermal conductivity at Site 1134 was measured from 0 to 155 mbsf, and values range from 0.9 to 1.4 W/(m·K) (Fig. F18). Thermal conductivity values increase through PP Unit 1 and 2 and decrease through PP Unit 3. These data correlate well to changes in bulk density (Fig. F18), confirming the importance of bulk density on thermal conductivity (see "Lithostratigraphy," p. 3).

F18. Thermal conductivity and bulk density measurements, p. 50.

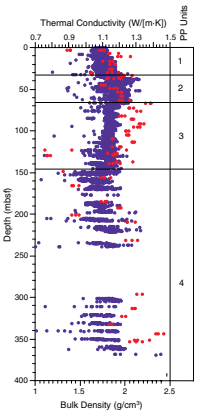

In Situ Temperature Measurements

One Adara formation temperature determination was made at Site 1134. The mudline temperature was 9.30°C ± 0.012°C, and the formation temperature at 33 mbsf was 9.67°C ± 0.014°C. The values are similar to those measured at Site 1126, which is located at a similar water depth.

DOWNHOLE MEASUREMENTS

Logging Operations

After completion of drilling operations at Hole 1134A, the hole was prepared for logging (see "Operations," p. 2). The end of the bottom-hole assembly was placed at 105 mbsf. The wireline heave compensator (WHC) was used during all logging runs and performed moderately well in the medium-to-high heave conditions, except on the first pass with the FMS/sonic tool string. Three different logging strings were deployed in the following order: (1) triple combo, (2) FMS/sonic tool, and (3) WST (Table T17; see "Logging Tools and Tool Strings," p. 27, in the "Explanatory Notes" chapter). Approximately 10 m of fill caused by loose sands was recorded at the base of the hole during the first logging run.

T17. Tool strings, intervals logged, and logging speeds; Hole 1134A, p. 79.

Before the main run with the triple combo, a short quality control run was made from 386 mbsf (11 m short of drilled depth) to 296 mbsf. The main run was logged from 386 mbsf to mudline. Two passes were made with the FMS/sonic. During the first pass from 386 to 118 mbsf, the WHC reached the maximum limit of heave correction at 158 mbsf and the FMS calipers were closed immediately to protect them from downheave. During the second pass from 386 to 129 mbsf, the WHC operated normally. Seven check-shot stations were recorded between 381 and 138 mbsf. Seven shots were stacked per station, with individual stations located near log breaks and at estimated depths of significant seismic reflectors (see "Seismic Stratigraphy," p. 26).

Data Quality

The general data quality from the triple combo and FMS/sonic tool strings was good, although borehole rugosity may have affected porosity measurements in some intervals (Fig. F19). Negative potassium concentrations between 230 and 250 mbsf are probably an artifact of the tool's inability to measure low potassium concentrations. Formation MicroScanner images were affected by moderate to rough heave conditions, and further shorebased processing will be necessary to fully compensate for heave effects. Although the sonic digital tool (DTCO output) performed well, the analog modes provided poor-quality data with only 50%–60% coverage of the logged interval. The signal recorded by the WST was clipped, as gun pressure was increased to 1500 psi to obtain consistent first-break arrival times. A comparison between downhole logging and sediment physical properties measurements is difficult because of poor core recovery below 145 mbsf (see "Physical Properties," p. 21).

F19. Triple combo and sonic logs vs. depth for the open-hole logged interval, p. 51.

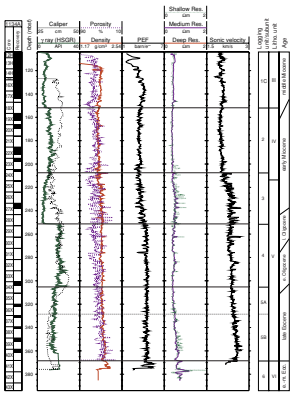

Preliminary Observations

The overall log pattern at Hole 1134A is similar to Hole 1126D, which is situated in a similar setting further to the east, although gamma radiation is higher in Hole 1134A than in Hole 1126D. The succession has been divided into six logging units on the basis of variations in measured parameters. The logging unit boundaries correlate closely with most lithostratigraphic boundaries (see "Lithostratigraphy," p. 3).

Logging Unit 1: 0–152 mbsf

Logging Unit 1 was logged through pipe to 105 mbsf and is divided into three subunits on the basis of the spectral gamma-ray log (Fig. F20). Subunit 1A (0–31 mbsf) is characterized by relatively high gamma-ray values (8–10 American Petroleum Institute [API] units), with three distinct gamma-ray lows. Subunit 1A can be correlated with logging Unit 1 in Hole 1126D, where a similar gamma-ray pattern is observed (Fig. F26, p. 75, in the "Site 1126" chapter). This elevated gamma radiation is likely to be diagenetic in origin. The lower boundary of Subunit 1A is defined by a decrease in gamma radiation, which correlates with the base of lithostratigraphic Unit I (see "Lithostratigraphy," p. 3). Logging Subunit 1B (31–57 mbsf) is characterized by variable NGR, with a marked decrease at the base of the unit (Fig. F20). Subunit 1C (57–152 mbsf) is characterized by low gamma-ray values in the pipe and in the open-hole logged interval (Figs. F20, F21). The origin of the positive separation of density and porosity logs for most of this unit is unclear. The base of Unit 1 is marked by an increase in NGR values (Fig. F21).

F20. Spectral gamma-ray logs from HNGS for interval logged through pipe, p. 52.

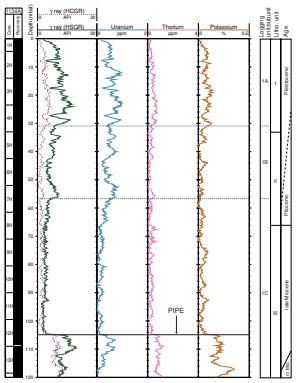

F21. Spectral gamma-ray logs from the HNGS, plotted vs. depth for the open-hole logged interval, p. 53.

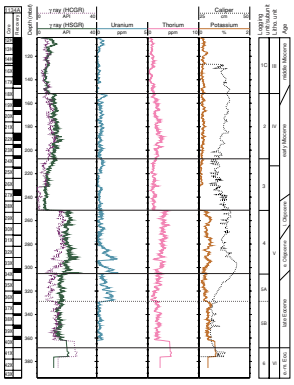

Logging Unit 2: 152–207 mbsf

Logging Unit 2 is characterized by an increase in gamma radiation compared to Unit 1 (~12–14 API units), caused mainly by increased thorium concentrations (Fig. F21). Separation of the density and porosity logs is less than in Unit 1, and photoelectric effect (PEF) values are relatively constant near 3.6 barn/e$^-$, with low variability in resistivity, density, and sonic logs (Fig. F19). This unit correlates to lithostrati-

graphic Unit IV, which is composed of an alternation of wackestones, grainstones, and chalk with variable lithification (see "Lithostratigraphy," p. 3). Except for the basal 15 m of this unit, where there is some evidence for fluid invasion, resistivity values remain nearly constant (Fig. F19). In the basal 15 m, thin chert beds occur, which appear as low-porosity peaks and coincide with decreased PEF and peaks in shallow resistivity. This is confirmed by FMS images, which show several thin (< 10 cm), resistive layers, alternating with thicker (1–3 m), more conductive layers. The base of Unit 2 is defined by a marked change in the character of all logs toward more variable values (Fig. F19), and by increasing frequency and thickness of the chert layers as indicated by the FMS images. Despite the fact that the gamma radiation values are higher in Unit 2, this unit may be correlated with logging Unit 3 in Hole 1126D, mainly on the basis of porosity-density, PEF, and sonic logs.

Logging Unit 3: 207–251 mbsf

Logging Unit 3 is characterized by decreasing trends in gamma radiation, increasing bulk density, and increased variability in all other measured parameters (Figs. F19, F21). Within logging Unit 3, there are numerous low-porosity excursions that cross over the bulk density curve and correlate with peaks in shallow resistivity and sonic velocity (Fig. F19). These variations reflect thin chert layers observed in recovered sediments (see "Lithostratigraphy," p. 3) and appear as thin (10–50 cm) resistive layers alternating with thicker (1–2 m), more conductive layers in the FMS images. Values of PEF increase slightly within logging Unit 3 (~3.4–4.1 barn/e^-). Excursions in shallow resistivity within Unit 3 indicate that fluid invasion is occurring within this sedimentary sequence (Fig. F19). The high variability in the sonic logs is easily correlatable to the upper part of logging Unit 4 at Site 1126. The base of Unit 3 occurs at a marked increase in gamma-ray values (28–22 API units), dominantly caused by increased thorium and potassium (Fig. F21). Logging Unit 3 corresponds to the upper part of lithostratigraphic Unit V (see "Lithostratigraphy," p. 3).

Logging Unit 4: 251–306 mbsf

Logging Unit 4 is characterized by relatively high gamma-ray values (~20–28 API units), with variability controlled by the uranium content of the formation (Fig. F21). As with the above units, porosity-density crossovers correlated to sonic velocity and shallow resistivity peaks indicate chert horizons (Fig. F19). Formation MicroScanner images clearly show that chert layers are thinner (5–20 cm) and less frequent (~2–4 m separation) than in logging Unit 3. Photoelectric effect values show a slight increasing trend with increasing depth in the unit. Resistivity values are generally constant within logging Unit 4, and there are fewer excursions of shallow resistivity compared to the unit above. Sonic velocity increases slightly within Unit 4 and has reduced variability relative to logging Unit 3. Logging Unit 4 corresponds to the middle part of lithostratigraphic Unit V, which contains mudstone to packstones, although recovery was poor for this interval (see "Lithostratigraphy," p. 3). The base of Unit 4 is marked by a peak in uranium gamma radiation, followed by an abrupt decrease, defining the boundary between Units 4 and 5 (Fig. F21).

Logging Unit 5: 306–368 mbsf

Total gamma-ray values display low variability and nearly constant values within logging Unit 5. However, individual radioactive elements display marked variations, defining two subunits within Unit 5 (Fig. F21). Subunit 5A is defined by a downhole increase in uranium and a decrease in thorium concentrations. The base of Subunit 5A is marked by an abrupt decrease in uranium and slight increases in thorium and potassium (Fig. F21). Within logging Unit 5, PEF values remain constant (~4.6 barn/e$^-$), whereas porosity decreases, and density, resistivity, and velocity increase, characteristic of a normal compaction trend (Fig. F19). As with the units above, porosity-density crossovers, corresponding to resistivity and sonic peaks, are interpreted as thin chert beds and/or partly silicified layers. This is confirmed by FMS images, which show a succession of thin (5–10 cm) resistive beds alternating with thicker (1–3 m) more conductive layers. Near the base of physical properties Unit 5, there are excursions of shallow resistivity indicating minor fluid invasion. Logging Unit 5 corresponds to the basal part of lithostratigraphic Unit V (see "Lithostratigraphy," p. 3), and is correlated with logging Units 6 and 7 in Hole 1126D.

Logging Unit 6: 368–385 mbsf

Density, PEF, caliper, and resistivity are the only logs available for logging Unit 6, as the length of the tool strings and sediment fill in the hole prevented acquisition of a full logging suite. This unit is characterized by two PEF peaks (~5.8 barn/e$^-$) associated with high density values (~2.1 g/cm^3), and highly variable resistivity with major excursions of shallow resistivity (Fig. F19). This unit corresponds to the poorly recovered lithostratigraphic Unit VI, consisting of limonitic sandstones (see "Lithostratigraphy," p. 3). Logging Unit 6 correlates with logging Unit 8 of Hole 1126D.

SEISMIC STRATIGRAPHY

Introduction

Site 1134 (Fig. F22) penetrated Cenozoic seismic Sequences 2, 3, 4, 6A, and 7 (sequences defined in Feary and James, 1998, reprinted as Chap. 2). It is unclear whether the basal Cenozoic unconformity was intersected before unstable hole conditions terminated coring. Postdrilling correlation indicates significant differences between the predrill seismic stratigraphy (Fig. F23) and the actual succession intersected at Site 1134. The base of Sequence 2 was predicted to occur at a much shallower depth than was the case, with the slumped interval at the base of Sequence 2 erroneously assigned to Sequence 3. In addition, a previously unrecognized sequence assignable to regional Sequence 7 (Feary and James, 1998, reprinted as Chap. 2) was intersected toward or at the base of Hole 1134A. It appears likely that the base Cenozoic unconformity either occurs immediately below the base of hole or more probably was intersected in the final two cores (from which no sediment was recovered). The high-resolution site-survey seismic data (Fig. F23), together with the regional seismic database, indicate that significant hiatuses should occur at all sequence boundaries and also at intrasequence horizons within Sequences 3 and 6A.

F22. Seismic site-survey tracks for Site 1134 in relation to other Leg 182 sites and the AGSO169 site-survey seismic lines, p. 54.

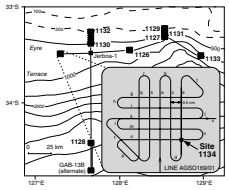

F23. Portion of seismic Line AGSO169/01e, p. 55.

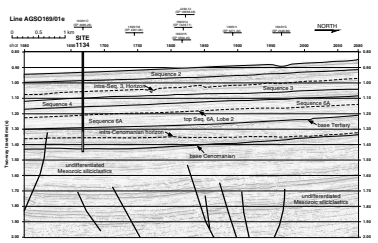

Time–Depth Conversion

A check-shot survey using the single-channel WST was undertaken at this site to determine the time–depth relationship for the Cenozoic succession. The parameters and procedures undertaken during the check-shot survey at this site are described in "Downhole Measurements," p. 23, and the seven time–depth tie-points established by the check-shot survey are presented in Fig. F24. These points were plotted on a depth to two-way–traveltime graph (Fig. F25A) to (1) determine the relationship between depths encountered at Site 1134 and sequence boundaries and horizons located on seismic data and (2) to compare the check-shot-corrected time–depth relationship with predictions based on stacking velocities. This plot shows that the actual time–depth relationship defined by the check-shot survey falls at the lower limit of the envelope (defined by the six stacking velocity curves from the immediate vicinity of Site 1134), with a relatively small difference (≤11 m) between predicted and actual depths to boundaries/horizons (Table T18). The plot of check-shot data and velocity (Fig. F25B) shows a reasonably good correlation, and the integrated sonic trace (Fig. F25), derived from interval transit-time data, is in excellent agreement with stacking velocities.

Seismic Sequence Characteristics

The data collected at Site 1134, particularly lithostratigraphic and biostratigraphic information, offer the opportunity to view the site data within a more regional context and to describe the characteristics of the seismic sequences intersected at this site (see "Lithostratigraphy," p. 3, and "Biostratigraphy," p. 8). Downhole data were correlated with seismic stratigraphy (Fig. F26) based both on the regional moderate-resolution multichannel seismic data collected by the Japan National Oil Corporation (JNOC) in 1990 (Feary and James, 1998, reprinted as Chap. 2) and on the high-resolution site-survey seismic data collected by the Australian Geological Survey Organisation (AGSO) in 1996 (Feary, 1997).

Sequence 2

Sequence 2 is relatively thin (66 m) at Site 1134, with seismic data indicating that the basal sequence boundary is a marked unconformity/hiatus surface containing erosional channels that cut into the underlying Sequence 3 succession. Reflections within the upper part of Sequence 2 (corresponding to the bioturbated nannofossil and foraminifer ooze of lithostratigraphic Unit I) are low amplitude, evenly stratified, and conformable. Reflections within the lower part of Sequence 2 (corresponding to the slumped nannofossil and foraminifer ooze, unlithified wackestone, packstone, and rudstone of lithostratigraphic Unit II) are irregular and discontinuous. Biostratigraphic datums indicate that Sequence 2 is of Pleistocene age, although probably containing a very thin Pliocene interval at the base (see "Biostratigraphy," p. 8). The predrill estimate of the depth to the base of Sequence 2 was at variance with the intersected succession because the base Sequence 2 unconformity was misidentified as occurring above instead of below the poorly stratified and irregular reflections corresponding to the slumped facies of lithostratigraphic Unit II.

F24. Check-shot stations and acquisition geometry for the WST survey at Hole 1134A, p. 56.

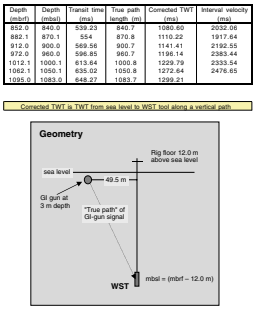

F25. Differences between depths to key horizons and corrected depths, p. 57.

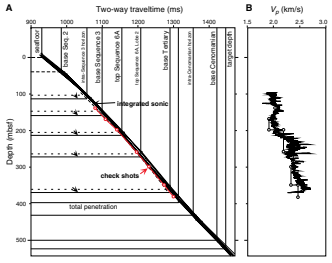

T18. Differences between depths to key horizons and corrected depths, p. 80.

F26. Lithostratigraphic units, seismic sequences, biostratigraphic hiatuses, and ages, p. 58.

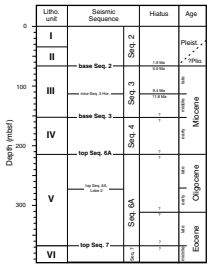

Sequence 3

From a regional perspective, Sequence 3 is thickest (~240 m) beneath the modern shelf and thins downslope to a feather edge beneath the modern middle shelf. Site 1134 intersects Sequence 3 beneath the upper slope, where it is 86 m thick. Sequence 3 correlates with lithostratigraphic Unit III (of middle and late Miocene age), which consists of dominantly pelagic, calcareous nannofossil and nannofossil foraminifer ooze. The upper Sequence 3 boundary represents a significant unconformity surface, corresponding to a hiatus of ~3 m.y. The high-resolution site-survey seismic data show that Sequence 3 includes a surface at ~112–114 mbsf (intra-Sequence 3 horizon on Fig. **F23**) that is a definite unconformity/hiatus associated with significant erosional downcutting. Biostratigraphic and lithostratigraphic data (see **"Biostratigraphy,"** p. 8, and **"Lithostratigraphy,"** p. 3) indicate that, despite apparent lithostratigraphic uniformity, this surface represents a hiatus of between 2 to 5 m.y., corresponding to the middle–upper Miocene boundary.

Sequence 4

Within the Eucla Basin, seismic Sequence 4 is a relatively thin, aggradational unit characterized by conformable internal reflections (Feary and James, 1998, reprinted as **Chap. 2**). This sequence is 62 m thick at Site 1134, corresponding to lithostratigraphic Unit IV (Fig. **F26**) of early Miocene age. Lithostratigraphic data indicate that the intensely bioturbated, unlithified or partially lithified wackestone/packstone, foraminifer chalk, and minor packstone of Sequence 4 are less calcareous than overlying sequences. The variable amplitude, evenly stratified reflections constituting Sequence 4 probably represent the foraminifer chalk to wackestone/packstone alternations characteristic of this unit.

Sequence 6A

Sites 1126 and 1134 offered the only opportunities during this leg to characterize the lithology and age of seismic Sequence 6A, shown on regional seismic data to consist of three deep-water sediment lobes derived from the north (Feary and James, 1998, reprinted as **Chap. 2**). The 154-m section through Sequence 6A intersected at Site 1134 was first encountered at 214 mbsf, corresponding to a lithostratigraphic and velocity boundary (see **"Lithostratigraphy,"** p. 3, and **"Downhole Measurements,"** p. 23). Sequence 6A correlates with lithostratigraphic Unit V, which consists of strongly bioturbated, texturally variable, calcareous nannofossil chalk interbedded with silicified equivalents and ranges in age from late Eocene to late Oligocene. Although limited recovery prevented the formal identification of lithostratigraphic subunits, substantial lithologic variations were noted (see **"Lithostratigraphy,"** p. 3). However, the poorly constrained lithostratigraphic boundaries do not appear to correlate with seismic stratigraphic boundaries. The downhole transition from wackestone to mudstone at 252 mbsf corresponds to a dramatic increase in gamma-ray values (see **"Downhole Measurements,"** p. 23) but correlates only with a pronounced reflection at 1190 ms two-way traveltime (Fig. **F23**). No apparent lithostratigraphic break was detected coinciding with the boundary between the lower Oligocene Lobe 2 and upper Oligocene Lobe 3 at ~270 mbsf (see Fig. **F23**), which was expected to occur as a minor hiatus surface. The transition

from packstone into the underlying mudstone facies at ~305 mbsf (possibly corresponding to the Eocene–Oligocene unconformity located biostratigraphically at ~315 mbsf) does not correlate with any seismic stratigraphic horizon.

Sequence 7

As noted above, intersection of an interval of Sequence 7 sandstones was unexpected at this site. Only 30 cm of limonitic, coarse-grained sandstone containing abundant skeletal grains was recovered and assigned to lithostratigraphic Unit VI. Biostratigraphic data show that this sandstone is of middle Eocene age and indicate a likely hiatus of ~3 m.y. at the top Sequence 7 boundary. Reinterpretation of the site-survey seismic data indicates that this previously unrecognized interval is a thin feather edge of Sequence 7 overlying the irregular basal Cenozoic unconformity. Although no Mesozoic material was recovered, it is likely that either of the two deepest cores in Hole 1134A (from which no material was recovered) may have penetrated into the Cretaceous sequence. Alternatively, the basal Cenozoic unconformity may be present immediately below the base of Hole 1134A.

REFERENCES

Berggren, W.A., 1992. Paleogene planktonic foraminifer magnetobiostratigraphy of the Southern Kerguelen Plateau (Sites 747–749). *In* Wise, S.W., Jr., Schlich, R., et al., *Proc. ODP, Sci. Results,* 120 (Pt. 2): College Station, TX (Ocean Drilling Program), 551–568.

Berggren, W.A., Kent, D.V., Swisher, C.C., III, and Aubry, M.-P., 1995. A revised Cenozoic geochronology and chronostratigraphy. *In* Berggren, W.A., Kent, D.V., Aubry, M.-P., and Hardenbol, J. (Eds.), *Geochronology, Time Scales and Global Stratigraphic Correlation*. Spec. Publ.—Soc. Econ. Paleontol. Mineral. (Soc. Sediment. Geol.), 54:129–212.

Boyce, R.E., 1976. Definitions and laboratory techniques of compressional sound velocity parameters and wet-water content, wet-bulk density, and porosity parameters by gravimetric and gamma-ray attenuation techniques. *In* Schlanger, S.O., Jackson, E.D., et al., *Init. Repts. DSDP,* 33: Washington (U.S. Govt. Printing Office), 931–958.

Chaproniere, G.C.H., Shafik, S., Truswell, E.M., MacPhail, M.K., and Partridge, A.D., 1995. Cainozoic. In *Australian Phanerozoic Time Scale.* Geol. Surv. Aust., 10.

Feary, D.A., 1997. ODP pollution prevention and safety panel: Leg 182 safety package—Cenozoic cool-water carbonates of the Great Australian Bight. *Aust. Geol. Surv. Org.,* 28.

Feary, D.A., and James, N.P., 1998. Seismic stratigraphy and geological evolution of the Cenozoic, cool-water, Eucla Platform, Great Australian Bight. *AAPG Bull.,* 82:792–816.

Jenkins, D.G., 1993. Cenozoic Southern mid- and high-latitude biostratigraphy and chronostratigraphy based on planktonic foraminifera. *In* Kennett, J.P., and Warnke, D.A. (Eds.), *The Antarctic Paleoenvironment: A Perspective on Global Change.* Antarct. Res. Ser., 60:125–144.

McGowran, B., Li, Q., and Moss, G., 1997. The Cenozoic neritic record in southern Australia: the biogeohistorical framework. *In* James, N.P., and Clarke, J., *Cool-Water Carbonates*. Spec. Publ.— Soc. Econ. Petrol. Mineral., 56:185–203.

Shafik, S., 1990. The Maastrichtian and early Tertiary record of the Great Australian Bight Basin and its onshore equivalents on the Australian southern margin: a nannofossil study. *BMR J. Australian Geol. Geophys.,* 11:473–497.

van Morkhoven, F.P.C.M., Berggren, W.A., and Edwards, A.S., 1986. Cenozoic cosmopolitan deep-water benthic foraminifera. *Bull. Cent. Rech. Explor.—Prod. Elf-Aquitaine,* 11.

Figure F1. Map showing the location of Site 1134 (on the Eyre Terrace) in relation to other Leg 182 sites and the Australian Geological Survey Organisation Survey 169 (AGSO169) seismic lines.

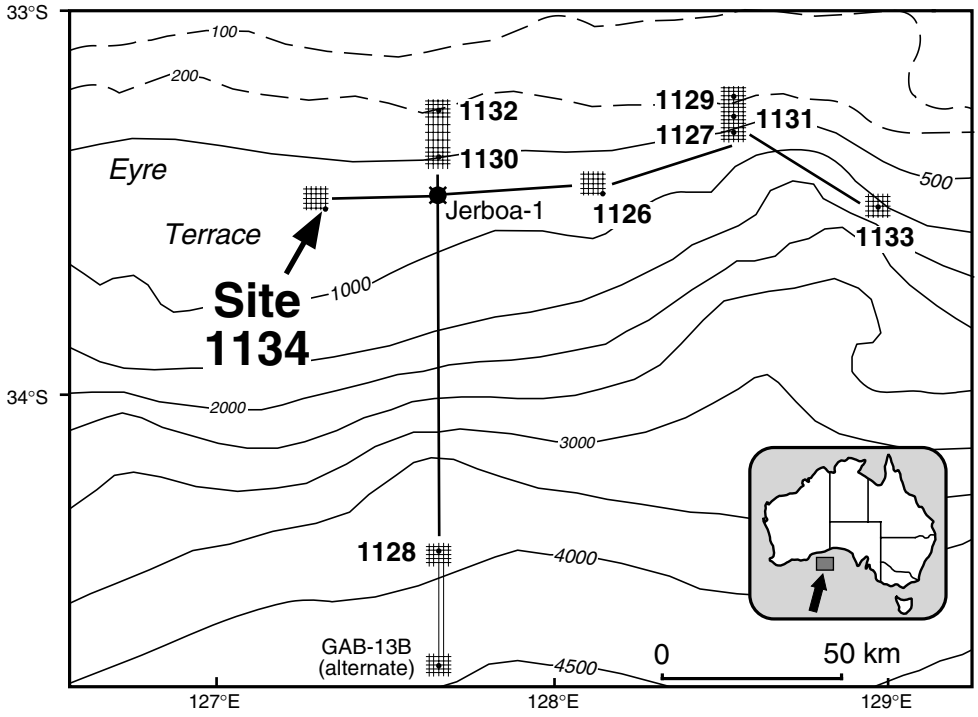

Figure F2. Portion of seismic Line AGSO169/01e showing interpreted seismic stratigraphic sequences planned (shown in white) and actually intersected (shown in black) at Site 1134.

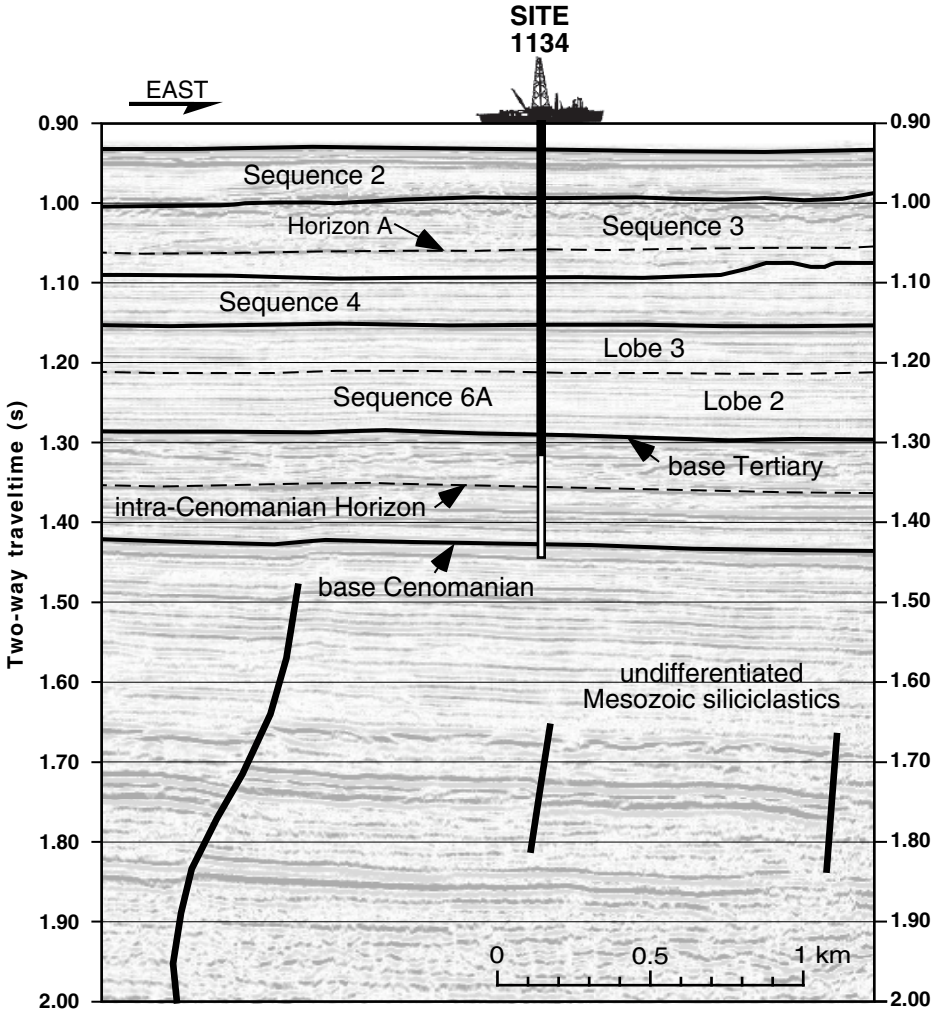

Figure F3. Summary of sediments and lithostratigraphy, Site 1134. Age assignments follow data provided in "Biostratigraphy," p. 8. SB = sequence boundary. (Continued on next page.)

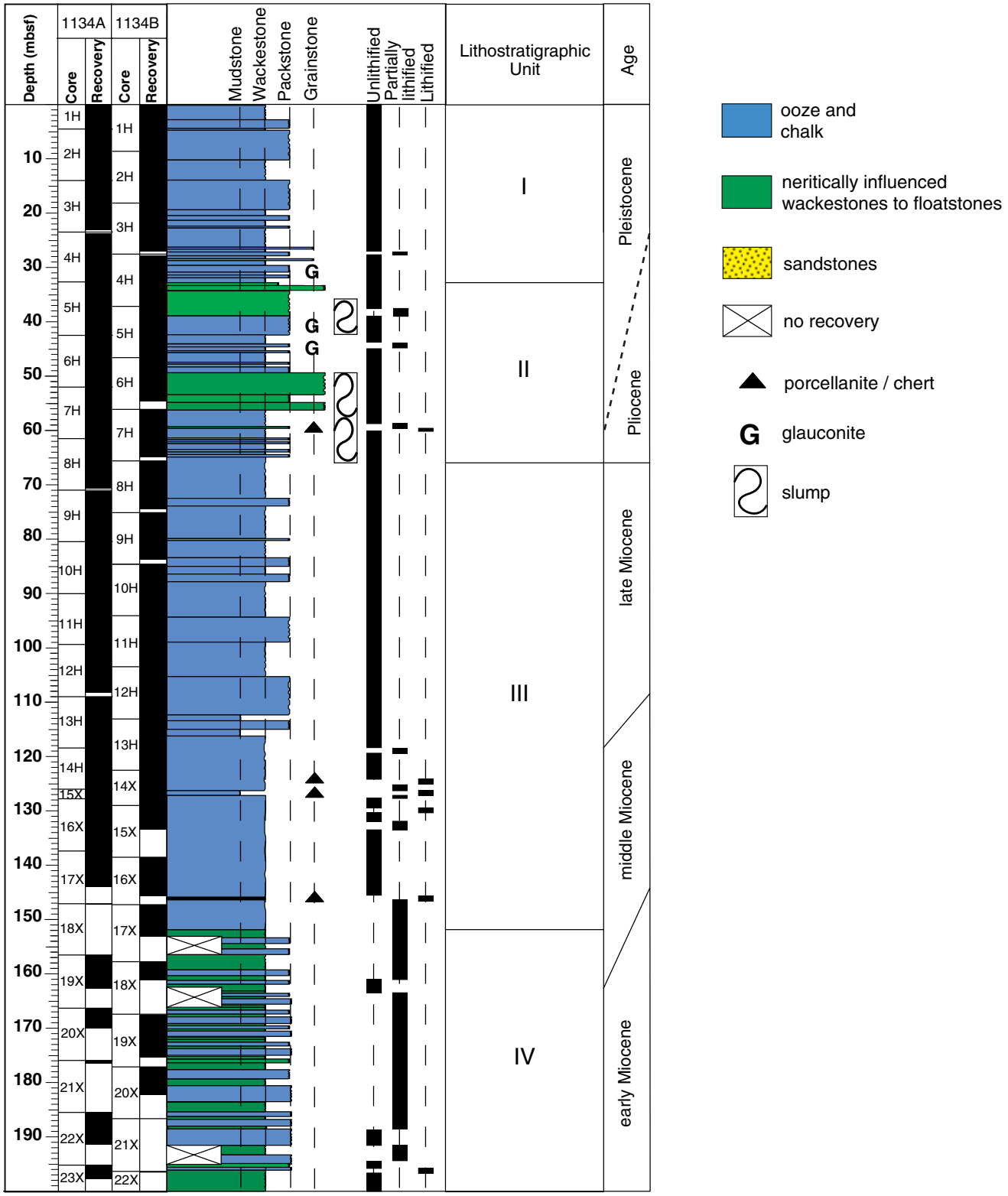

Figure F3 (continued).

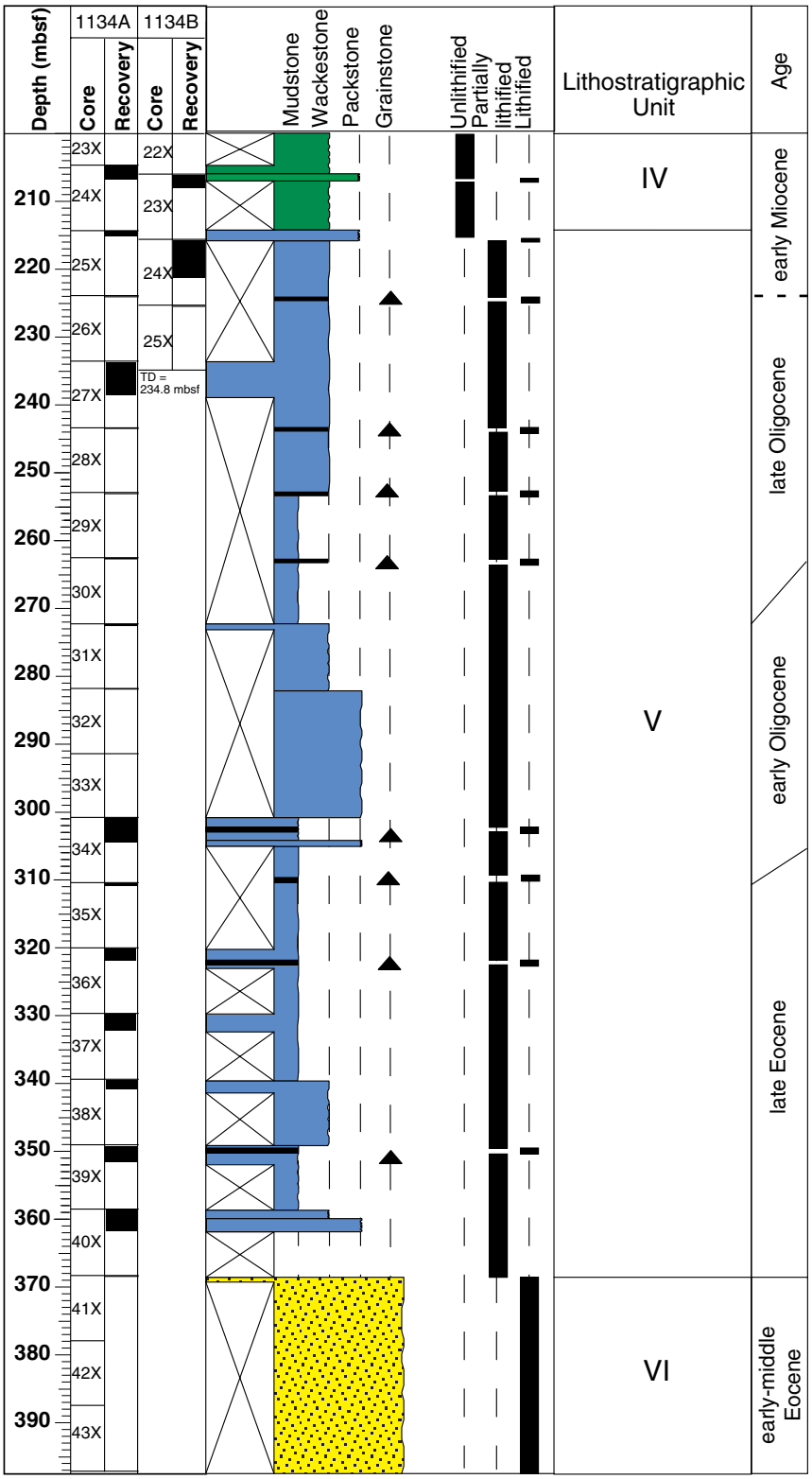

Figure F4. Stratigraphic position of calcareous nannofossil and planktonic foraminiferal zones and benthic foraminiferal assemblages at Site 1134. Dashed boundaries imply uncertainty. No data = there is insufficient data to assign an age. Lithostratigraphic units are taken from "Lithostratigraphy," p. 3.

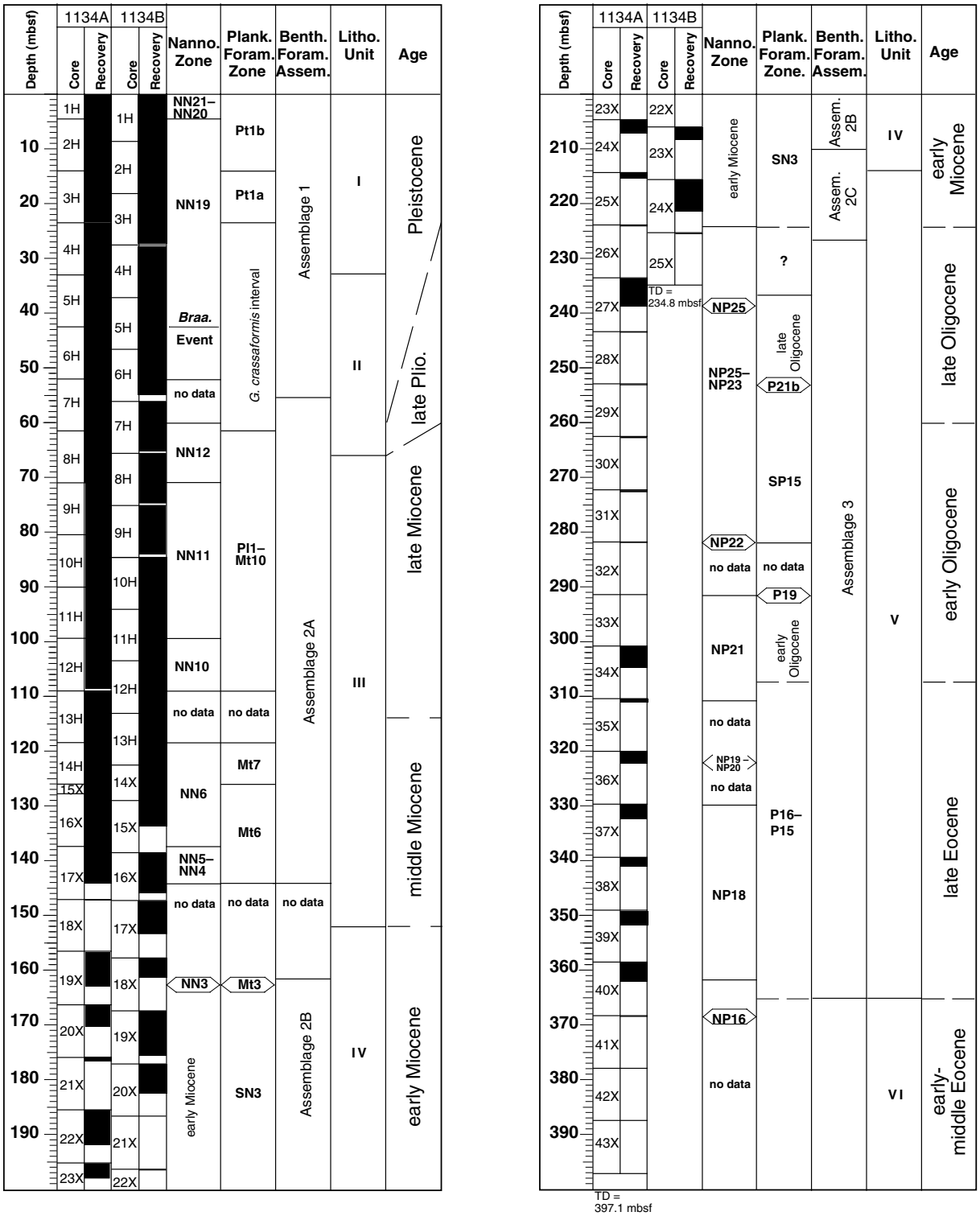

Figure F5. Sedimentation-rate curve constructed from the datum levels listed in Table T2, p. 61. Stratigraphic errors are indicated by the length of the error bars. Datum levels are coded from 1 to 28, with every fifth one labeled on the chart.

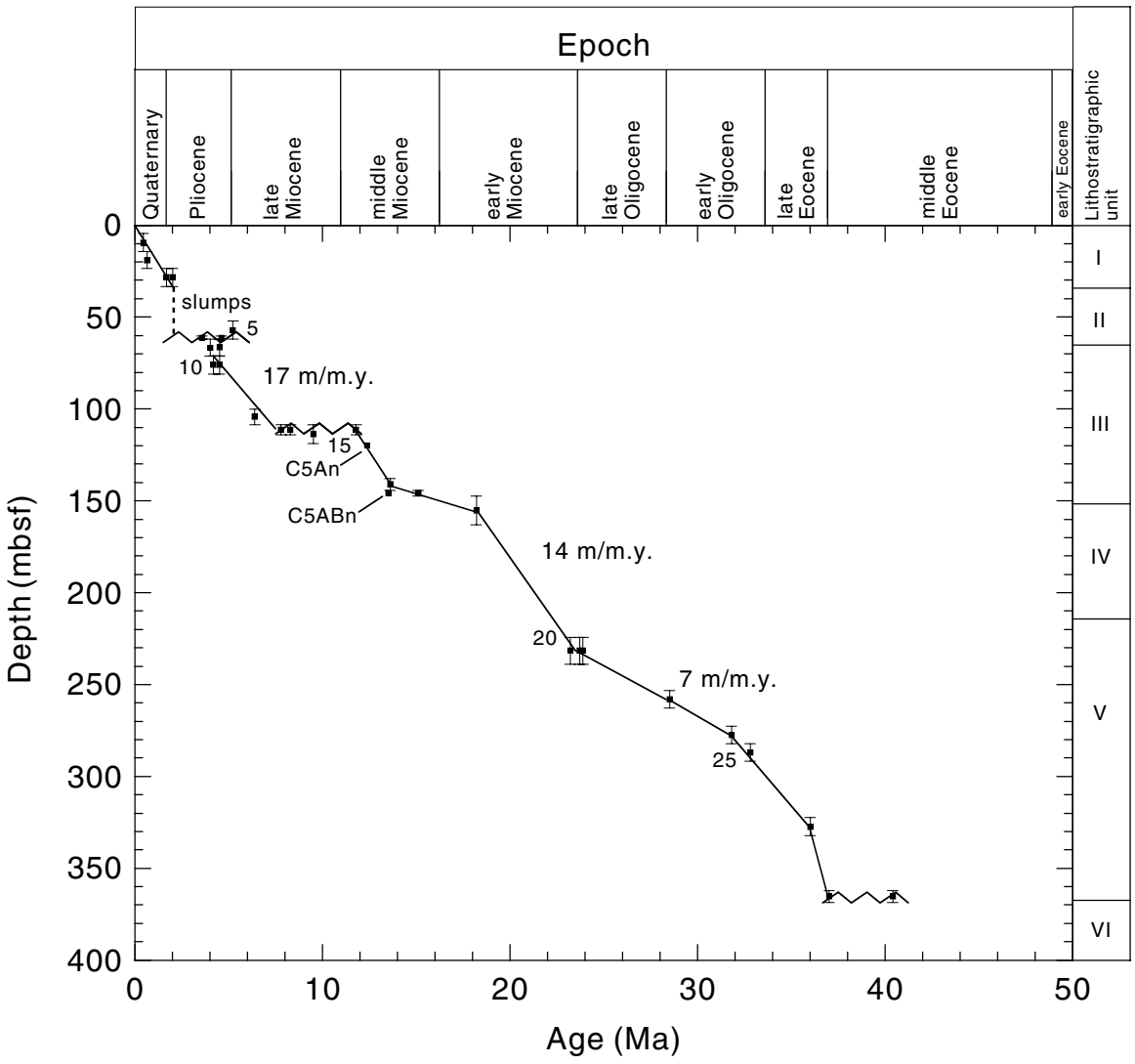

Figure F6. Intensity of magnetization in Hole 1134A showing a decrease in intensity in uppermost 100 mbsf followed by an increase correlated with the appearance of cherts in the hole.

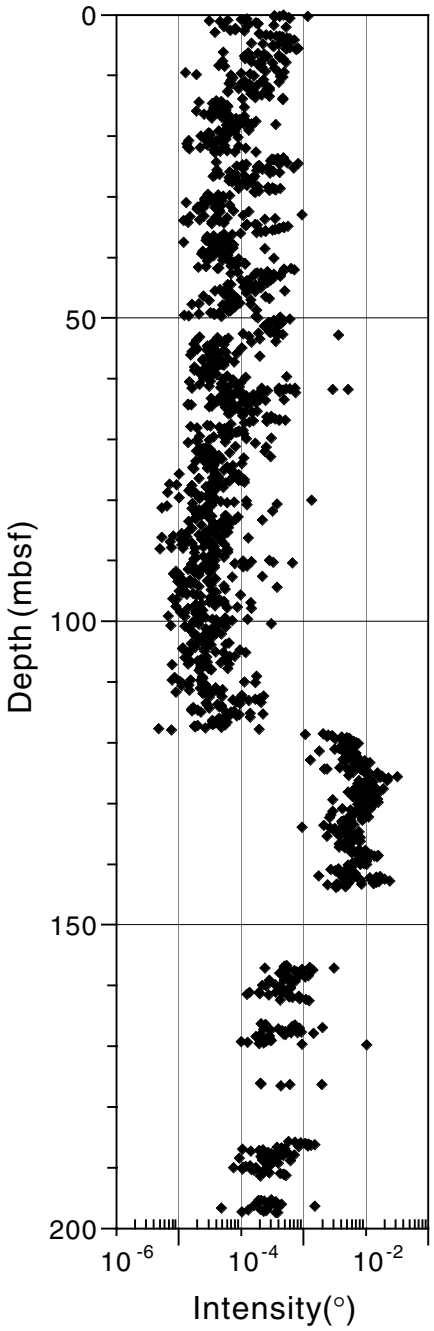

Figure F7. Alternating field demagnetization of Sample 182-1134A-10H-CC showing stable normal magnetization.

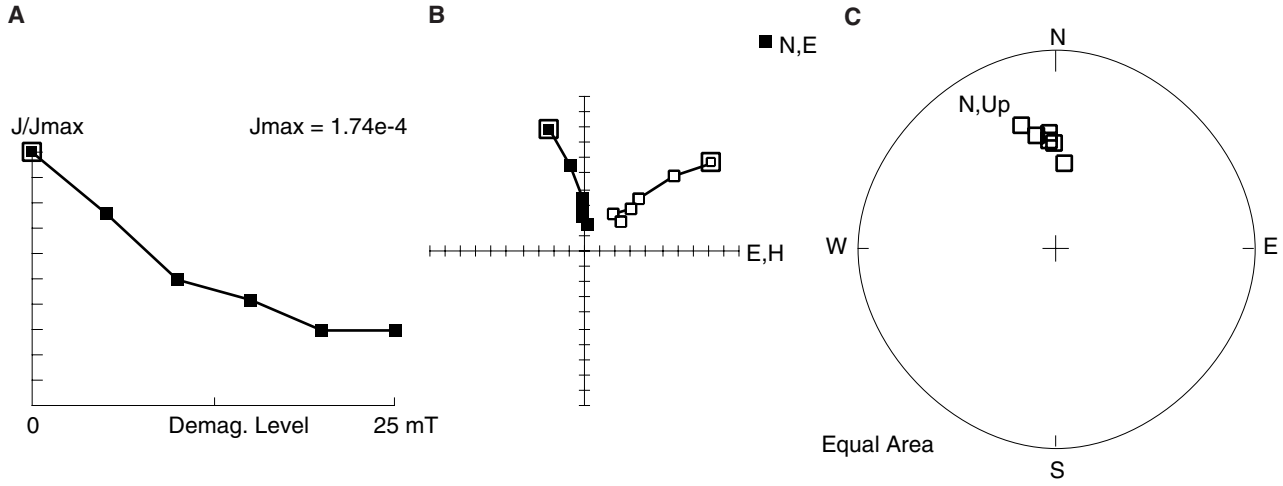

Figure F8. Inclination data and interpreted magnetostratigraphy for Holes 1134A and 1134B. Immediately to the right of the inclination data are two magnetostratigraphic columns. The diagonal pattern indicates intervals of indeterminate polarity. On the extreme right, an interpreted column for Site 1134 is correlated with the geomagnetic polarity time scale (GPTS).

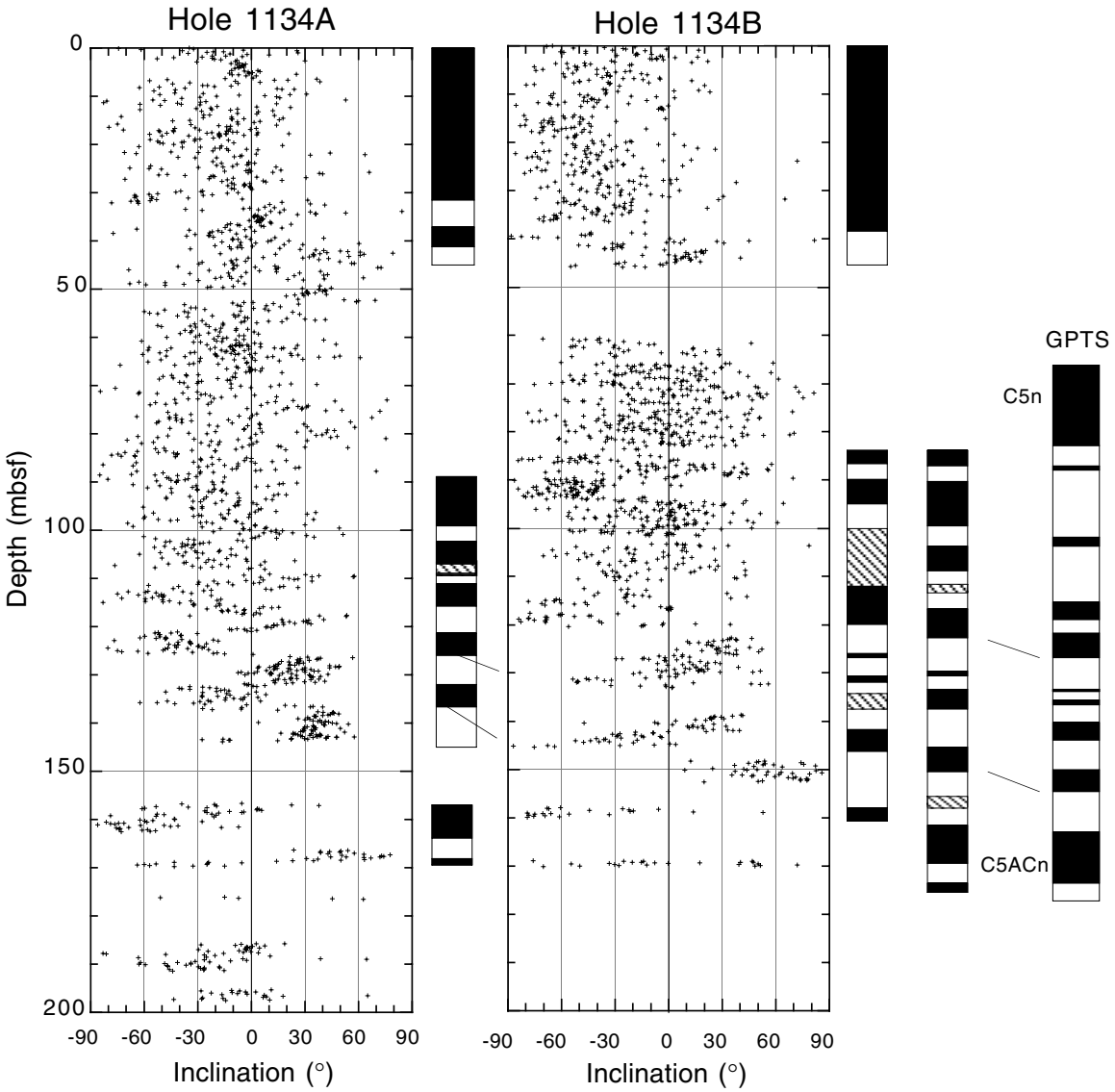

Figure F9. Composite depth section produced using the Splicer software. The black line represents data from Hole 1134A, and the red line represents data from Hole 1134B. Data from Hole 1134B are offset for ease of comparison. All depths use the meters composite depth (mcd) scale. For conversions from mcd to mbsf, see Table T3, p. 62. GRA = gamma-ray attenuation. (Continued on next page.)

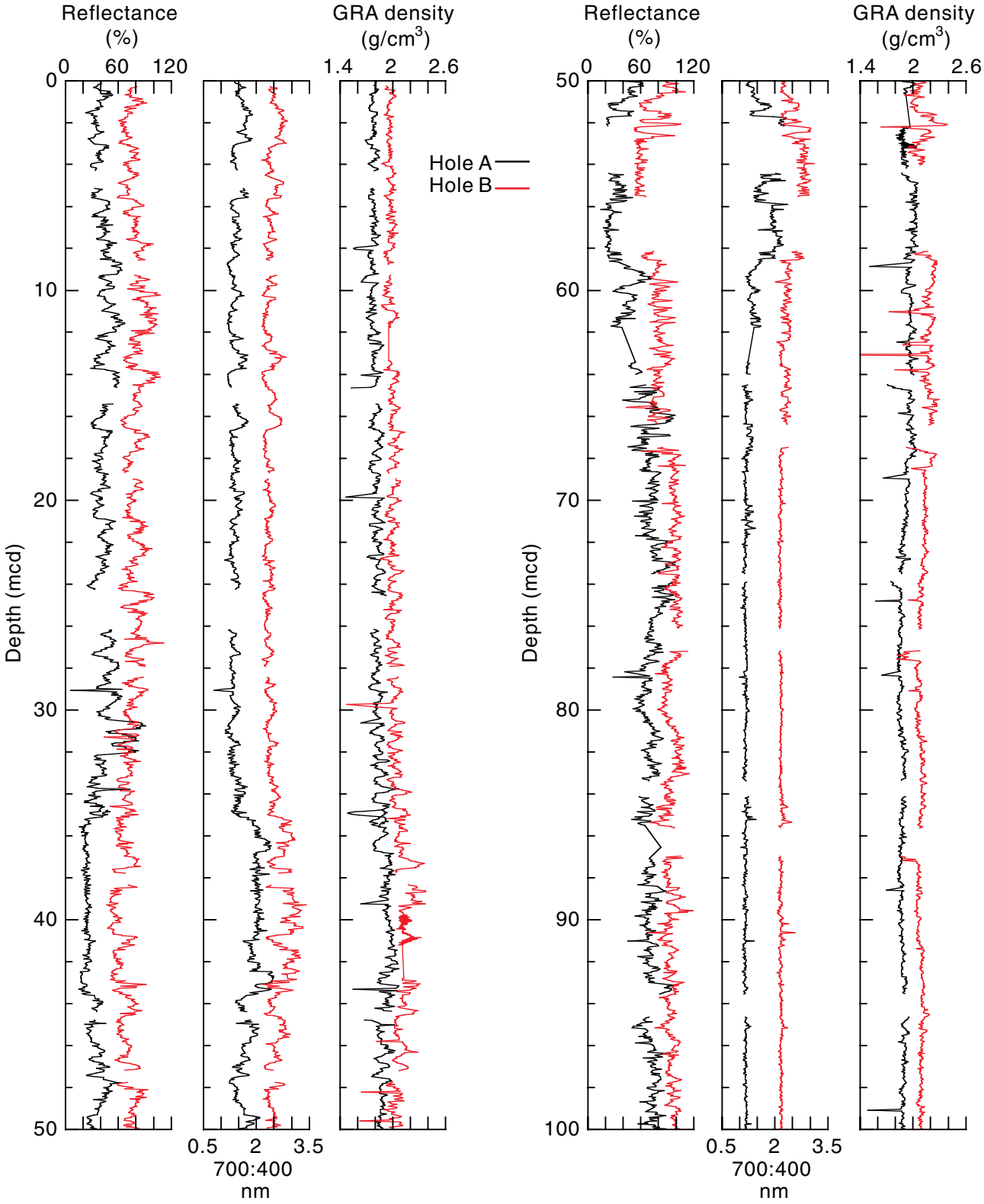

Figure F9 (continued).

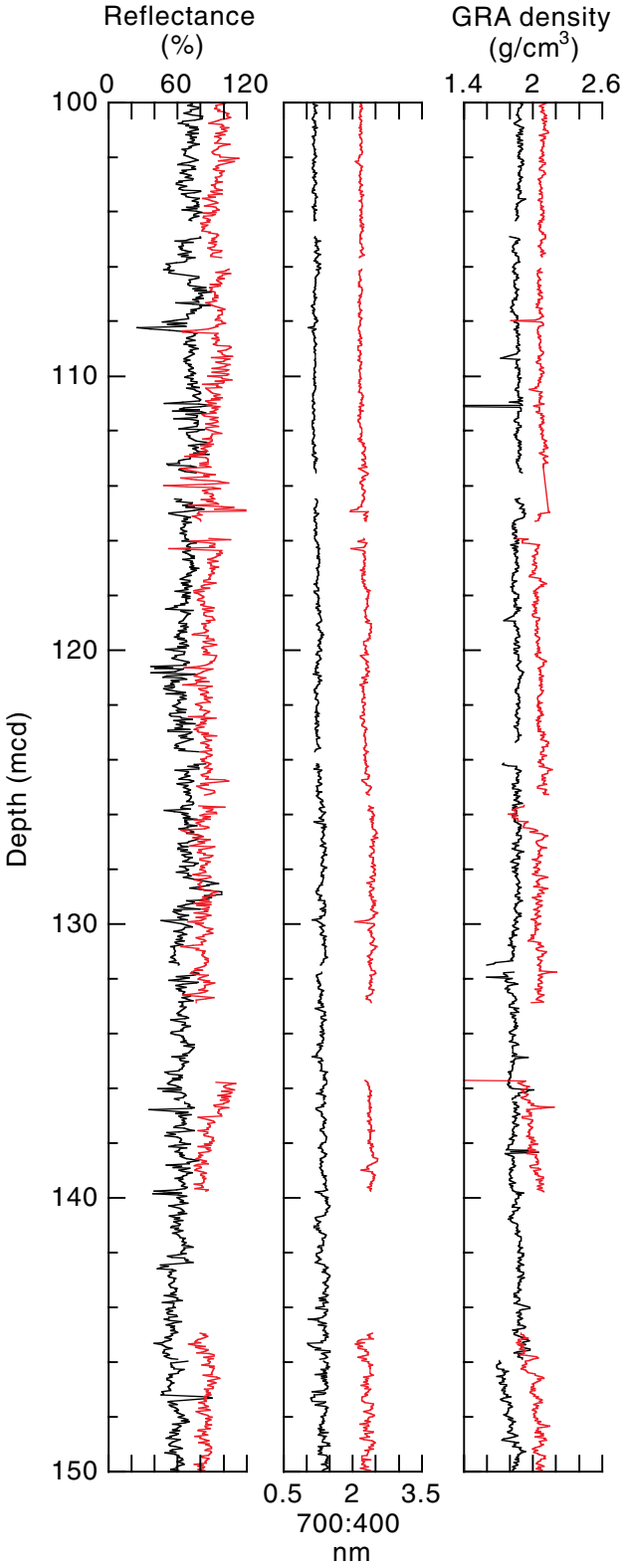

Figure F10. Spliced section of smoothed 400-nm color reflectance data, smoothed color reflectance ratio data (700:400 nm), smoothed gamma-ray attenuation (GRA) density data, and smoothed natural gamma radiation (NGR) data produced using the Splicer software. These data are a spliced composite of correlated data from Holes 1134A and 1134B. Lithostratigraphic units are described in **"Lithostratigraphy,"** p. 3, and ages are derived from biostratigraphic data (see **"Biostratigraphy,"** p. 8).

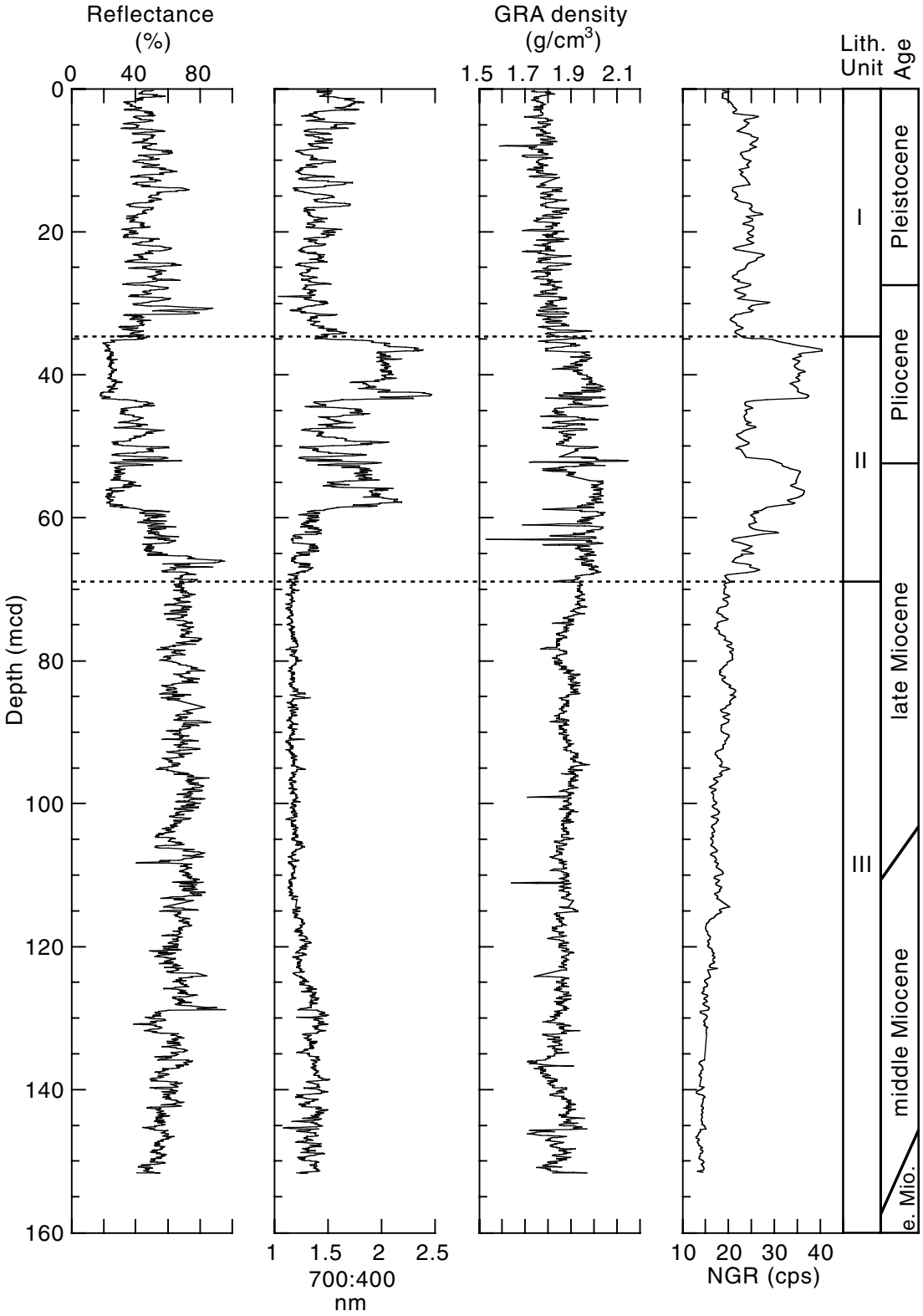

Figure F11. Calcium carbonate content in samples from Hole 1134A.

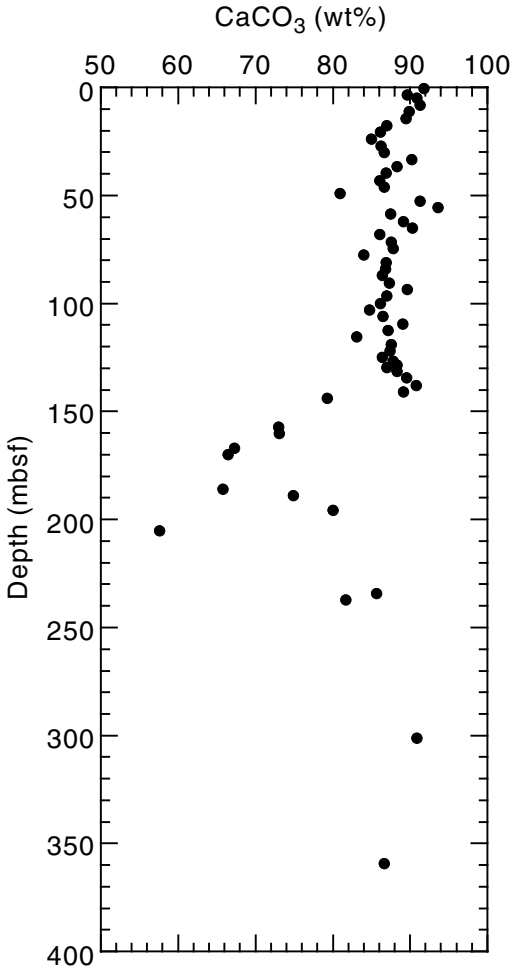

Figure F12. Concentrations from Site 1134 for (**A**) salinity, (**B**) Cl^-, (**C**) Na^+, (**D**) K^+, and (**E**) Na^+/Cl^-. Although the trends of the concentrations in these ions show a diffusive profile, the Na^+/Cl^- value shows a maximum between 90 and 120 mbsf.

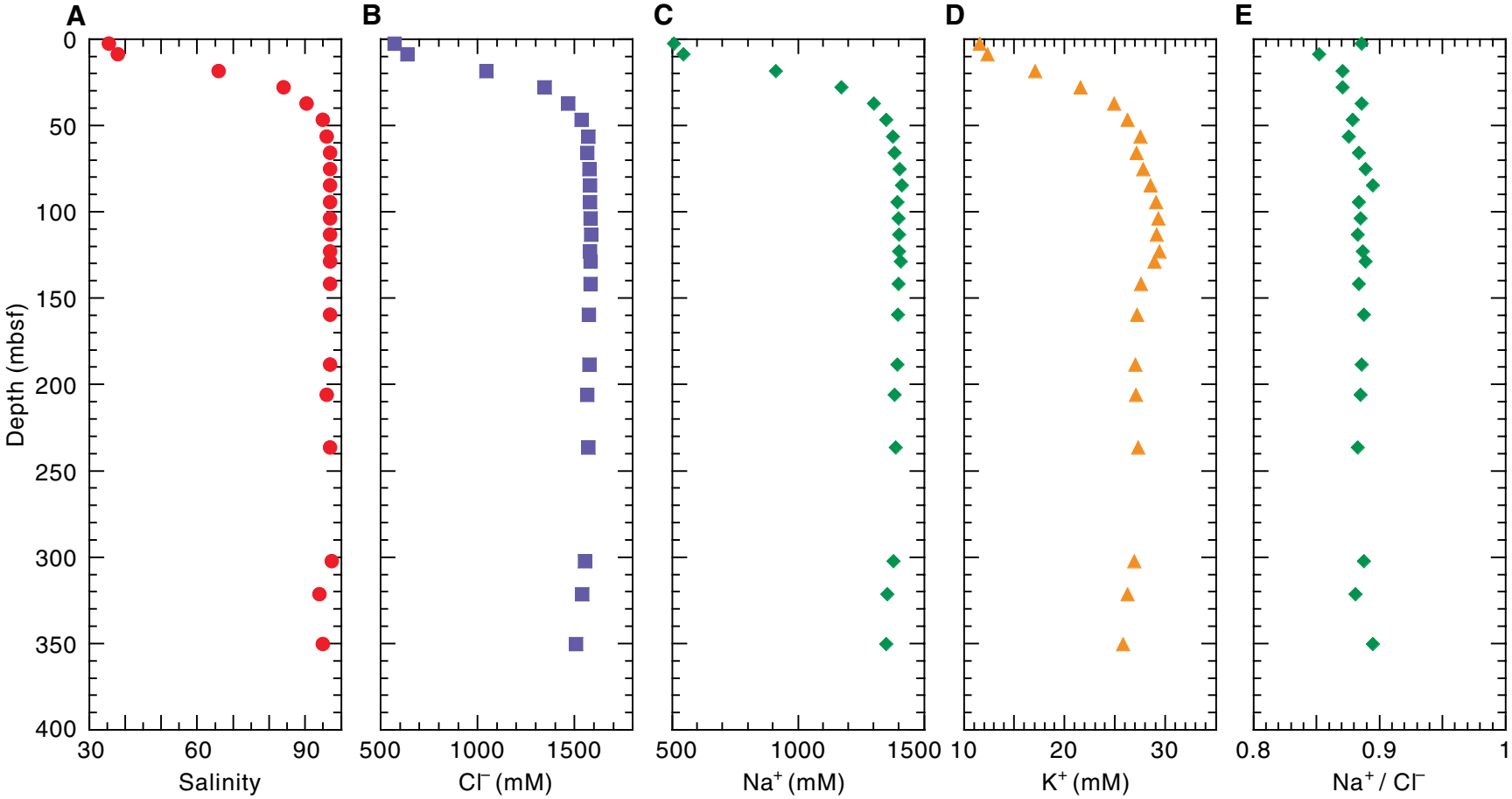

Figure F13. Concentrations of (**A**) Mg^{2+}, (**B**) Ca^{2+}, (**C**) Sr^{2+}, (**D**) Li^{+}, and (**E**) $H_4SiO_4^0$ at Site 1134.

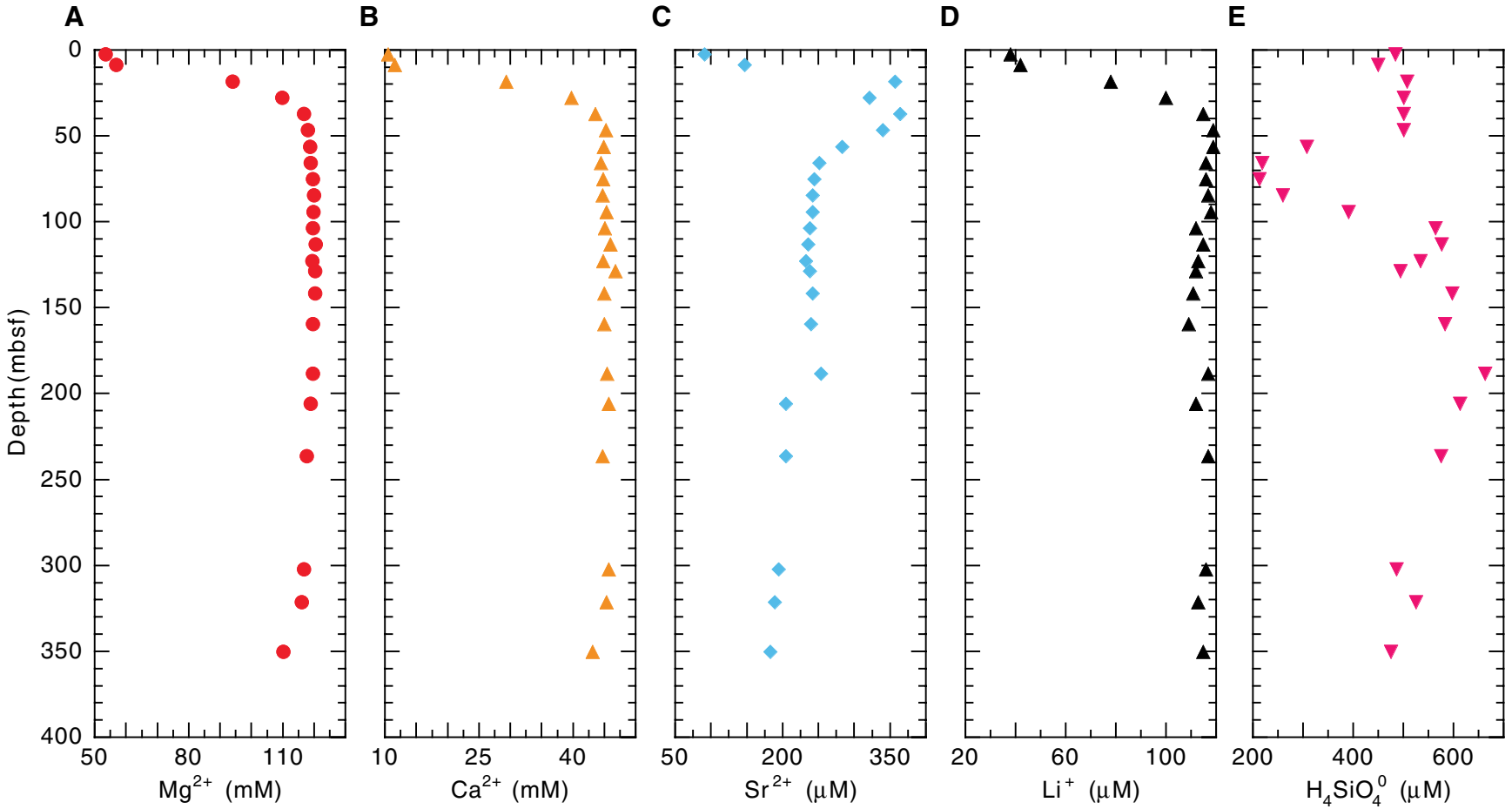

Figure F14. Variations in (**A**) pH, (**B**) alkalinity, (**C**) excess SO_4^{2-}, (**D**) NH_4^+, and (**E**) Fe^{2+} from Site 1134. Open triangles represent pH as measured by the punch-in electrode method.

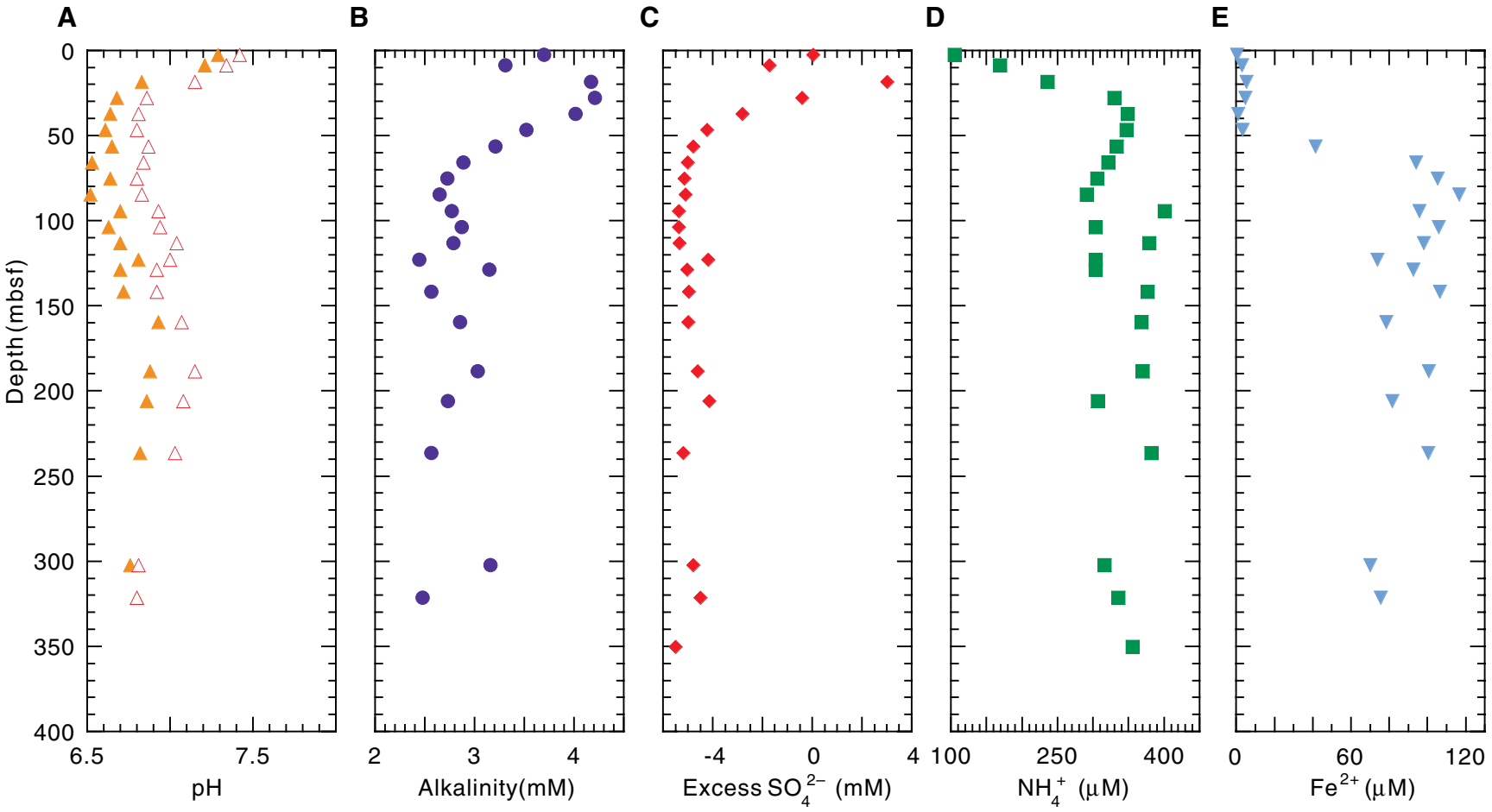

Figure F15. Combined plot of discrete *P*-wave velocity, gamma-ray attenuation bulk density (blue dots) and moisture-and-density (MAD) bulk density (light blue dots), magnetic susceptibility, MAD porosity, and natural gamma radiation (NGR), Site 1134. Physical properties units (PP units) are indicated on the right, and a recovery column is shown on the left.

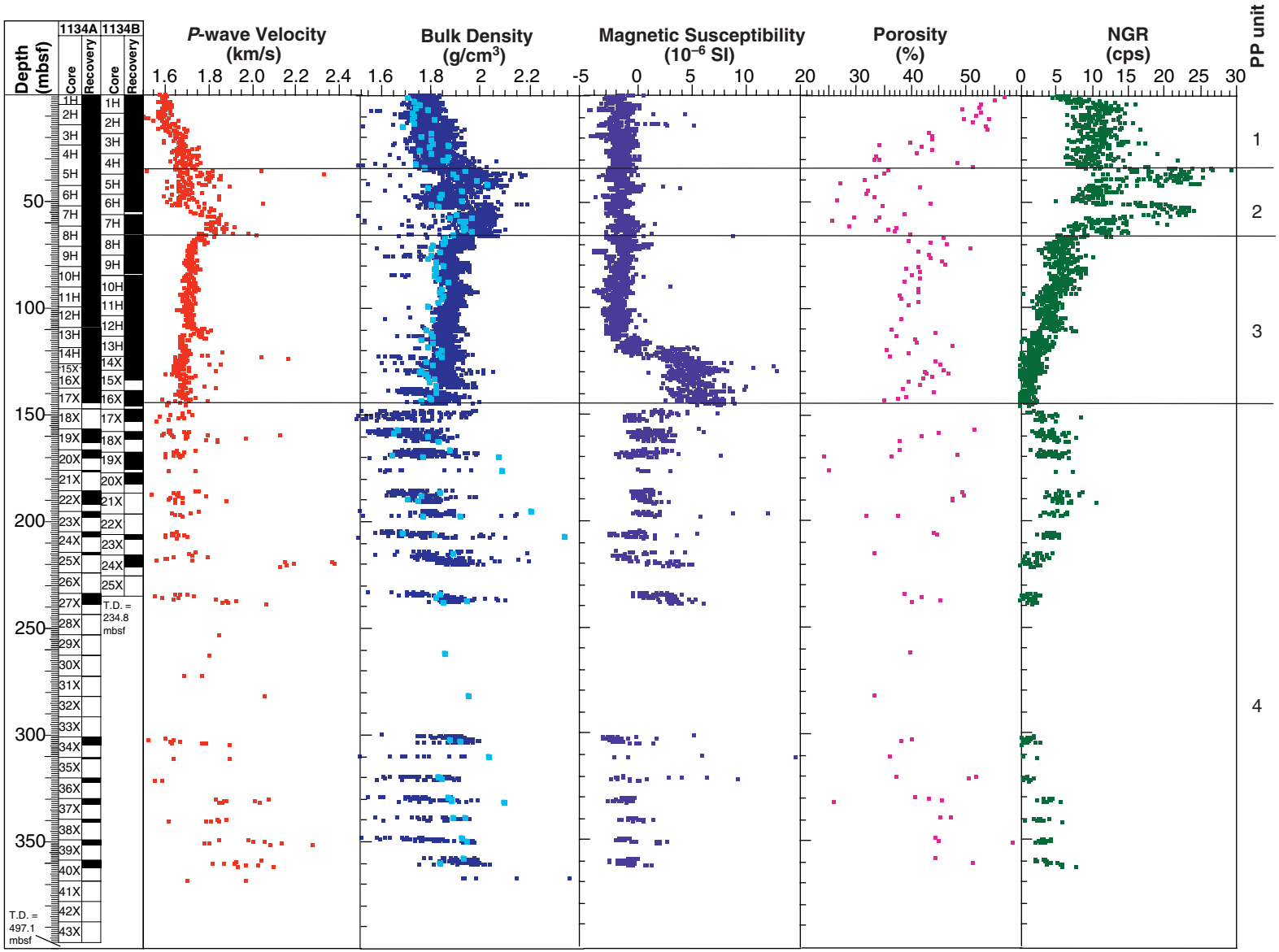

Figure F16. Comparison of downhole logging data and physical properties measurements on recovered sediments from Site 1134. **A.** Natural gamma radiation (NGR) data from the multisensor track (blue dots) and log data (red dots). **B.** Bulk density (g/cm^3) from GRA densiometry (blue dots) and downhole measurements (red dots). **C.** *P*-wave velocity (km/s) from discrete measurements (blue dots) and sonic log (red dots) with physical properties units (PP units).

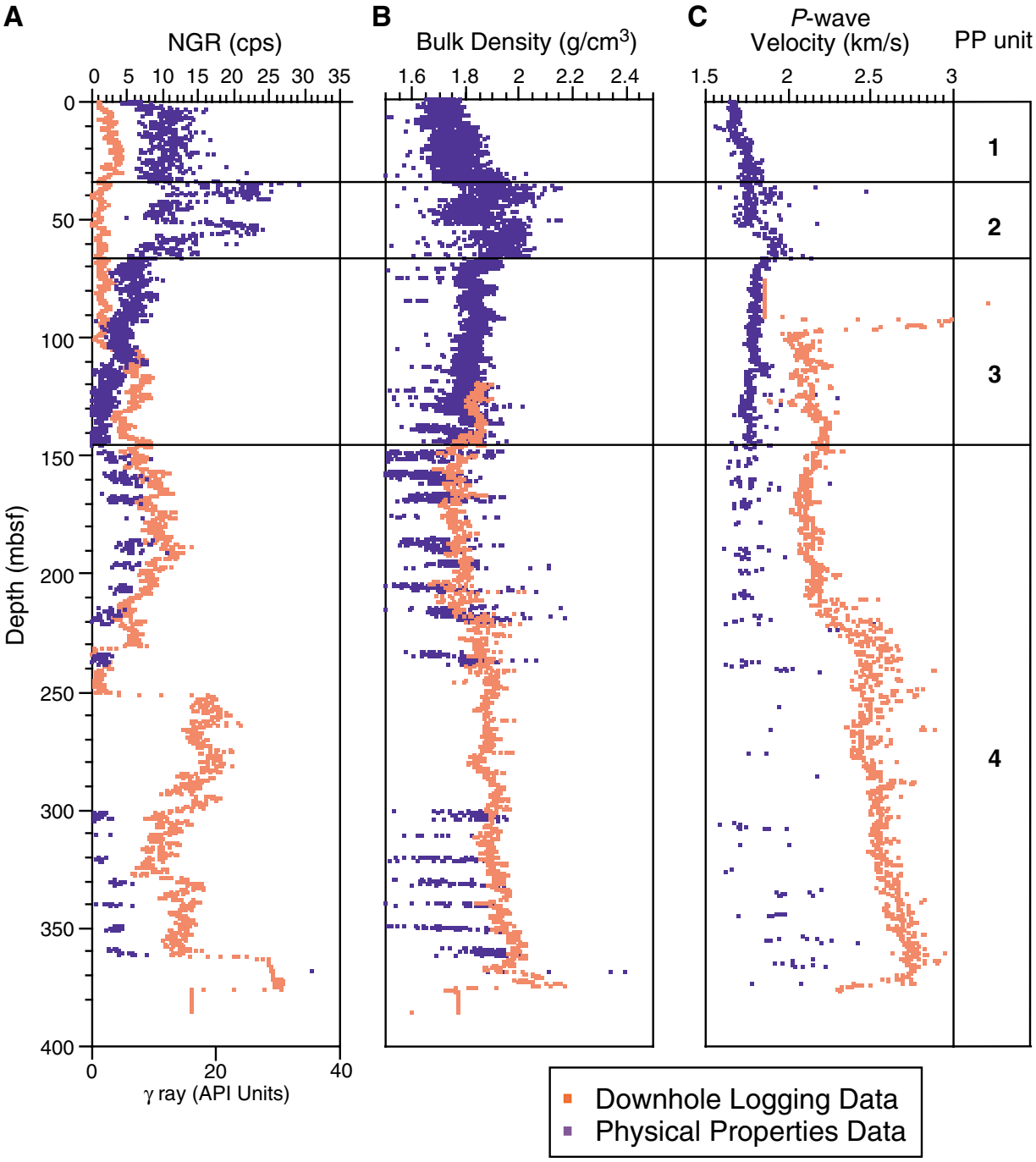

Figure F17. Shear strength measurements from Site 1134. Physical properties units (PP units) are indicated on the right.

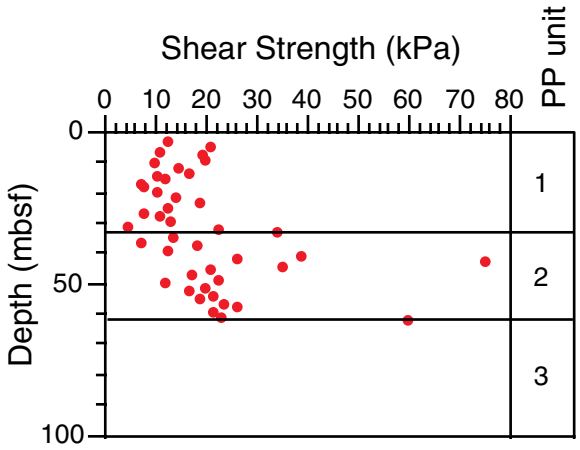

Figure F18. Thermal conductivity (blue dots) and moisture-and-density bulk density (red dots) measurements from Site 1134. Physical properties units (PP units) are indicated on the right.

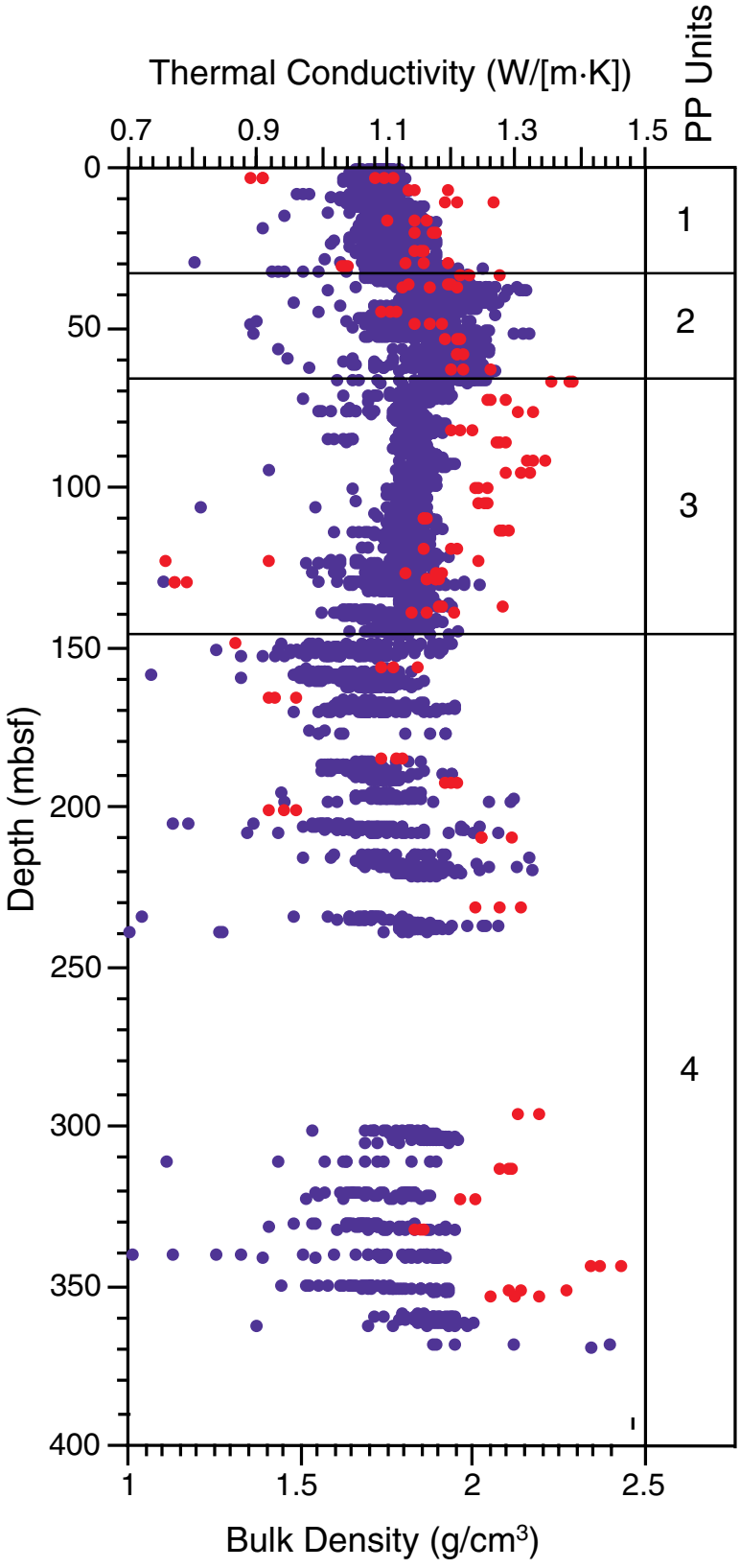

Figure F19. Summary of triple combination logging tool and sonic logs vs. depth for the open-hole logged interval. From left to right, columns are core recovery; total gamma radiation (HSGR) and caliper; porosity and density; photoelectric effect (PEF); shallow, medium, and deep resistivity; sonic velocity; logging units; lithostratigraphic units; and biostratigraphic ages.

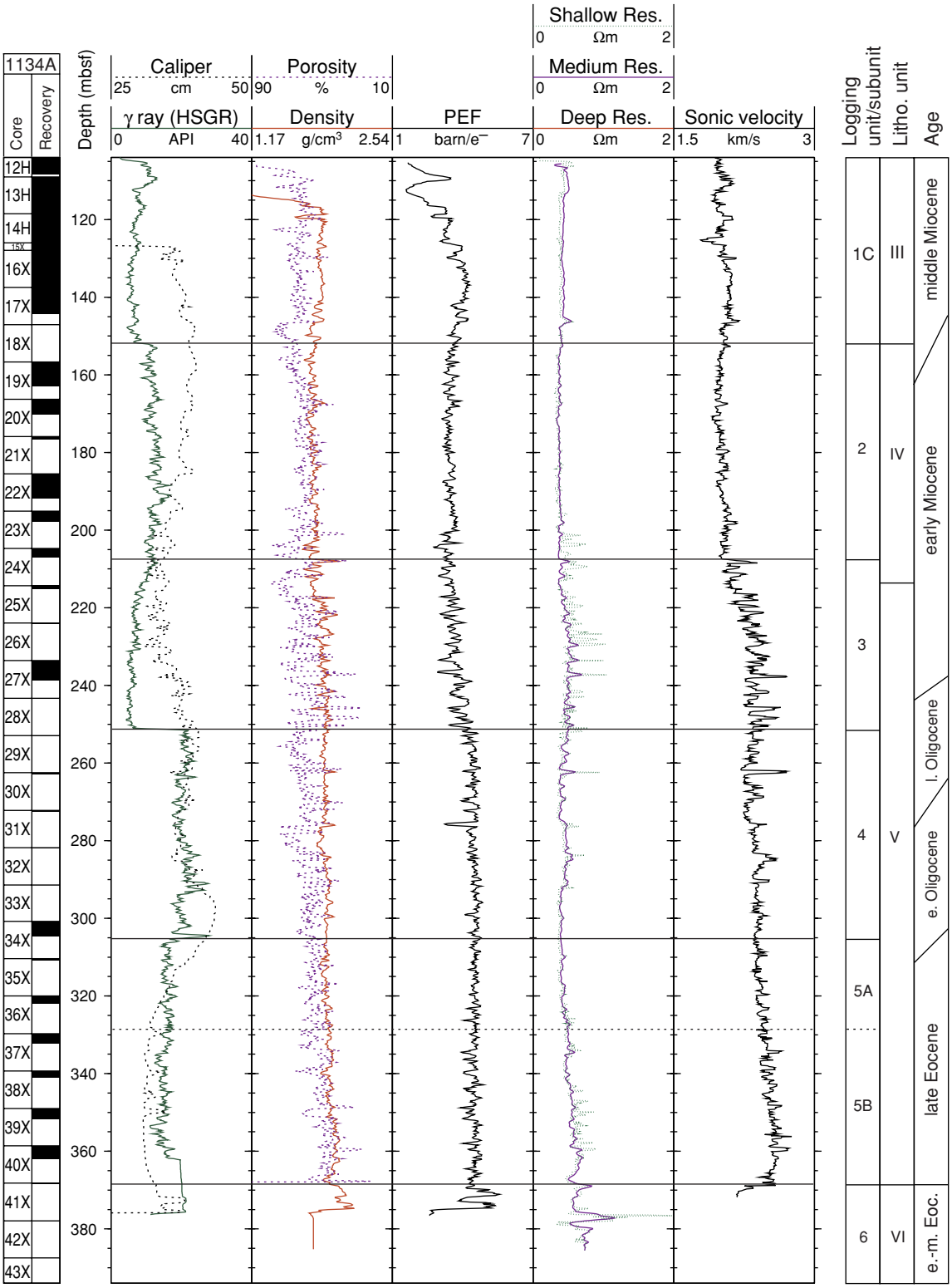

Figure F20. Summary of spectral gamma-ray logs from the hostile environment natural gamma-ray sonde plotted on an expanded depth scale to highlight variations in the interval logged through pipe. From left to right, columns are core recovery, total gamma radiation (HSGR) and computed (uranium-free) gamma radiation (HCGR), uranium, thorium, potassium, logging units, lithostratigraphic units, and biostratigraphic ages.

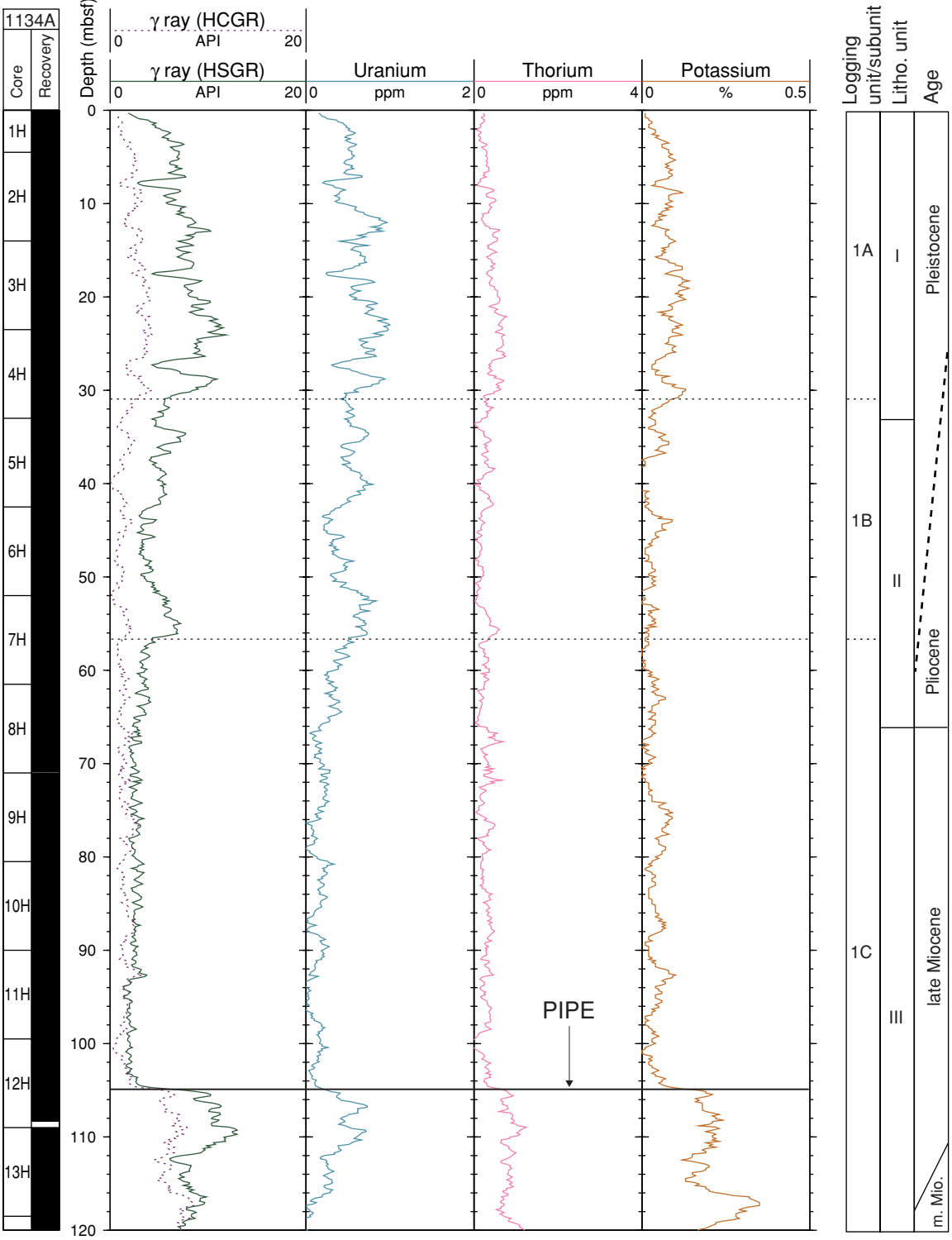

Figure F21. Summary of spectral gamma-ray logs from the hostile environment natural gamma-ray sonde, plotted vs. depth for the open-hole logged interval. From left to right, columns are core recovery, total gamma radiation (HSGR) and computed (uranium-free) gamma radiation (HCGR), uranium, thorium, potassium and caliper, logging units, lithostratigraphic units, and biostratigraphic ages.

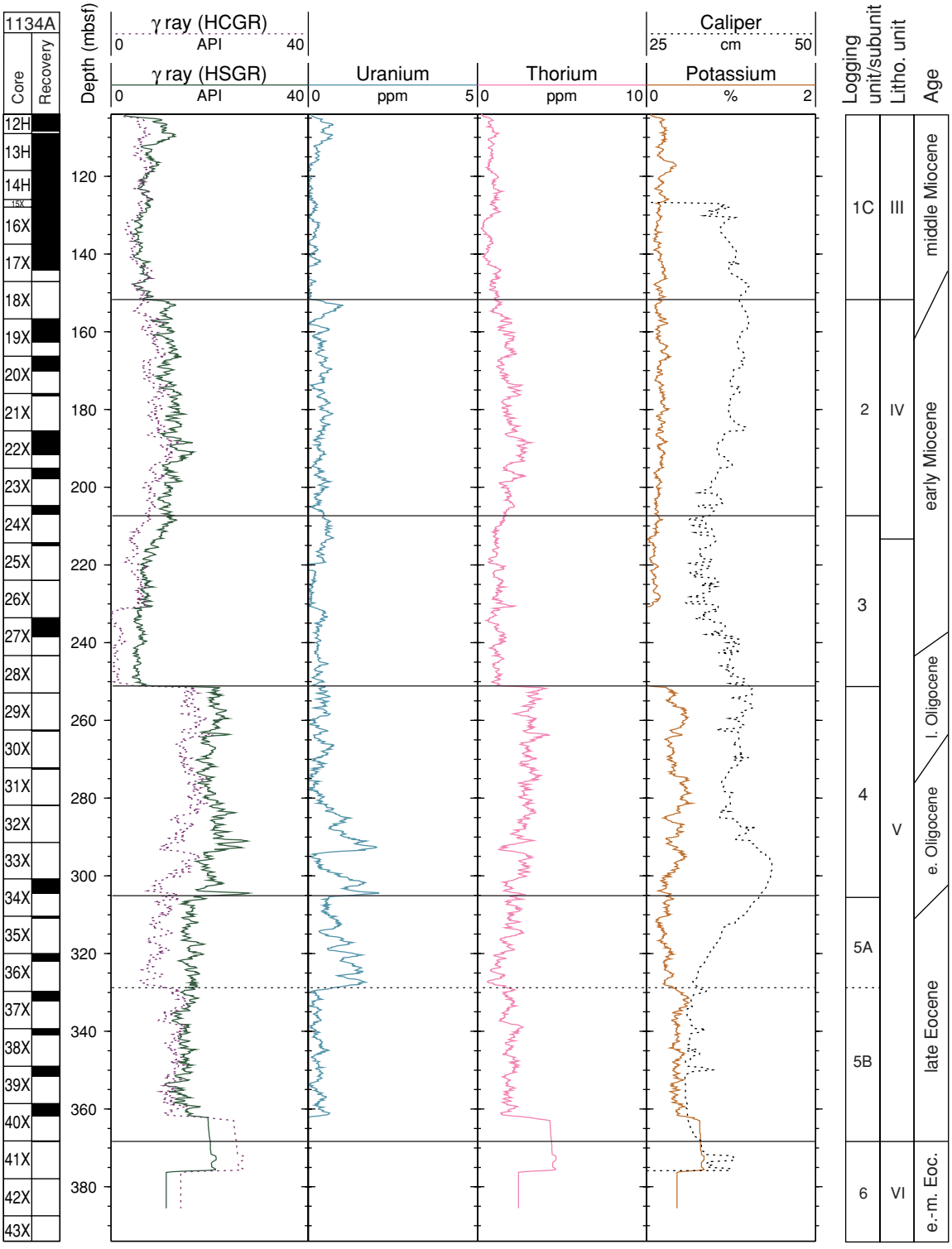

Figure F22. Map showing seismic site-survey tracks for Site 1134 (Line AGSO169/01) in relation to other Leg 182 sites and the AGSO169 site-survey seismic lines. The bold trackline (AGSO169/01e) corresponds to the seismic line segment shown in Figure F23, p. 55.

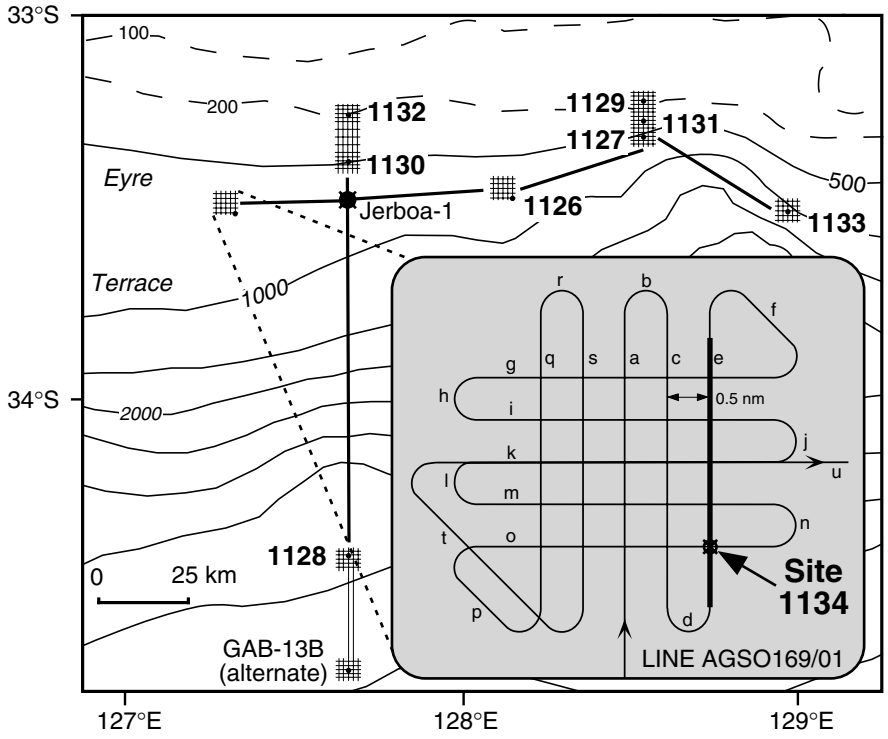

Figure F23. Portion of seismic Line AGSO169/01e showing predrill interpreted seismic stratigraphic sequences planned (shown in white) and actually intersected (shown in black) at Site 1134.

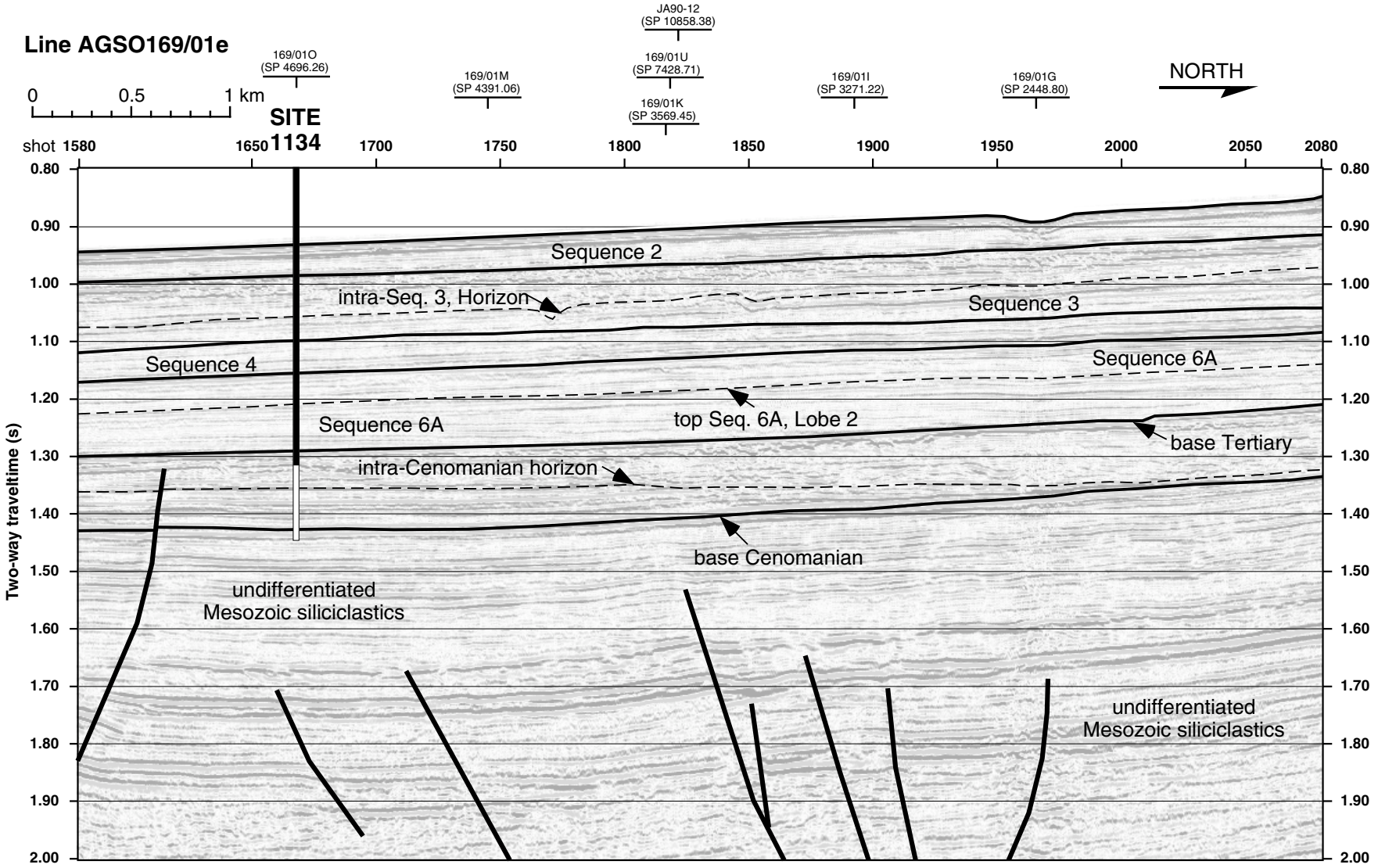

Figure F24. Check-shot stations and acquisition geometry for the well seismic tool (WST) survey at Hole 1134A, with corrected two-way traveltimes (TWT) and derived interval velocities. GI = generator-injector.

Depth (mbrf)	Depth (mbsl)	Transit time (ms)	True path length (m)	Corrected TWT (ms)	Interval velocity (ms)
852.0	840.0	539.23	840.7	1080.60	2032.06
882.1	870.1	554	870.8	1110.22	1917.64
912.0	900.0	569.56	900.7	1141.41	2192.55
972.0	960.0	596.85	960.7	1196.14	2383.44
1012.1	1000.1	613.64	1000.8	1229.79	2333.54
1062.1	1050.1	635.02	1050.8	1272.64	2476.65
1095.0	1083.0	648.27	1083.7	1299.21	

Corrected TWT is TWT from sea level to WST tool along a vertical path

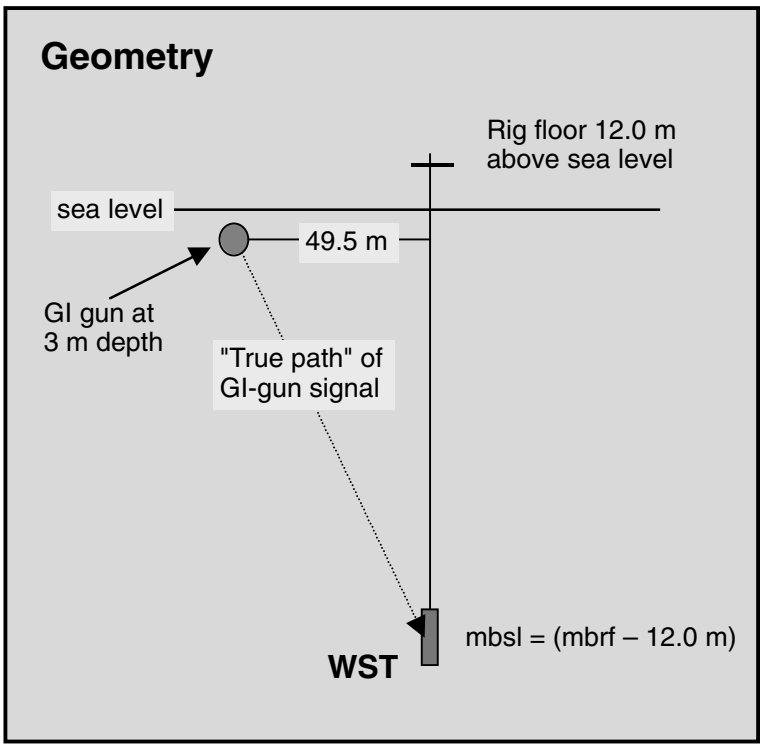

Figure F25. A. Plot showing relationship between predicted depths to key horizons and sequence boundaries (dashed) and corrected depths (arrowed). Corrected depths are based on the check-shot survey data (heavy line), shown plotted at the lower limit of the envelope of stacking velocities (derived from six common depth points from site-survey seismic data adjacent to this site). The integrated sonic log, based on interval transit-time data, is plotted as a heavy dashed line. **B.** Interval velocities derived from the seven check-shot stations shown overlying the velocity log (derived from the compressional sonic trace).

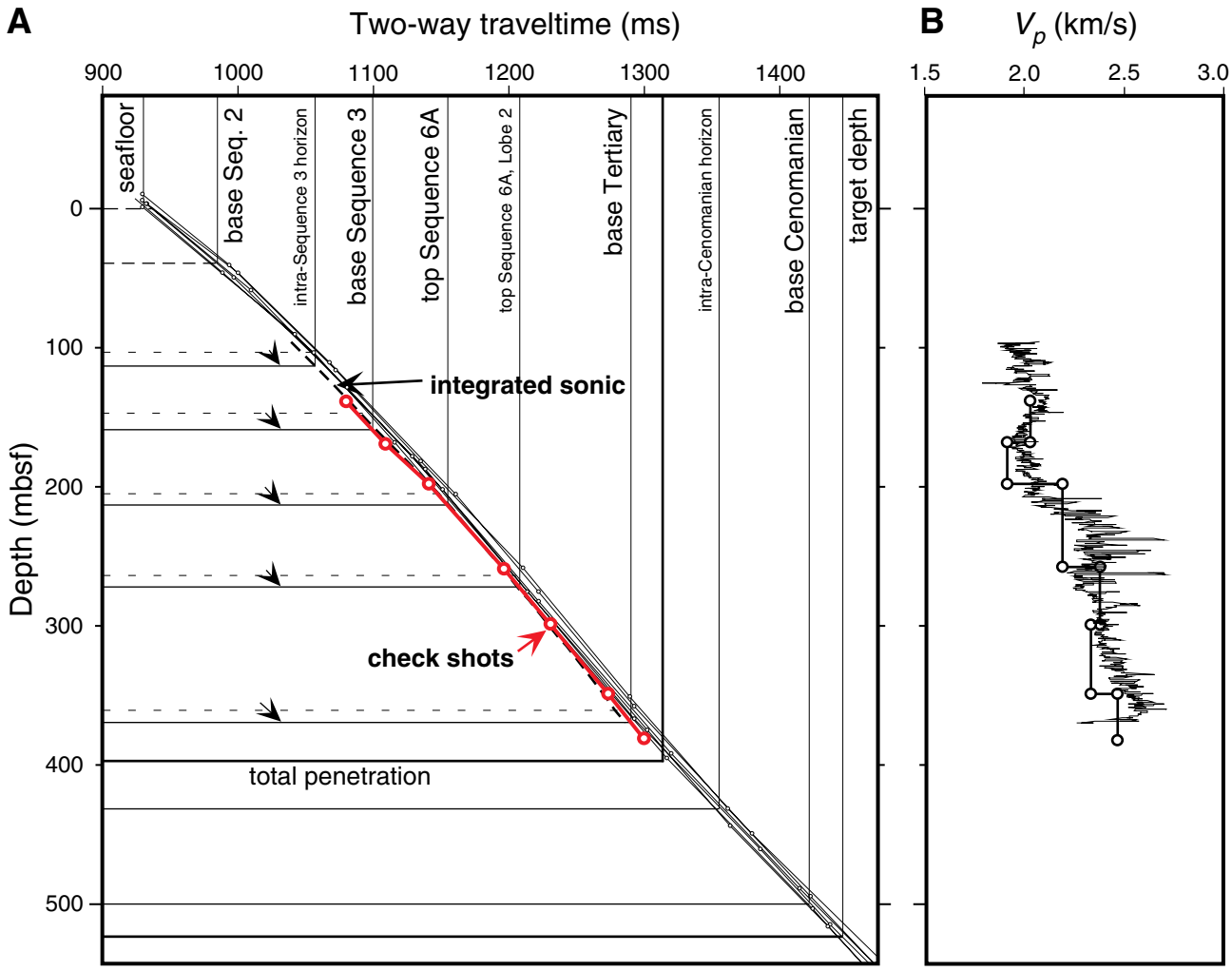

Figure F26. Tentative summary correlation between lithostratigraphic units, seismic sequences, biostratigraphic hiatuses, and ages at Site 1134. Note that the middle Eocene unit at the base of the succession was expected to be of Mesozoic age, based on predrill seismic stratigraphic correlations. This unit (lithostratigraphic Unit VI) is now interpreted as a previously unrecognized portion of the Cenozoic siliciclastic Sequence 7, overlying the basal Cenozoic unconformity. ? = seismic data shows missing section corresponding to these surfaces, although biostratigraphic data provide no constraint on the length of missing time.

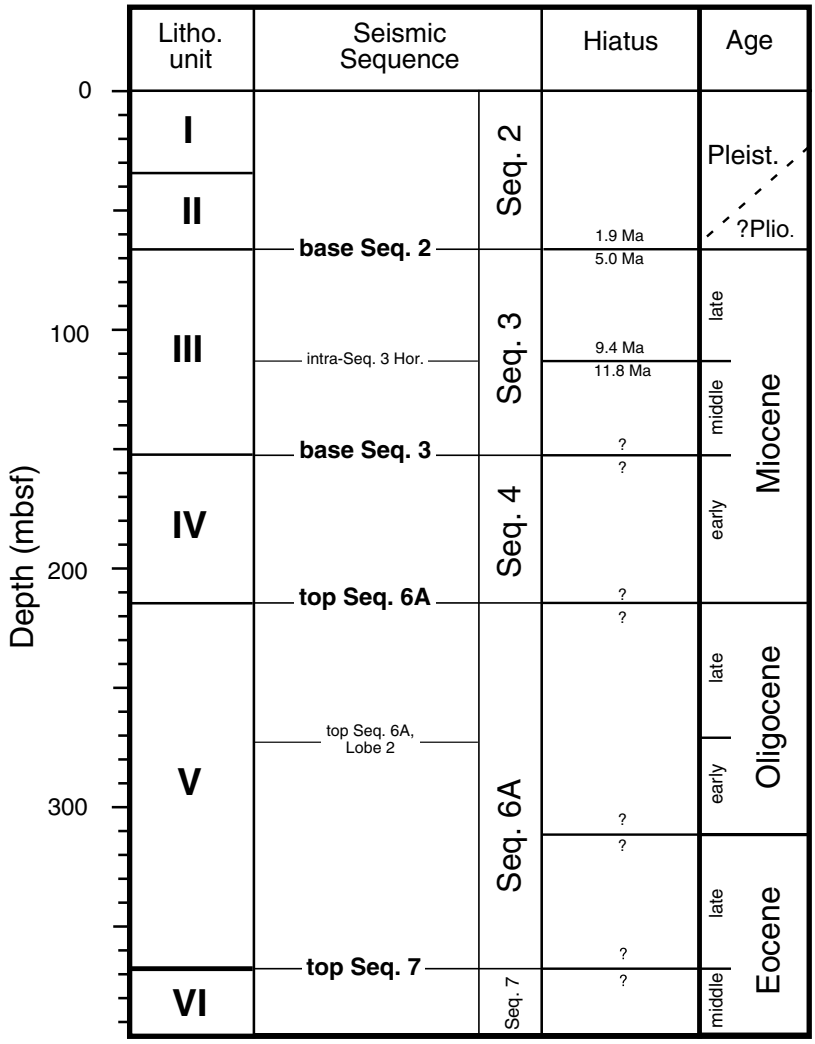

Table T1. Site 1134 coring summary. (See table note. Continued on next page.)

Hole 1134A

Latitude: –33.528740° (33°31.7244′S)
Longitude: 127.264000° (127°15.8400′E)
Seafloor (drill-pipe measurement from rig floor, mbrf): 713.0
Distance between rig floor and sea level (m): 12.0
Water depth (drill-pipe measurement from sea level, m): 701.0
Total depth (from rig floor, mbrf): 1110.1
Penetration (mbsf): 397.1
Total number of cores: 43
Total length of cored section (m): 397.1
Total core recovered (m): 195.54
Core recovery (%): 49.2

Hole 1134B

Latitude: –33.528980° (33°31.7388′S)
Longitude: 127.263960° (127°15.8376′E)
Seafloor (drill-pipe measurement from rig floor, mbrf): 711.9
Distance between rig floor and sea level (m): 12.0
Water depth (drill-pipe measurement from sea level, m): 699.9
Total depth (from rig floor, mbrf): 946.7
Penetration (mbsf): 234.8
Total number of cores: 25
Total length of cored section (m): 234.8
Total core recovered (m): 158.76
Core recovery (%): 67.6

Core	Date (Nov 1998)	Time (UTC + 8 hr)	Depth (mbsf)	Length cored (m)	Length recovered (m)	Recovery (%)	Comment
182-1134A-							
1H	1	0850	0.00-4.50	4.5	4.50	100.0	
2H	1	0925	4.50-14.00	9.5	9.74	102.5	
3H	1	1000	14.00-23.50	9.5	9.44	99.4	Oriented; nonmagnetic shoe
4H	1	1115	23.50-33.00	9.5	9.65	101.6	Oriented; Adara
5H	1	1155	33.00-42.50	9.5	9.91	104.3	Oriented; nonmagnetic shoe
6H	1	1225	42.50-52.00	9.5	9.55	100.5	Oriented
7H	1	1255	52.00-61.50	9.5	9.92	104.4	Oriented; nonmagnetic shoe
8H	1	1330	61.50-71.00	9.5	9.37	98.6	Oriented
9H	1	1400	71.00-80.50	9.5	9.77	102.8	Oriented; nonmagnetic shoe
10H	1	1430	80.50-90.00	9.5	9.72	102.3	Oriented
11H	1	1505	90.00-99.50	9.5	9.99	105.2	Oriented; nonmagnetic shoe
12H	1	1550	99.50-109.00	9.5	8.88	93.5	Oriented
13H	1	1625	109.00-118.50	9.5	9.58	100.8	Oriented; nonmagnetic shoe
14H	1	1700	118.50-126.00	7.5	7.67	102.3	Oriented
15X	1	1810	126.00-127.90	1.9	4.97	261.6	
16X	1	1840	127.90-137.50	9.6	9.84	102.5	
17X	1	1910	137.50-147.10	9.6	6.70	69.8	
18X	1	1945	147.10-156.70	9.6	0.03	0.3	
19X	1	2010	156.70-166.30	9.6	6.17	64.3	
20X	1	2100	166.30-175.90	9.6	3.86	40.2	
21X	1	2130	175.90-185.50	9.6	0.71	7.4	
22X	1	2200	185.50-195.10	9.6	6.30	65.6	
23X	1	2245	195.10-204.70	9.6	2.76	28.8	
24X	1	2325	204.70-214.30	9.6	2.25	23.4	
25X	2	0030	214.30-223.90	9.6	0.92	9.6	
26X	2	0120	223.90-233.60	9.7	0.18	1.9	
27X	2	0210	233.60-243.30	9.7	5.07	52.3	
28X	2	0315	243.30-252.90	9.6	0.14	1.5	
29X	2	0420	252.90-262.50	9.6	0.21	2.2	
30X	2	0515	262.50-272.20	9.7	0.25	2.6	
31X	2	0600	272.20-281.80	9.6	0.40	4.2	
32X	2	0655	281.80-291.40	9.6	0.19	2.0	
33X	2	0745	291.40-300.80	9.4	0.02	0.2	
34X	2	0855	300.80-310.40	9.6	3.74	39.0	
35X	2	0950	310.40-320.00	9.6	0.55	5.7	
36X	2	1105	320.00-329.70	9.7	2.12	21.9	
37X	2	1225	329.70-339.30	9.6	2.49	25.9	
38X	2	1340	339.30-349.00	9.7	1.67	17.2	
39X	2	1440	349.00-358.60	9.6	2.67	27.8	
40X	2	1545	358.60-368.20	9.6	3.34	34.8	

Table T1 (continued).

Core	Date (Nov 1998)	Time (UTC + 8 hr)	Depth (mbsf)	Length cored (m)	Length recovered (m)	Recovery (%)	Comment
41X	2	1615	368.20-377.90	9.7	0.30	3.1	
42X	2	1700	377.90-387.50	9.6	0.00	0.0	No recovery
43X	2	1755	387.50-397.10	9.6	0.00	0.0	No recovery
Totals:				397.1	195.54	49.2	
182-1134B-							
1H	3	1500	0.00-8.60	8.6	8.60	100.0	
2H	3	1540	8.60-18.10	9.5	9.69	102.0	
3H	3	1615	18.10-27.60	9.5	9.19	96.7	Oriented; nonmagnetic barrel
4H	3	1645	27.60-37.10	9.5	9.75	102.6	Oriented
5H	3	1720	37.10-46.60	9.5	9.54	100.4	Oriented; nonmagnetic barrel; some material from bottom lost
6H	3	1800	46.60-56.10	9.5	8.14	85.7	Crushed liner; highly disturbed
7H	3	1835	56.10-65.60	9.5	8.93	94.0	Oriented; nonmagnetic barrel; core stuck in core barrel; cut into sections on drill floor; highly disturbed
8H	3	1910	65.60-75.10	9.5	9.02	95.0	Oriented
9H	3	1950	75.10-84.60	9.5	8.76	92.2	Oriented; nonmagnetic barrel
10H	3	2025	84.60-94.10	9.5	9.77	102.8	Oriented
11H	3	2100	94.10-103.60	9.5	9.74	102.5	Oriented; nonmagnetic barrel
12H	3	2140	103.60-113.10	9.5	9.53	100.3	Oriented
13H	3	2205	113.10-122.60	9.5	9.82	103.4	Oriented; nonmagnetic barrel
14X	3	2315	122.60-129.00	6.4	7.57	118.3	
15X	4	0005	129.00-138.60	9.6	4.51	47.0	
16X	4	0040	138.60-148.20	9.6	7.14	74.4	
17X	4	0115	148.20-157.80	9.6	5.06	52.7	
18X	4	0145	157.80-167.40	9.6	2.44	25.4	
19X	4	0245	167.40-177.10	9.7	2.96	30.5	
20X	4	0300	177.10-186.70	9.6	0.33	3.4	
21X	4	0340	186.70-196.30	9.6	0.00	0.0	No recovery
22X	4	0415	196.30-206.00	9.7	0.17	1.8	
23X	4	0500	206.00-215.60	9.6	2.16	22.5	
24X	4	0545	215.60-225.20	9.6	5.76	60.0	
25X	4	0630	225.20-234.80	9.6	0.18	1.9	
Totals:				234.8	158.76	67.6	

Note: UTC = Universal Time Coordinated, Adara = Adara temperature tool.

Table T2. Datum levels used for the calculation of Site 1134 sedimentation rates.

Datum type	Datum level	Age (Ma)	Midpoint (mbsf)	Stratigraphic error (m)	Fossil group	Datum code	Upper sample: Core, section, interval (cm)	Upper sample: Depth (mbsf)	Lower sample: Core, section, interval (cm)	Lower sample: Depth (mbsf)
							182-1134A-		182-1134A-	
T	*P. lacunosa*	0.45	9.37	4.87	1	1	1H-CC, 13-16	4.47	2H-CC, 8-11	14.21
T	*G. tosaensis*	0.65	18.84	4.60	4	2	2H-CC, 8-11	14.21	3H-CC, 15-18	23.41
B	*G. truncatulinoides*	2	28.27	4.86	4	3	3H-CC, 15-18	23.41	4H-CC, 21-24	33.12
T	*C. macintyrei*	1.67	28.30	4.86	1	4	3H-CC, 15-18	23.41	4H-CC, 21-24	33.12
T	*T. rugosus*	5.23	56.99	4.94	1	5	6H-CC, 0-4	52.01	7H-4, 55-57	57.05
T	*G. margaritae*	3.58	61.00	0.93	4	6	7H-6, 55-57	60.05	7H-CC, 13-16	61.89
B	*G. puncticulata*	4.5	66.36	4.47	4	7	7H-CC, 13-16	61.89	8H-CC, 19-23	70.83
T	*G. cibaoensis*	4.6	61.00	0.93	4	8	7H-6, 55-57	60.05	7H-CC, 13-16	61.89
T	*A. tricorniculatus*	4	66.40	4.48	1	9	7H-CC, 13-16	61.89	8H-CC, 19-23	70.83
B	*G. crassaformis*	4.5	75.78	4.95	4	10	8H-CC, 19-23	70.83	9H-CC, 14-18	80.73
T	*Z. nepenthes*	4.2	75.82	4.95	4	11	8H-CC, 19-23	70.83	9H-CC, 14-18	80.73
B	*G. margaritae*	6.4	104.16	4.20	4	12	11H-CC, 16-19	99.96	12H-CC, 11-14	108.35
B	*G. cibaoensis*	7.8	111.17	2.82	4	13	12H-CC, 11-14	108.35	13H-4, 49-54	113.99
B	*G. plesiotumida*	8.3	111.17	2.82	4	14	12H-CC, 11-14	108.35	13H-4, 49-54	113.99
B	*Z. nepenthes*	11.8	111.17	2.82	4	15	12H-CC, 11-14	108.35	13H-4, 49-54	113.99
B	*M. convallis*	9.5	113.45	5.10	1	16	13H-4, 49-54	113.99	13H-CC, 10-13	118.54
B	C5An	12.401	119.80							
T	*S. heteromorphus*	13.6	140.97	3.23	1	17	16X-CC, 30-33	137.71	17X-CC, 31-34	144.17
B	C5ABn	13.51	145.40							
B	*O. suturalis*	15.1	145.64	1.47	4	18	17X-CC, 31-34	144.17	18X-CC, 0-3	147.10
B	*S. heteromorphus*	18.2	154.97	7.87	1	19	18X-CC, 0-3	147.10	19X-CC, 29-32	162.84
B	*G. dehiscens*	23.2	231.35	7.29	4	20	26X-CC, 15-18	224.05	27X-CC, 34-37	238.64
T	*S. capricornutus*	23.7	231.38	7.29	1	21	26X-CC, 15-18	224.05	27X-CC, 34-37	238.64
T	*D. bisectus*	23.9	231.38	7.29	1	22	26X-CC, 15-18	224.05	27X-CC, 34-37	238.64
T	*C. cubensis*	28.5	257.90	4.82	4	23	29X-CC, 18-21	253.08	30X-CC, 22-25	262.72
T	*I. recurvus*	31.8	277.28	4.72	1	24	31X-CC, 0-4	272.56	32X-CC, 16-19	281.96
T	*C. formosus*	32.8	286.71	4.72	1	25	32X-CC, 16-19	281.96	33X-CC, 0-2	291.40
B	*I. recurvus*	36	327.13	5.04	1	26	36X-CC, 29-32	322.09	37X-CC, 32-35	332.16
B	*C. oamaruensis*	37	365.16	3.24	1	27	40X-CC, 31-34	361.91	41X-CC, 20-22	368.40
T	*C. solitus*	40.4	365.18	3.24	1	28	40X-CC, 31-34	361.91	41X-CC, 20-22	368.40

Notes: T = top of taxon stratigraphic range, B = bottom of taxon stratigraphic range. Midpoint = the middle depth between the sample where the taxon occurs and the adjacent sample where it does not occur. Stratigraphic error = one-half the distance between the sample where the taxon occurs and the adjacent sample where it does not occur. Datum code = the number assigned to the datum level on Figure F5, p. 36. Fossil groups: 1 = calcareous nannofossils, 4 = planktonic foraminifers.

Table T3. Core and section depths in mcd and mbsf, Site 1134. (**See table notes.** Continued on next three pages.)

Leg	Site	Hole	Core	Type	Section	Depth (mbsf)	Offset	Depth (mcd)
182	1134	A	1	H	1	0.00	0.00	0.00
182	1134	A	1	H	2	1.50	0.00	1.50
182	1134	A	1	H	3	3.00	0.00	3.00
182	1134	A	2	H	1	4.50	0.58	5.08
182	1134	A	2	H	2	6.00	0.58	6.58
182	1134	A	2	H	3	7.50	0.58	8.08
182	1134	A	2	H	4	9.00	0.58	9.58
182	1134	A	2	H	5	10.50	0.58	11.08
182	1134	A	2	H	6	12.00	0.58	12.58
182	1134	A	2	H	7	13.50	0.58	14.08
182	1134	A	3	H	1	14.00	1.34	15.34
182	1134	A	3	H	2	15.50	1.34	16.84
182	1134	A	3	H	3	17.00	1.34	18.34
182	1134	A	3	H	4	18.50	1.34	19.84
182	1134	A	3	H	5	20.00	1.34	21.34
182	1134	A	3	H	6	21.50	1.34	22.84
182	1134	A	3	H	7	23.00	1.34	24.34
182	1134	A	4	H	1	23.50	2.60	26.10
182	1134	A	4	H	2	25.00	2.60	27.60
182	1134	A	4	H	3	26.50	2.60	29.10
182	1134	A	4	H	4	28.00	2.60	30.60
182	1134	A	4	H	5	29.50	2.60	32.10
182	1134	A	4	H	6	31.00	2.60	33.60
182	1134	A	4	H	7	32.50	2.60	35.10
182	1134	A	5	H	1	33.00	1.72	34.72
182	1134	A	5	H	2	34.50	1.72	36.22
182	1134	A	5	H	3	36.00	1.72	37.72
182	1134	A	5	H	4	37.50	1.72	39.22
182	1134	A	5	H	5	39.00	1.72	40.72
182	1134	A	5	H	6	40.50	1.72	42.22
182	1134	A	5	H	7	42.00	1.72	43.72
182	1134	A	6	H	1	42.50	2.22	44.72
182	1134	A	6	H	2	44.00	2.22	46.22
182	1134	A	6	H	3	45.50	2.22	47.72
182	1134	A	6	H	4	47.00	2.22	49.22
182	1134	A	6	H	6	50.00	2.22	52.22
182	1134	A	6	H	7	51.50	2.22	53.72
182	1134	A	7	H	1	52.00	2.34	54.34
182	1134	A	7	H	2	53.50	2.34	55.84
182	1134	A	7	H	3	55.00	2.34	57.34
182	1134	A	7	H	4	56.50	2.34	58.84
182	1134	A	7	H	5	58.00	2.34	60.34
182	1134	A	7	H	6	59.50	2.34	61.84
182	1134	A	7	H	7	61.00	2.34	63.34
182	1134	A	8	H	1	61.50	2.93	64.43
182	1134	A	8	H	2	63.00	2.93	65.93
182	1134	A	8	H	3	64.50	2.93	67.43
182	1134	A	8	H	4	66.00	2.93	68.93
182	1134	A	8	H	5	67.50	2.93	70.43
182	1134	A	8	H	6	69.00	2.93	71.93
182	1134	A	8	H	7	70.00	2.93	72.93
182	1134	A	9	H	1	71.00	2.83	73.83
182	1134	A	9	H	2	72.50	2.83	75.33
182	1134	A	9	H	3	74.00	2.83	76.83
182	1134	A	9	H	4	75.50	2.83	78.33
182	1134	A	9	H	5	77.00	2.83	79.83
182	1134	A	9	H	6	78.50	2.83	81.33
182	1134	A	9	H	7	80.00	2.83	82.83
182	1134	A	10	H	1	80.50	3.57	84.07
182	1134	A	10	H	2	82.00	3.57	85.57
182	1134	A	10	H	3	83.50	3.57	87.07
182	1134	A	10	H	4	85.00	3.57	88.57
182	1134	A	10	H	5	86.50	3.57	90.07
182	1134	A	10	H	6	88.00	3.57	91.57
182	1134	A	10	H	7	89.50	3.57	93.07
182	1134	A	11	H	1	90.00	4.58	94.58

Table T3 (continued).

Leg	Site	Hole	Core	Type	Section	Depth (mbsf)	Offset	Depth (mcd)
182	1134	A	11	H	2	91.50	4.58	96.08
182	1134	A	11	H	3	93.00	4.58	97.58
182	1134	A	11	H	4	94.50	4.58	99.08
182	1134	A	11	H	5	96.00	4.58	100.58
182	1134	A	11	H	6	97.50	4.58	102.08
182	1134	A	11	H	7	99.00	4.58	103.58
182	1134	A	12	H	1	99.50	5.34	104.84
182	1134	A	12	H	2	101.00	5.34	106.34
182	1134	A	12	H	3	102.50	5.34	107.84
182	1134	A	12	H	4	104.00	5.34	109.34
182	1134	A	12	H	5	105.50	5.34	110.84
182	1134	A	12	H	6	107.00	5.34	112.34
182	1134	A	13	H	1	109.00	5.40	114.40
182	1134	A	13	H	2	110.50	5.40	115.90
182	1134	A	13	H	3	112.00	5.40	117.40
182	1134	A	13	H	4	113.50	5.40	118.90
182	1134	A	13	H	5	115.00	5.40	120.40
182	1134	A	13	H	6	116.50	5.40	121.90
182	1134	A	14	H	1	118.50	5.58	124.08
182	1134	A	14	H	2	119.88	5.58	125.46
182	1134	A	14	H	3	121.38	5.58	126.96
182	1134	A	14	H	4	122.88	5.58	128.46
182	1134	A	14	H	5	124.38	5.58	129.96
182	1134	A	14	H	6	125.38	5.58	130.96
182	1134	A	15	X	1	126.00	5.70	131.70
182	1134	A	15	X	2	127.50	5.70	133.20
182	1134	A	15	X	3	129.00	5.70	134.70
182	1134	A	15	X	4	130.10	5.70	135.80
182	1134	A	16	X	1	127.90	8.54	136.44
182	1134	A	16	X	2	129.40	8.54	137.94
182	1134	A	16	X	3	130.90	8.54	139.44
182	1134	A	16	X	4	132.40	8.54	140.94
182	1134	A	16	X	5	133.90	8.54	142.44
182	1134	A	16	X	6	135.40	8.54	143.94
182	1134	A	16	X	7	136.90	8.54	145.44
182	1134	A	17	X	1	137.50	8.40	145.90
182	1134	A	17	X	2	139.00	8.40	147.40
182	1134	A	17	X	3	140.50	8.40	148.90
182	1134	A	17	X	4	142.00	8.40	150.40
182	1134	A	17	X	5	143.30	8.40	151.70
182	1134	A	19	X	1	156.70	8.40	165.10
182	1134	A	19	X	2	158.20	8.40	166.60
182	1134	A	19	X	3	159.70	8.40	168.10
182	1134	A	19	X	4	161.20	8.40	169.60
182	1134	A	20	X	1	166.30	8.40	174.70
182	1134	A	20	X	2	167.80	8.40	176.20
182	1134	A	20	X	3	169.30	8.40	177.70
182	1134	A	21	X	1	175.90	8.40	184.30
182	1134	A	21	X	2	176.11	8.40	184.51
182	1134	A	22	X	1	185.50	8.40	193.90
182	1134	A	22	X	2	187.00	8.40	195.40
182	1134	A	22	X	3	188.50	8.40	196.90
182	1134	A	22	X	4	190.00	8.40	198.40
182	1134	A	23	X	1	195.10	8.40	203.50
182	1134	A	23	X	2	196.60	8.40	205.00
182	1134	A	23	X	3	197.51	8.40	205.91
182	1134	A	24	X	1	204.70	8.40	213.10
182	1134	A	24	X	2	206.20	8.40	214.60
182	1134	A	25	X	1	214.30	8.40	222.70
182	1134	A	25	X	2	214.85	8.40	223.25
182	1134	A	27	X	1	233.60	8.40	242.00
182	1134	A	27	X	2	235.10	8.40	243.50
182	1134	A	27	X	3	236.60	8.40	245.00
182	1134	A	27	X	4	237.80	8.40	246.20
182	1134	A	27	X	5	238.30	8.40	246.70
182	1134	A	34	X	1	300.80	8.40	309.20
182	1134	A	34	X	2	302.30	8.40	310.70
182	1134	A	34	X	3	303.80	8.40	312.20
182	1134	A	34	X	4	304.20	8.40	312.60

Table T3 (continued).

Leg	Site	Hole	Core	Type	Section	Depth (mbsf)	Offset	Depth (mcd)
182	1134	A	35	X	1	310.40	8.40	318.80
182	1134	A	36	X	1	320.00	8.40	328.40
182	1134	A	36	X	2	321.50	8.40	329.90
182	1134	A	36	X	3	321.80	8.40	330.20
182	1134	A	37	X	1	329.70	8.40	338.10
182	1134	A	37	X	2	331.20	8.40	339.60
182	1134	A	37	X	3	331.84	8.40	340.24
182	1134	A	38	X	1	339.30	8.40	347.70
182	1134	A	38	X	2	340.54	8.40	348.94
182	1134	A	39	X	1	349.00	8.40	357.40
182	1134	A	39	X	2	350.50	8.40	358.90
182	1134	A	40	X	1	358.60	8.40	367.00
182	1134	A	40	X	2	360.10	8.40	368.50
182	1134	A	40	X	3	361.60	8.40	370.00
182	1134	A	41	X	1	368.20	8.40	376.60
182	1134	B	1	H	1	0.00	0.20	0.20
182	1134	B	1	H	2	1.50	0.20	1.70
182	1134	B	1	H	3	3.00	0.20	3.20
182	1134	B	1	H	4	4.50	0.20	4.70
182	1134	B	1	H	5	6.00	0.20	6.20
182	1134	B	1	H	6	7.50	0.20	7.70
182	1134	B	1	H	7	8.44	0.20	8.64
182	1134	B	2	H	1	8.60	0.61	9.21
182	1134	B	2	H	2	9.71	0.61	10.32
182	1134	B	2	H	4	12.71	0.61	13.32
182	1134	B	2	H	5	14.21	0.61	14.82
182	1134	B	2	H	6	15.71	0.61	16.32
182	1134	B	2	H	7	17.21	0.61	17.82
182	1134	B	3	H	1	18.10	0.82	18.92
182	1134	B	3	H	2	19.60	0.82	20.42
182	1134	B	3	H	3	21.10	0.82	21.92
182	1134	B	3	H	4	22.60	0.82	23.42
182	1134	B	3	H	5	24.10	0.82	24.92
182	1134	B	3	H	6	25.60	0.82	26.42
182	1134	B	3	H	7	26.60	0.82	27.42
182	1134	B	4	H	1	27.60	0.76	28.36
182	1134	B	4	H	2	29.10	0.76	29.86
182	1134	B	4	H	3	30.60	0.76	31.36
182	1134	B	4	H	4	32.10	0.76	32.86
182	1134	B	4	H	5	33.60	0.76	34.36
182	1134	B	4	H	6	35.10	0.76	35.86
182	1134	B	4	H	7	36.60	0.76	37.36
182	1134	B	5	H	1	37.10	1.18	38.28
182	1134	B	5	H	2	38.60	1.18	39.78
182	1134	B	5	H	2	38.60	1.18	39.78
182	1134	B	5	H	4	41.60	1.18	42.78
182	1134	B	5	H	5	43.10	1.18	44.28
182	1134	B	5	H	6	44.60	1.18	45.78
182	1134	B	6	H	1	46.60	1.08	47.68
182	1134	B	6	H	2	48.10	1.08	49.18
182	1134	B	6	H	3	49.60	1.08	50.68
182	1134	B	6	H	4	51.10	1.08	52.18
182	1134	B	6	H	5	51.52	1.08	52.60
182	1134	B	7	H	1	56.10	1.97	58.07
182	1134	B	7	H	2	57.60	1.97	59.57
182	1134	B	7	H	3	59.10	1.97	61.07
182	1134	B	7	H	4	60.60	1.97	62.57
182	1134	B	7	H	5	61.76	1.97	63.73
182	1134	B	7	H	6	63.26	1.97	65.23
182	1134	B	8	H	1	65.60	1.83	67.43
182	1134	B	8	H	2	67.10	1.83	68.93
182	1134	B	8	H	3	68.60	1.83	70.43
182	1134	B	8	H	4	70.10	1.83	71.93
182	1134	B	8	H	5	71.60	1.83	73.43
182	1134	B	8	H	6	73.10	1.83	74.93
182	1134	B	9	H	1	75.10	2.03	77.13
182	1134	B	9	H	2	76.60	2.03	78.63
182	1134	B	9	H	3	78.10	2.03	80.13
182	1134	B	9	H	4	79.60	2.03	81.63

Table T3 (continued).

Leg	Site	Hole	Core	Type	Section	Depth (mbsf)	Offset	Depth (mcd)
182	1134	B	9	H	5	81.10	2.03	83.13
182	1134	B	9	H	6	82.60	2.03	84.63
182	1134	B	10	H	1	84.60	2.32	86.92
182	1134	B	10	H	2	86.10	2.32	88.42
182	1134	B	10	H	3	87.60	2.32	89.92
182	1134	B	10	H	4	89.10	2.32	91.42
182	1134	B	10	H	5	90.60	2.32	92.92
182	1134	B	10	H	6	92.10	2.32	94.42
182	1134	B	10	H	7	93.60	2.32	95.92
182	1134	B	11	H	1	94.10	2.14	96.24
182	1134	B	11	H	2	95.60	2.14	97.74
182	1134	B	11	H	3	97.10	2.14	99.24
182	1134	B	11	H	4	98.60	2.14	100.74
182	1134	B	11	H	5	100.10	2.14	102.24
182	1134	B	11	H	6	101.60	2.14	103.74
182	1134	B	11	H	7	103.10	2.14	105.24
182	1134	B	12	H	1	103.60	2.42	106.02
182	1134	B	12	H	2	105.10	2.42	107.52
182	1134	B	12	H	3	106.60	2.42	109.02
182	1134	B	12	H	4	108.10	2.42	110.52
182	1134	B	12	H	5	109.60	2.42	112.02
182	1134	B	12	H	6	111.10	2.42	113.52
182	1134	B	12	H	7	112.50	2.42	114.92
182	1134	B	13	H	1	113.10	2.76	115.86
182	1134	B	13	H	2	114.60	2.76	117.36
182	1134	B	13	H	3	116.10	2.76	118.86
182	1134	B	13	H	4	117.60	2.76	120.36
182	1134	B	13	H	5	119.10	2.76	121.86
182	1134	B	13	H	5	119.10	2.76	121.86
182	1134	B	13	H	6	120.60	2.76	123.36
182	1134	B	13	H	7	122.10	2.76	124.86
182	1134	B	14	X	1	122.60	3.02	125.62
182	1134	B	14	X	2	124.10	3.02	127.12
182	1134	B	14	X	3	125.60	3.02	128.62
182	1134	B	14	X	4	127.10	3.02	130.12
182	1134	B	14	X	5	128.60	3.02	131.62
182	1134	B	15	X	1	129.00	6.64	135.64
182	1134	B	15	X	2	130.50	6.64	137.14
182	1134	B	15	X	3	132.00	6.64	138.64
182	1134	B	16	X	1	138.60	6.28	144.88
182	1134	B	16	X	2	140.10	6.28	146.38
182	1134	B	16	X	3	141.60	6.28	147.88
182	1134	B	16	X	4	143.10	6.28	149.38
182	1134	B	16	X	5	144.60	6.28	150.88
182	1134	B	17	X	1	148.20	6.28	154.48
182	1134	B	17	X	2	149.70	6.28	155.98
182	1134	B	17	X	3	151.20	6.28	157.48
182	1134	B	17	X	4	152.70	6.28	158.98
182	1134	B	18	X	1	157.80	6.28	164.08
182	1134	B	18	X	2	159.30	6.28	165.58
182	1134	B	18	X	3	159.96	6.28	166.24
182	1134	B	19	X	1	167.40	6.28	173.68
182	1134	B	19	X	2	168.90	6.28	175.18
182	1134	B	19	X	3	170.08	6.28	176.36
182	1134	B	23	X	1	206.00	6.28	212.28
182	1134	B	23	X	2	207.50	6.28	213.78
182	1134	B	23	X	3	207.81	6.28	214.09
182	1134	B	24	X	1	215.60	6.28	221.88
182	1134	B	24	X	2	217.10	6.28	223.38
182	1134	B	24	X	3	218.60	6.28	224.88
182	1134	B	24	X	4	220.10	6.28	226.38

Notes: Depths are measured at the top of each section. This table is also available in **ASCII format.**

Table T4. Splice tie points, Site 1134.

Site	Hole	Core	Type	Section	Interval (cm)	Depth (mbsf)	Depth (mcd)		Site	Hole	Core	Type	Section	Interval (cm)	Depth (mbsf)	Depth (mcd)
1134	B	1	H	5	84	6.84	7.04	Tie to	1134	A	2	H	2	45	6.46	7.04
1134	A	2	H	5	144	11.94	12.52	Tie to	1134	B	2	H	3	69	11.91	12.52
1134	B	2	H	6	44	16.15	16.76	Tie to	1134	A	3	H	1	141	15.42	16.76
1134	A	3	H	5	52	20.52	21.86	Tie to	1134	B	3	H	2	144	21.04	21.86
1134	B	3	H	6	36	25.96	26.78	Tie to	1134	A	4	H	1	68	24.18	26.78
1134	A	4	H	4	92	28.92	31.52	Tie to	1134	B	4	H	3	16	30.76	31.52
1134	B	4	H	5	60	34.20	34.96	Tie to	1134	A	5	H	1	24	33.24	34.96
1134	A	5	H	6	116	41.66	43.38	Tie to	1134	B	5	H	4	60	42.20	43.38
1134	B	5	H	6	92	45.52	46.70	Tie to	1134	A	6	H	2	48	44.48	46.70
1134	A	6	H	5	72	49.22	51.44	Tie to	1134	B	6	H	3	76	50.36	51.44
1134	B	6	H	6	68	53.70	54.78	Tie to	1134	A	7	H	1	44	52.44	54.78
1134	A	7	H	4	32	56.82	59.16	Tie to	1134	B	7	H	1	107.5	57.19	59.16
1134	B	7	H	5	139	63.15	65.12	Tie to	1134	A	8	H	1	66	62.19	65.12
1134	A	8	H	4	11	66.11	69.04	Tie to	1134	B	8	H	2	11	67.21	69.04
1134	B	8	H	6	104	74.14	75.97	Tie to	1134	A	9	H	2	64	73.14	75.97
1134	A	9	H	6	140	79.90	82.73	Tie to	1134	B	9	H	4	109	80.70	82.73
1134	B	9	H	6	11	82.71	84.74	Tie to	1134	A	10	H	1	67	81.17	84.74
1134	A	10	H	6	104	89.04	92.61	Tie to	1134	B	10	H	4	118.5	90.29	92.61
1134	B	10	H	6	140	93.50	95.82	Tie to	1134	A	11	H	1	124	91.24	95.82
1134	A	11	H	5	52	96.52	101.10	Tie to	1134	B	11	H	4	36	98.96	101.10
1134	B	11	H	7	4	103.14	105.28	Tie to	1134	A	12	H	1	44	99.94	105.28
1134	A	12	H	6	120	108.20	113.54	Append to	1134	A	13	H	1	0	109.00	114.40
1134	A	13	H	7	32	118.32	123.72	Append to	1134	A	14	H	1	0	118.50	124.08
1134	A	14	H	4	43	123.31	128.89	Tie to	1134	B	14	X	3	27	125.87	128.89
1134	B	14	X	5	59	129.19	132.21	Tie to	1134	A	15	X	1	51	126.51	132.21
1134	A	15	X	4	11	130.21	135.91	Tie to	1134	B	15	X	1	27	129.27	135.91
1134	B	15	X	3	19	132.19	138.83	Tie to	1134	A	16	X	2	88	130.29	138.83
1134	A	16	X	7	19	137.09	145.63	Tie to	1134	B	16	X	1	75	139.35	145.63
1134	B	16	X	5	84	145.44	151.72									

Note: This table is also available in **ASCII format.**

Table T5. Composition of headspace gases, Hole 1134A.

Core, section	Depth (mbsf)	C_1 (ppmv)
182-1134A-		
1H-3	3.00	2
2H-4	9.00	2
3H-4	18.50	2
4H-4	28.00	3
5H-4	37.50	3
6H-4	47.00	3
7H-4	56.50	3
8H-4	66.00	4
9H-4	75.50	4
10H-4	85.00	3
11H-4	94.50	3
12H-4	104.00	3
13H-4	113.50	4
14H-4	122.88	4
15X-3	129.00	4
16X-4	132.40	5
17X-4	142.00	4
19X-3	159.70	5
20X-2	167.80	4
21X-1	175.90	4
22X-3	188.50	4
23X-2	196.60	5
24X-2	206.20	4
25X-1	214.30	3
27X-3	236.60	2
29X-CC	252.90	2
31X-1	272.54	2
35X-1	310.92	3
36X-2	321.50	8
37X-2	331.20	8
38X-1	339.30	6
39X-2	350.50	3
40X-2	360.10	5
41X-CC	368.47	3

Table T6. Calcium carbonate ($CaCO_3$) content of samples, Hole 1134A.

Core, section, interval (cm)	Depth (mbsf)	$CaCO_3$ (wt%)
182-1134A-		
1H-1, 60-61	0.60	91.8
1H-3, 60-61	3.60	89.7
2H-1, 60-61	5.10	90.9
2H-3, 60-61	8.10	91.3
2H-5, 60-61	11.10	89.9
3H-1, 60-61	14.60	89.5
3H-3, 60-61	17.60	87.0
3H-5, 60-61	20.60	86.2
4H-1, 60-61	24.10	85.0
4H-3, 60-61	27.10	86.3
4H-5, 60-61	30.10	86.7
5H-1, 60-62	33.60	90.2
5H-3, 60-62	36.60	88.3
5H-5, 60-62	39.60	86.9
6H-1, 60-62	43.10	86.1
6H-3, 60-62	46.10	86.7
6H-5, 60-62	49.10	81.0
7H-1, 60-62	52.60	91.3
7H-3, 60-62	55.60	93.6
7H-5, 60-62	58.60	87.5
8H-1, 60-62	62.10	89.2
8H-3, 60-62	65.10	90.3
8H-5, 60-62	68.10	86.1
9H-1, 60-62	71.60	87.6
9H-3, 60-62	74.60	87.8
9H-3, 60-62	77.60	84.0
10H-1, 60-62	81.10	86.9
10H-3, 60-62	84.10	86.8
10H-5, 60-62	87.10	86.4
11H-1, 60-62	90.60	87.3
11H-3, 60-62	93.60	89.7
11H-5, 60-62	96.60	87.0
12H-1, 60-62	100.10	86.2
12H-3, 60-62	103.10	84.8
12H-5, 60-62	106.10	86.5
13H-1, 60-62	109.60	89.1
13H-3, 60-62	112.60	87.2
13H-5, 60-62	115.60	83.1
14H-1, 60-62	119.10	87.6
14H-3, 60-62	121.98	87.4
14H-5, 60-62	124.98	86.4
15X-1, 60-62	126.60	87.8
15X-3, 60-62	129.60	87.0
16X-1, 60-62	128.50	88.3
16X-3, 60-62	131.50	88.3
16X-5, 60-62	134.50	89.6
17X-1, 60-62	138.10	90.8
17X-3, 60-62	141.10	89.2
17X-5, 45-46	143.75	79.3
19X-1, 60-61	157.30	73.0
19X-3, 60-61	160.30	73.1
20X-1, 82-83	167.12	67.3
20X-CC, 9-10	169.95	66.5
22X-1, 60-61	186.10	65.8
22X-3, 62-63	189.12	74.9
23X-1, 60-61	195.70	80.1
24X-1, 60-61	205.30	57.6
27X-1, 60-62	234.20	85.7
27X-3, 60-62	237.20	81.7
34X-1, 60-62	301.40	90.9
40X-1, 60-62	359.20	86.7

Table T7. Interstitial water geochemistry, Site 1134.

Core, section, interval (cm)	Depth (mbsf)	pH	ppH	Alkalinity (mM)	Salinity	Cl^- (mM)	SO_4^{2-} (mM)	Na^+ (mM)	K^+ (mM)	Mg^{2+} (mM)	Ca^{2+} (mM)	Sr^{2+} (µM)	Li^+ (µM)	$H_4SiO_4^0$ (µM)	NH_4^+ (µM)	Fe^{2+} (µM)
1H-2, 140-150	2.90	7.29	7.42	3.70	35.5	574	29.8	509	11.6	53.4	10.6	91	38	484	105	1
2H-3, 140-150	8.90	7.21	7.34	3.31	38.0	639	31.2	545	12.4	57.0	11.6	147	42	450	169	3
3H-3, 140-150	18.40	6.83	7.15	4.17	66.0	1046	60.0	911	17.1	94.0	29.3	357	78	507	236	5
4H-3, 140-150	27.90	6.68	6.86	4.21	84.0	1345	68.8	1172	21.6	109.8	39.8	321	100	501	330	5
5H-3, 140-150	37.40	6.64	6.81	4.01	90.5	1468	68.8	1301	24.9	116.7	43.6	364	115	501	349	1
6H-3, 140-150	46.90	6.61	6.80	3.52	95.0	1536	68.1	1350	26.3	118.1	45.3	340	119	501	347	3
7H-3, 140-150	56.40	6.65	6.87	3.21	96.0	1573	68.1	1378	27.6	118.8	45.0	283	119	308	333	42
8H-3, 140-150	65.90	6.53	6.84	2.89	97.0	1566	67.3	1384	27.1	119.0	44.5	251	116	219	322	94
9H-3, 140-150	75.40	6.64	6.80	2.73	97.0	1578	67.4	1403	27.8	119.6	44.8	244	116	213	306	105
10H-3, 140-150	84.90	6.52	6.83	2.65	97.0	1580	67.6	1413	28.5	120.1	44.7	242	117	260	291	117
11H-3, 140-150	94.40	6.70	6.93	2.77	97.0	1580	66.8	1396	29.1	119.8	45.4	242	118	391	401	96
12H-3, 140-150	103.90	6.63	6.94	2.87	97.0	1582	66.9	1400	29.3	119.8	45.2	238	112	564	304	106
13H-3, 140-150	113.40	6.70	7.04	2.79	97.0	1587	67.2	1401	29.1	120.6	46.0	236	115	577	379	98
14H-3, 140-150	122.90	6.81	7.00	2.45	97.0	1581	70.2	1402	29.4	119.4	44.8	233	113	534	304	74
15X-2, 140-150	128.90	6.70	6.92	3.15	97.0	1583	67.9	1407	28.9	120.4	46.8	238	112	494	304	93
17X-3, 140-150	141.90	6.72	6.92	2.56	97.0	1583	68.1	1400	27.6	120.3	45.1	242	111	598	377	107
19X-2, 140-150	159.60	6.93	7.07	2.86	97.0	1574	67.7	1398	27.2	119.8	45.1	240	109	583	368	79
22X-2, 140-150	188.40	6.88	7.15	3.03	97.0	1576	68.8	1395	27.0	119.7	45.4	254	117	663	370	101
24X-1, 140-150	206.10	6.86	7.08	2.73	96.0	1564	69.6	1383	27.1	119.0	45.8	205	112	613	307	82
27X-1, 140-150	236.50	6.82	7.03	2.56	97.0	1572	67.0	1388	27.3	117.6	44.7	205	117	575	382	100
34X-1, 140-150	302.20	6.76	6.81	3.16	97.5	1553	67.3	1379	26.9	116.9	45.8	195	116	486	316	70
36X-1, 140-150	321.40	6.80	6.80	2.48	94.0	1540	67.5	1356	26.2	116.2	45.4	189	113	526	336	76
39X-1, 140-150	350.40	NM	NM	NM	95.0	1508	63.4	1350	25.8	110.3	43.2	183	115	475	356	NM

Note: NM = not measured.

Table T8. Summary of X-ray diffraction analysis, Site 1134.

Leg	Site	Hole	Core	Type	Section	Top (cm)	Bottom (cm)	Depth (mbsf)	Aragonite (wt%)	Quartz (wt%)	LMC (wt%)	HMC (wt%)	Dolomite (wt%)
182	1134	A	1	H	1	60	61	0.60	13	0	31	56	0
182	1134	A	1	H	3	60	61	3.60	22	1	51	26	1
182	1134	A	2	H	1	60	61	5.10	20	1	56	22	1
182	1134	A	2	H	3	60	61	8.10	11	1	88	0	0
182	1134	A	2	H	5	60	61	11.10	3	1	96	0	0
182	1134	A	3	H	1	60	61	14.60	17	1	51	30	1
182	1134	A	3	H	3	60	61	17.60	19	2	79	0	0
182	1134	A	3	H	5	60	61	20.60	17	2	81	0	0
182	1134	A	4	H	1	60	61	24.10	9	1	90	0	0
182	1134	A	4	H	3	60	61	27.10	15	1	81	0	3
182	1134	A	4	H	5	60	61	30.10	17	2	81	0	1
182	1134	A	5	H	1	60	62	33.60	14	0	84	0	2
182	1134	A	5	H	3	60	62	36.60	18	2	75	0	5
182	1134	A	5	H	5	60	62	39.60	23	1	67	0	9
182	1134	A	6	H	1	60	62	43.10	15	1	51	32	1
182	1134	A	6	H	3	60	62	46.10	8	1	58	32	1
182	1134	A	6	H	5	60	62	49.10	19	5	75	0	2
182	1134	A	7	H	1	60	62	52.60	14	1	80	0	5
182	1134	A	7	H	3	60	62	55.60	11	2	74	0	13
182	1134	A	7	H	5	60	62	58.60	0	1	98	0	1
182	1134	A	8	H	1	60	62	62.10	0	1	99	0	0
182	1134	A	8	H	3	60	62	65.10	0	1	99	0	0
182	1134	A	8	H	5	60	62	68.10	0	1	99	0	0
182	1134	A	9	H	1	60	62	71.60	0	1	99	0	0
182	1134	A	9	H	3	60	62	74.60	0	2	98	0	0
182	1134	A	9	H	5	60	62	77.60	0	1	99	0	0
182	1134	A	10	H	1	60	62	81.10	0	1	99	0	0
182	1134	A	10	H	3	60	62	84.10	0	1	99	0	0
182	1134	A	10	H	5	60	62	87.10	0	1	99	0	0
182	1134	A	11	H	1	60	62	90.60	0	1	99	0	0
182	1134	A	11	H	3	60	62	93.60	0	1	99	0	0
182	1134	A	11	H	5	60	62	96.60	0	1	99	0	0
182	1134	A	12	H	1	60	62	100.10	0	0	100	0	0
182	1134	A	12	H	3	60	62	103.10	0	1	99	0	0
182	1134	A	12	H	5	60	62	106.10	0	1	99	0	0
182	1134	A	13	H	1	60	62	109.60	0	1	99	0	0
182	1134	A	13	H	3	60	62	112.60	0	0	100	0	0
182	1134	A	13	H	5	60	62	115.60	0	1	99	0	0
182	1134	A	14	H	1	60	62	119.10	0	1	99	0	0
182	1134	A	14	H	3	60	62	121.98	0	1	99	0	0
182	1134	A	14	H	5	60	62	124.98	0	1	99	0	0
182	1134	A	15	X	1	60	62	126.60	0	1	99	0	0
182	1134	A	15	X	3	60	62	129.60	0	1	99	0	0
182	1134	A	16	X	1	60	62	128.50	0	1	99	0	0
182	1134	A	16	X	3	60	62	131.50	0	1	99	0	0
182	1134	A	16	X	5	60	62	134.50	0	0	100	0	0
182	1134	A	17	X	1	60	62	138.10	0	0	100	0	0
182	1134	A	17	X	3	60	62	141.10	0	0	100	0	0
182	1134	A	17	X	5	45	46	143.75	0	3	97	0	0
182	1134	A	19	X	1	60	61	157.30	0	4	96	0	0
182	1134	A	19	X	3	60	61	160.30	0	12	88	0	0
182	1134	A	20	X	1	82	83	167.12	6	7	87	0	0
182	1134	A	20	X	CC	9	10	169.95	6	26	68	0	0
182	1134	A	22	X	1	60	61	186.10	5	22	73	0	0
182	1134	A	22	X	3	62	63	189.12	3	6	91	0	0
182	1134	A	23	X	1	60	61	195.70	0	3	97	0	0
182	1134	A	24	X	1	60	61	205.30	0	2	98	0	0
182	1134	A	27	X	1	60	62	234.20	0	2	98	0	0
182	1134	A	27	X	3	60	62	237.20	0	1	99	0	0
182	1134	A	34	X	1	60	62	301.40	0	1	99	0	0
182	1134	A	40	X	1	60	62	359.20	0	2	98	0	0

Notes: LMC = low-Mg calcite, HMC = high-Mg calcite. This table is also available in **ASCII format.**

Table T9. *P*-wave velocity measurements from the multisensor track, Site 1134.

Leg	Site	Hole	Core	Type	Section	Interval (cm)	Depth (mbsf)	V_p (km/s)
182	1134	A	1	H	1	3.0	0.03	2.4055
182	1134	A	1	H	1	7.0	0.07	3.3284
182	1134	A	1	H	1	11.0	0.11	1.1467
182	1134	A	1	H	1	15.0	0.15	3.3270
182	1134	A	1	H	1	19.0	0.19	2.4098
182	1134	A	1	H	1	23.0	0.23	3.3311
182	1134	A	1	H	1	27.0	0.27	2.4113
182	1134	A	1	H	1	31.0	0.31	1.8913
182	1134	A	1	H	1	35.0	0.35	3.3284
182	1134	A	1	H	1	39.0	0.39	1.8908
182	1134	A	1	H	1	43.0	0.43	5.3642
182	1134	A	1	H	1	47.0	0.47	3.3270
182	1134	A	1	H	1	51.0	0.51	3.3284
182	1134	A	1	H	1	55.0	0.55	3.3201
182	1134	A	1	H	1	59.0	0.59	2.4077
182	1134	A	1	H	1	67.0	0.67	3.3188
182	1134	A	1	H	1	71.0	0.71	1.3183
182	1134	A	1	H	1	75.0	0.75	5.3499
182	1134	A	1	H	1	79.0	0.79	2.4091
182	1134	A	1	H	1	83.0	0.83	2.4019
182	1134	A	1	H	1	87.0	0.87	3.3270
182	1134	A	1	H	1	91.0	0.91	1.5552
182	1134	A	1	H	1	95.0	0.95	3.5409
182	1134	A	1	H	1	99.0	0.99	3.8383
182	1134	A	1	H	1	103.0	1.03	5.0668
182	1134	A	1	H	1	107.0	1.07	3.3229
182	1134	A	1	H	1	111.0	1.11	4.8207
182	1134	A	1	H	1	115.0	1.15	3.3215
182	1134	A	1	H	1	119.0	1.19	2.8255
182	1134	A	1	H	1	123.0	1.23	5.1743
182	1134	A	1	H	1	127.0	1.27	4.9697
182	1134	A	1	H	1	131.0	1.31	5.3642
182	1134	A	1	H	1	135.0	1.35	4.6941
182	1134	A	1	H	1	139.0	1.39	5.3677
182	1134	A	1	H	1	147.0	1.47	4.1471
182	1134	A	1	H	2	3.0	1.53	2.4149
182	1134	A	1	H	2	7.0	1.57	5.4002
182	1134	A	1	H	2	11.0	1.61	3.3325
182	1134	A	1	H	2	15.0	1.65	3.3380
182	1134	A	1	H	2	19.0	1.69	3.3284
182	1134	A	1	H	2	23.0	1.73	1.5555
182	1134	A	1	H	2	27.0	1.77	1.8882
182	1134	A	1	H	2	31.0	1.81	5.3966
182	1134	A	1	H	2	35.0	1.85	2.4120
182	1134	A	1	H	2	39.0	1.89	2.4091
182	1134	A	1	H	2	43.0	1.93	5.3463
182	1134	A	1	H	2	47.0	1.97	2.4091
182	1134	A	1	H	2	51.0	2.01	2.4077
182	1134	A	1	H	2	55.0	2.05	3.3242
182	1134	A	1	H	2	59.0	2.09	5.3642
182	1134	A	1	H	2	63.0	2.13	3.3160
182	1134	A	1	H	2	67.0	2.17	1.8886
182	1134	A	1	H	2	71.0	2.21	2.4069
182	1134	A	1	H	2	75.0	2.25	3.3215
182	1134	A	1	H	2	79.0	2.29	1.8882
182	1134	A	1	H	2	83.0	2.33	3.3201
182	1134	A	1	H	2	87.0	2.37	1.8873
182	1134	A	1	H	2	91.0	2.41	2.4091
182	1134	A	1	H	2	95.0	2.45	5.3392
182	1134	A	1	H	2	99.0	2.49	5.3893
182	1134	A	1	H	2	103.0	2.53	2.4077
182	1134	A	1	H	2	107.0	2.57	4.7920
182	1134	A	1	H	2	111.0	2.61	4.3654
182	1134	A	1	H	2	115.0	2.65	5.0860
182	1134	A	1	H	2	119.0	2.69	3.2217

Note: Only a portion of this table appears here. The complete table is available in **ASCII format.**

Table T10. Gamma-ray attenuation densiometry measurements from the multisensor track, Site 1134.

Leg	Site	Hole	Core	Type	Section	Interval (cm)	Depth (mbsf)	Density (g/cm^3)	Corrected density (g/cm^3)
182	1134	A	1	H	1	3.0	0.03	1.76	1.70
182	1134	A	1	H	1	7.0	0.07	1.82	1.76
182	1134	A	1	H	1	11.0	0.11	1.81	1.75
182	1134	A	1	H	1	15.0	0.15	1.81	1.76
182	1134	A	1	H	1	19.0	0.19	1.81	1.76
182	1134	A	1	H	1	23.0	0.23	1.79	1.73
182	1134	A	1	H	1	27.0	0.27	1.81	1.76
182	1134	A	1	H	1	31.0	0.31	1.81	1.75
182	1134	A	1	H	1	35.0	0.35	1.80	1.74
182	1134	A	1	H	1	39.0	0.39	1.82	1.76
182	1134	A	1	H	1	43.0	0.43	1.84	1.78
182	1134	A	1	H	1	47.0	0.47	1.82	1.77
182	1134	A	1	H	1	51.0	0.51	1.83	1.78
182	1134	A	1	H	1	55.0	0.55	1.82	1.76
182	1134	A	1	H	1	59.0	0.59	1.79	1.73
182	1134	A	1	H	1	63.0	0.63	1.76	1.70
182	1134	A	1	H	1	67.0	0.67	1.74	1.68
182	1134	A	1	H	1	71.0	0.71	1.76	1.70
182	1134	A	1	H	1	75.0	0.75	1.78	1.72
182	1134	A	1	H	1	79.0	0.79	1.78	1.72
182	1134	A	1	H	1	83.0	0.83	1.76	1.70
182	1134	A	1	H	1	87.0	0.87	1.76	1.70
182	1134	A	1	H	1	91.0	0.91	1.78	1.72
182	1134	A	1	H	1	95.0	0.95	1.77	1.71
182	1134	A	1	H	1	99.0	0.99	1.77	1.71
182	1134	A	1	H	1	103.0	1.03	1.79	1.73
182	1134	A	1	H	1	107.0	1.07	1.78	1.72
182	1134	A	1	H	1	111.0	1.11	1.77	1.71
182	1134	A	1	H	1	115.0	1.15	1.77	1.71
182	1134	A	1	H	1	119.0	1.19	1.74	1.68
182	1134	A	1	H	1	123.0	1.23	1.75	1.69
182	1134	A	1	H	1	127.0	1.27	1.74	1.68
182	1134	A	1	H	1	131.0	1.31	1.73	1.67
182	1134	A	1	H	1	135.0	1.35	1.74	1.67
182	1134	A	1	H	1	139.0	1.39	1.74	1.68
182	1134	A	1	H	1	143.0	1.43	1.74	1.68
182	1134	A	1	H	1	147.0	1.47	1.76	1.70
182	1134	A	1	H	2	3.0	1.53	1.83	1.77
182	1134	A	1	H	2	7.0	1.57	1.82	1.76
182	1134	A	1	H	2	11.0	1.61	1.83	1.77
182	1134	A	1	H	2	15.0	1.65	1.82	1.77
182	1134	A	1	H	2	19.0	1.69	1.79	1.73
182	1134	A	1	H	2	23.0	1.73	1.80	1.74
182	1134	A	1	H	2	27.0	1.77	1.77	1.71
182	1134	A	1	H	2	31.0	1.81	1.76	1.70
182	1134	A	1	H	2	35.0	1.85	1.78	1.72
182	1134	A	1	H	2	39.0	1.89	1.78	1.72
182	1134	A	1	H	2	43.0	1.93	1.76	1.70
182	1134	A	1	H	2	47.0	1.97	1.77	1.71
182	1134	A	1	H	2	51.0	2.01	1.81	1.75
182	1134	A	1	H	2	55.0	2.05	1.81	1.75
182	1134	A	1	H	2	59.0	2.09	1.81	1.75
182	1134	A	1	H	2	63.0	2.13	1.78	1.72
182	1134	A	1	H	2	67.0	2.17	1.79	1.73
182	1134	A	1	H	2	71.0	2.21	1.80	1.74
182	1134	A	1	H	2	75.0	2.25	1.78	1.72
182	1134	A	1	H	2	79.0	2.29	1.78	1.72
182	1134	A	1	H	2	83.0	2.33	1.80	1.74
182	1134	A	1	H	2	87.0	2.37	1.77	1.71
182	1134	A	1	H	2	91.0	2.41	1.81	1.75
182	1134	A	1	H	2	95.0	2.45	1.79	1.73
182	1134	A	1	H	2	99.0	2.49	1.82	1.76
182	1134	A	1	H	2	103.0	2.53	1.78	1.72
182	1134	A	1	H	2	107.0	2.57	1.81	1.76

Note: Only a portion of this table appears here. The complete table is available in **ASCII format.**

Table T11. Magnetic susceptibility measurements from the multisensor track, Site 1134.

Leg	Site	Hole	Core	Type	Section	Interval (cm)	Depth (mbsf)	Magnetic susceptibility (10^{-6}; SI units)	Corrected susceptibility (10^{-6}; SI units)
182	1134	A	1	H	1	3.0	0.03	–0.5	–0.5
182	1134	A	1	H	1	11.0	0.11	–1.0	–1.0
182	1134	A	1	H	1	19.0	0.19	–0.4	–0.4
182	1134	A	1	H	1	27.0	0.27	–1.4	–1.4
182	1134	A	1	H	1	35.0	0.35	–1.6	–1.6
182	1134	A	1	H	1	43.0	0.43	–1.7	–1.7
182	1134	A	1	H	1	51.0	0.51	–2.7	–2.7
182	1134	A	1	H	1	59.0	0.59	–2.1	–2.1
182	1134	A	1	H	1	67.0	0.67	–2.4	–2.4
182	1134	A	1	H	1	75.0	0.75	–2.6	–2.6
182	1134	A	1	H	1	83.0	0.83	–2.7	–2.7
182	1134	A	1	H	1	91.0	0.91	–2.4	–2.4
182	1134	A	1	H	1	99.0	0.99	–2.8	–2.8
182	1134	A	1	H	1	107.0	1.07	–2.9	–2.9
182	1134	A	1	H	1	115.0	1.15	–2.7	–2.7
182	1134	A	1	H	1	123.0	1.23	–2.8	–2.8
182	1134	A	1	H	1	131.0	1.31	–3.0	–3.0
182	1134	A	1	H	1	139.0	1.39	–3.1	–3.1
182	1134	A	1	H	1	147.0	1.47	–2.1	–2.1
182	1134	A	1	H	2	3.0	1.53	–2.0	–2.0
182	1134	A	1	H	2	11.0	1.61	–1.8	–1.8
182	1134	A	1	H	2	19.0	1.69	–1.8	–1.8
182	1134	A	1	H	2	27.0	1.77	–1.9	–1.9
182	1134	A	1	H	2	35.0	1.85	–2.5	–2.5
182	1134	A	1	H	2	43.0	1.93	–2.5	–2.5
182	1134	A	1	H	2	51.0	2.01	–2.5	–2.5
182	1134	A	1	H	2	59.0	2.09	–2.5	–2.5
182	1134	A	1	H	2	67.0	2.17	–2.3	–2.3
182	1134	A	1	H	2	75.0	2.25	–2.7	–2.7
182	1134	A	1	H	2	83.0	2.33	–2.5	–2.5
182	1134	A	1	H	2	91.0	2.41	–2.8	–2.8
182	1134	A	1	H	2	99.0	2.49	–2.6	–2.6
182	1134	A	1	H	2	107.0	2.57	–2.6	–2.6
182	1134	A	1	H	2	115.0	2.65	–2.6	–2.6
182	1134	A	1	H	2	123.0	2.73	–2.4	–2.4
182	1134	A	1	H	2	131.0	2.81	–2.2	–2.2
182	1134	A	1	H	3	3.0	3.03	–1.9	–1.9
182	1134	A	1	H	3	11.0	3.11	–1.8	–1.8
182	1134	A	1	H	3	19.0	3.19	–2.1	–2.1
182	1134	A	1	H	3	27.0	3.27	–1.8	–1.8
182	1134	A	1	H	3	35.0	3.35	–2.4	–2.4
182	1134	A	1	H	3	43.0	3.43	–2.2	–2.2
182	1134	A	1	H	3	51.0	3.51	–2.2	–2.2
182	1134	A	1	H	3	59.0	3.59	–2.4	–2.4
182	1134	A	1	H	3	67.0	3.67	–1.8	–1.8
182	1134	A	1	H	3	75.0	3.75	–2.9	–2.9
182	1134	A	1	H	3	83.0	3.83	–1.9	–1.9
182	1134	A	1	H	3	91.0	3.91	–0.9	–0.9
182	1134	A	1	H	3	99.0	3.99	–0.7	–0.7
182	1134	A	1	H	3	107.0	4.07	–1.2	–1.2
182	1134	A	1	H	3	115.0	4.15	–1.4	–1.4
182	1134	A	1	H	3	123.0	4.23	–2.5	–2.5
182	1134	A	1	H	3	131.0	4.31	–1.0	–1.0
182	1134	A	2	H	1	3.0	4.53	0.1	0.1
182	1134	A	2	H	1	11.0	4.61	–0.3	–0.3
182	1134	A	2	H	1	19.0	4.69	–0.2	–0.2
182	1134	A	2	H	1	27.0	4.77	–0.9	–0.9
182	1134	A	2	H	1	35.0	4.85	–0.7	–0.7
182	1134	A	2	H	1	43.0	4.93	–0.8	–0.8
182	1134	A	2	H	1	51.0	5.01	–0.9	–0.9
182	1134	A	2	H	1	59.0	5.09	–0.4	–0.4
182	1134	A	2	H	1	67.0	5.17	–0.7	–0.7
182	1134	A	2	H	1	75.0	5.25	–0.9	–0.9
182	1134	A	2	H	1	83.0	5.33	–1.2	–1.2

Note: Only a portion of this table appears here. The complete table is available in **ASCII format.**

Table T12. Natural gamma-ray measurements from the multisensor track, Site 1134.

Leg	Site	Hole	Core	Type	Section	Interval (cm)	Depth (mbsf)	NGR (cps)
182	1134	A	1	H	1	11.0	0.11	5.77
182	1134	A	1	H	1	27.0	0.27	6.35
182	1134	A	1	H	1	43.0	0.43	5.08
182	1134	A	1	H	1	59.0	0.59	6.39
182	1134	A	1	H	1	75.0	0.75	6.00
182	1134	A	1	H	1	91.0	0.91	8.23
182	1134	A	1	H	1	107.0	1.07	6.19
182	1134	A	1	H	1	123.0	1.23	5.58
182	1134	A	1	H	1	139.0	1.39	8.50
182	1134	A	1	H	2	11.0	1.61	8.31
182	1134	A	1	H	2	27.0	1.77	9.73
182	1134	A	1	H	2	43.0	1.93	8.04
182	1134	A	1	H	2	59.0	2.09	8.15
182	1134	A	1	H	2	75.0	2.25	8.69
182	1134	A	1	H	2	91.0	2.41	6.69
182	1134	A	1	H	2	107.0	2.57	8.96
182	1134	A	1	H	2	123.0	2.73	10.92
182	1134	A	1	H	3	11.0	3.11	7.12
182	1134	A	1	H	3	27.0	3.27	7.96
182	1134	A	1	H	3	43.0	3.43	6.46
182	1134	A	1	H	3	59.0	3.59	13.12
182	1134	A	1	H	3	75.0	3.75	11.92
182	1134	A	1	H	3	91.0	3.91	14.69
182	1134	A	1	H	3	107.0	4.07	15.85
182	1134	A	1	H	3	123.0	4.23	10.92
182	1134	A	2	H	1	11.0	4.61	11.69
182	1134	A	2	H	1	27.0	4.77	12.65
182	1134	A	2	H	1	43.0	4.93	10.92
182	1134	A	2	H	1	59.0	5.09	8.46
182	1134	A	2	H	1	75.0	5.25	11.92
182	1134	A	2	H	1	91.0	5.41	7.81
182	1134	A	2	H	1	107.0	5.57	9.54
182	1134	A	2	H	1	123.0	5.73	12.39
182	1134	A	2	H	2	11.0	6.11	12.00
182	1134	A	2	H	2	27.0	6.27	10.46
182	1134	A	2	H	2	43.0	6.43	13.27
182	1134	A	2	H	2	59.0	6.59	13.69
182	1134	A	2	H	2	75.0	6.75	12.85
182	1134	A	2	H	2	91.0	6.91	11.04
182	1134	A	2	H	2	107.0	7.07	13.35
182	1134	A	2	H	2	123.0	7.23	9.65
182	1134	A	2	H	2	139.0	7.39	12.12
182	1134	A	2	H	3	11.0	7.61	14.50
182	1134	A	2	H	3	27.0	7.77	11.65
182	1134	A	2	H	3	43.0	7.93	10.69
182	1134	A	2	H	3	59.0	8.09	12.50
182	1134	A	2	H	3	75.0	8.25	11.00
182	1134	A	2	H	3	91.0	8.41	9.00
182	1134	A	2	H	3	107.0	8.57	8.54
182	1134	A	2	H	3	123.0	8.73	10.77
182	1134	A	2	H	4	11.0	9.11	9.12
182	1134	A	2	H	4	27.0	9.27	10.96
182	1134	A	2	H	4	43.0	9.43	9.73
182	1134	A	2	H	4	59.0	9.59	13.77
182	1134	A	2	H	4	75.0	9.75	10.04
182	1134	A	2	H	4	91.0	9.91	11.54
182	1134	A	2	H	4	107.0	10.07	10.81
182	1134	A	2	H	4	123.0	10.23	9.85
182	1134	A	2	H	4	139.0	10.39	13.50
182	1134	A	2	H	5	11.0	10.61	9.62
182	1134	A	2	H	5	27.0	10.77	8.58
182	1134	A	2	H	5	43.0	10.93	8.81
182	1134	A	2	H	5	59.0	11.09	10.92
182	1134	A	2	H	5	75.0	11.25	9.69

Notes: NGR = natural gamma radiation. Only a portion of this table appears here. The complete table is available in **ASCII format.**

Table T13. Thermal conductivity measurements, Site 1134.

Leg	Site	Hole	Core	Type	Section	Interval (cm)	Depth (mbsf)	Thermal conductivity (W/[m·K])
182	1134	A	1	H	3	75.0	3.75	1.085
182	1134	A	2	H	3	75.0	8.25	1.149
182	1134	A	3	H	3	75.0	17.75	1.126
182	1134	A	4	H	3	75.0	27.25	1.140
182	1134	A	4	H	6	75.0	31.75	1.025
182	1134	A	5	H	2	75.0	35.25	1.229
182	1134	A	5	H	4	75.0	38.25	1.165
182	1134	A	6	H	3	75.0	46.25	1.093
182	1134	A	7	H	3	75.0	55.75	1.193
182	1134	A	8	H	3	75.0	65.25	1.216
182	1134	A	9	H	3	75.0	74.75	1.257
182	1134	A	10	H	3	75.0	84.25	1.205
182	1134	A	11	H	3	75.0	93.75	1.320
182	1134	A	12	H	3	75.0	103.25	1.235
182	1134	A	13	H	3	75.0	112.75	1.161
182	1134	A	14	H	3	75.0	122.13	1.167
182	1134	A	15	X	3	75.0	129.75	1.153
182	1134	A	16	X	3	75.0	131.65	1.198
182	1134	A	17	X	3	75.0	141.25	1.161
182	1134	A	19	X	3	75.0	160.45	1.045
182	1134	A	20	X	3	40.0	169.70	0.979
182	1134	A	22	X	3	75.0	189.25	1.150
182	1134	A	27	X	3	75.0	237.35	1.284
182	1134	A	34	X	2	75.0	303.05	1.284
182	1134	A	36	X	1	75.0	320.75	1.158
182	1134	A	24	X	1	75.0	205.45	1.022
182	1134	A	23	X	2	75.0	197.35	1.206
182	1134	A	25	X	CC	18.0	215.03	1.243
182	1134	A	37	X	1	75.0	330.45	1.193
182	1134	A	38	X	1	90.0	340.20	1.200
182	1134	A	40	X	2	75.0	360.85	1.320
182	1134	A	39	X	2	55.0	351.05	1.409
182	1134	A	40	X	1	55.0	359.15	1.158
182	1134	B	1	H	3	75.0	3.75	0.890
182	1134	B	2	H	3	75.0	11.96	1.213
182	1134	B	3	H	3	75.0	21.85	1.154
182	1134	B	4	H	3	75.0	31.35	1.151
182	1134	B	5	H	2	75.0	39.35	1.158
182	1134	B	6	H	3	75.0	50.35	1.155
182	1134	B	7	H	3	75.0	59.85	1.201
182	1134	B	8	H	3	75.0	69.35	1.366
182	1134	B	9	H	3	75.0	78.85	1.300
182	1134	B	10	H	3	75.0	88.35	1.267
182	1134	B	11	H	3	75.0	97.85	1.297
182	1134	B	12	H	3	75.0	107.35	1.240
182	1134	B	13	H	3	75.0	116.85	1.272
182	1134	B	14	X	3	75.0	126.35	0.962
182	1134	B	15	X	3	75.0	132.75	0.868
182	1134	B	15	X	3	50.0	132.50	1.150
182	1134	B	16	X	3	75.0	142.35	1.067

Note: This table is also available in **ASCII format.**

Table T14. Discrete *P*-wave velocity measurements using PWS1, PWS2, and PWS3, Site 1134.

Leg	Site	Hole	Core	Type	Section	Interval (cm)	Depth (mbsf)	PWS 1, 2, or 3	V_p (km/s)
182	1134	A	1	H	1	13.8	0.14	1	1.5793
182	1134	A	1	H	1	54.6	0.55	1	1.6102
182	1134	A	1	H	1	101.0	1.01	1	1.5839
182	1134	A	1	H	2	14.2	1.64	1	1.5933
182	1134	A	1	H	2	55.0	2.05	1	1.5884
182	1134	A	1	H	2	96.0	2.46	1	1.6014
182	1134	A	1	H	2	135.6	2.86	1	1.6083
182	1134	A	1	H	3	8.9	3.09	1	1.5829
182	1134	A	1	H	3	51.0	3.51	1	1.6102
182	1134	A	1	H	3	82.5	3.83	1	1.6165
182	1134	A	1	H	3	115.7	4.16	1	1.6014
182	1134	A	2	H	1	18.8	4.69	1	1.6284
182	1134	A	2	H	1	60.2	5.10	1	1.6316
182	1134	A	2	H	1	93.1	5.43	1	1.6245
182	1134	A	2	H	1	139.3	5.89	1	1.6336
182	1134	A	2	H	2	14.0	6.14	1	1.6162
182	1134	A	2	H	2	51.1	6.51	1	1.5882
182	1134	A	2	H	2	93.6	6.94	1	1.6245
182	1134	A	2	H	2	132.8	7.33	1	1.5906
182	1134	A	2	H	3	48.4	7.98	2	1.5947
182	1134	A	2	H	3	87.3	8.37	2	1.6274
182	1134	A	2	H	3	129.5	8.80	2	1.5691
182	1134	A	2	H	4	16.1	9.16	2	1.6312
182	1134	A	2	H	4	57.7	9.58	2	1.5885
182	1134	A	2	H	4	92.9	9.93	2	1.5799
182	1134	A	2	H	4	134.3	10.34	2	1.5691
182	1134	A	2	H	5	13.6	10.64	2	1.5922
182	1134	A	2	H	5	53.4	11.03	2	1.5799
182	1134	A	2	H	5	91.0	11.41	2	1.5204
182	1134	A	2	H	5	143.5	11.94	2	1.6590
182	1134	A	2	H	6	15.0	12.15	2	1.5461
182	1134	A	2	H	6	53.8	12.54	2	1.5959
182	1134	A	2	H	6	95.1	12.95	2	1.5922
182	1134	A	2	H	6	135.0	13.35	2	1.6109
182	1134	A	2	H	7	18.1	13.68	2	1.6287
182	1134	A	2	H	7	43.4	13.93	2	1.6470
182	1134	A	3	H	1	21.3	14.21	2	1.6206
182	1134	A	3	H	1	64.4	14.64	2	1.6198
182	1134	A	3	H	1	103.4	15.03	2	1.6211
182	1134	A	3	H	1	137.8	15.38	2	1.6644
182	1134	A	3	H	2	17.8	15.68	2	1.6002
182	1134	A	3	H	2	55.3	16.05	2	1.6882
182	1134	A	3	H	2	89.7	16.40	2	1.6027
182	1134	A	3	H	2	138.7	16.89	2	1.6385
182	1134	A	3	H	3	16.2	17.16	2	1.6140
182	1134	A	3	H	3	50.3	17.50	2	1.6583
182	1134	A	3	H	3	82.8	17.83	2	1.6437
182	1134	A	3	H	3	129.3	18.29	2	1.6596
182	1134	A	3	H	4	17.3	18.67	2	1.6450
182	1134	A	3	H	4	64.4	19.14	2	1.6557
182	1134	A	3	H	4	103.2	19.53	2	1.6868
182	1134	A	3	H	4	146.5	19.97	2	1.6828
182	1134	A	3	H	5	15.8	20.16	2	1.6910
182	1134	A	3	H	5	55.1	20.55	2	1.6731
182	1134	A	3	H	5	93.2	20.93	2	1.6814
182	1134	A	3	H	5	135.5	21.36	2	1.5953
182	1134	A	3	H	6	17.2	21.67	2	1.6431
182	1134	A	3	H	6	59.0	22.09	2	1.6724
182	1134	A	3	H	6	96.2	22.46	2	1.6711
182	1134	A	3	H	6	140.7	22.91	2	1.6779
182	1134	A	3	H	7	19.8	23.20	2	1.6890
182	1134	A	4	H	1	18.8	23.69	2	1.6677
182	1134	A	4	H	1	60.0	24.10	2	1.6855
182	1134	A	4	H	1	95.4	24.45	2	1.6841

Note: Only a portion of this table appears here. The complete table is available in **ASCII format.**

Table T15. Index properties measurements, Site 1134.

Leg	Site	Hole	Core	Type	Section	Top (cm)	Bottom (cm)	Depth (mbsf)	Bulk water content (%)	Dry water content (%)	Bulk density (g/cm³)	Dry density (g/cm³)	Grain density (g/cm³)	Porosity (%)	Void ratio
182	1134	A	1	H	1	72.0	74.0	0.72	34.1	51.7	1.71	1.13	2.61	56.9	1.32
182	1134	A	1	H	2	71.0	73.0	2.21	32.6	48.5	1.73	1.17	2.61	55.2	1.23
182	1134	A	1	H	3	74.0	76.0	3.74	30.7	44.3	1.75	1.22	2.56	52.6	1.11
182	1134	A	2	H	1	74.0	76.0	5.24	30.9	44.7	1.74	1.20	2.52	52.4	1.10
182	1134	A	2	H	2	76.0	78.0	6.76	28.2	39.3	1.79	1.28	2.53	49.2	0.97
182	1134	A	2	H	3	76.0	78.0	8.26	31.3	45.5	1.73	1.19	2.51	52.7	1.12
182	1134	A	2	H	4	76.0	78.0	9.76	30.6	44.1	1.73	1.20	2.50	51.8	1.08
182	1134	A	2	H	5	75.0	77.0	11.25	32.2	47.5	1.72	1.17	2.55	54.2	1.18
182	1134	A	2	H	5	98.0	100.0	11.48	28.1	39.0	1.81	1.30	2.59	49.7	0.99
182	1134	A	2	H	6	75.0	77.0	12.75	30.2	43.2	1.73	1.21	2.47	51.0	1.04
182	1134	A	3	H	1	73.0	75.0	14.73	32.5	48.1	1.69	1.14	2.45	53.5	1.15
182	1134	A	3	H	2	73.0	75.0	16.23	38.2	61.9	1.44	0.89	1.93	53.8	1.17
182	1134	A	3	H	3	52.0	54.0	17.52	24.4	32.3	1.80	1.36	2.39	43.0	0.76
182	1134	A	3	H	4	72.0	74.0	19.22	25.4	34.0	1.76	1.31	2.33	43.6	0.77
182	1134	A	3	H	5	71.0	73.0	20.71	24.9	33.2	1.80	1.35	2.40	43.7	0.78
182	1134	A	3	H	6	70.0	72.0	22.20	22.5	29.0	1.81	1.40	2.33	39.7	0.66
182	1134	A	3	H	7	12.0	14.0	23.12	18.8	23.1	1.87	1.52	2.31	34.2	0.52
182	1134	A	4	H	1	62.0	64.0	24.12	23.9	31.4	1.79	1.36	2.34	41.8	0.72
182	1134	A	4	H	2	80.0	82.0	25.80	25.5	34.3	1.75	1.30	2.31	43.6	0.78
182	1134	A	4	H	3	82.0	84.0	27.32	23.3	30.5	1.80	1.38	2.33	41.0	0.69
182	1134	A	4	H	4	84.0	86.0	28.84	18.4	22.5	1.87	1.53	2.30	33.5	0.51
182	1134	A	4	H	5	77.0	79.0	30.27	19.0	23.4	1.85	1.50	2.28	34.2	0.52
182	1134	A	4	H	5	96.0	98.0	30.46	18.3	22.4	1.86	1.52	2.28	33.2	0.50
182	1134	A	4	H	6	78.0	80.0	31.78	28.5	39.9	1.74	1.24	2.40	48.3	0.94
182	1134	A	5	H	1	75.0	77.0	33.75	29.6	42.0	1.77	1.25	2.55	51.2	1.05
182	1134	A	5	H	2	73.0	75.0	35.23	18.9	23.3	1.94	1.57	2.45	35.8	0.56
182	1134	A	5	H	3	73.0	75.0	36.73	19.1	23.6	1.89	1.53	2.36	35.2	0.54
182	1134	A	5	H	4	71.0	73.0	38.21	18.1	22.1	1.90	1.56	2.35	33.6	0.51
182	1134	A	5	H	5	70.0	72.0	39.70	16.2	19.4	1.99	1.66	2.43	31.5	0.46
182	1134	A	5	H	6	100.0	102.0	41.50	13.7	15.9	2.03	1.75	2.40	27.2	0.37
182	1134	A	6	H	1	70.0	72.0	43.20	23.9	31.4	1.78	1.36	2.33	41.6	0.71
182	1134	A	6	H	2	70.0	72.0	44.70	17.1	20.6	1.92	1.59	2.34	32.1	0.47
182	1134	A	6	H	3	78.0	80.0	46.28	17.7	21.4	1.84	1.52	2.22	31.7	0.47
182	1134	A	6	H	4	78.0	80.0	47.78	18.6	22.8	1.84	1.50	2.24	33.3	0.50
182	1134	A	6	H	5	79.0	81.0	49.29	14.1	16.5	1.93	1.65	2.25	26.6	0.36
182	1134	A	6	H	6	98.0	100.0	50.98	24.7	32.9	1.80	1.36	2.40	43.5	0.77
182	1134	A	6	H	7	19.0	21.0	51.69	19.5	24.2	1.83	1.47	2.25	34.7	0.53
182	1134	A	7	H	3	103.0	105.0	56.03	20.9	26.4	1.90	1.50	2.46	38.7	0.63
182	1134	A	7	H	4	77.0	79.0	57.27	18.7	23.1	1.87	1.52	2.32	34.3	0.52
182	1134	A	7	H	4	91.0	93.0	57.41	15.5	18.3	1.96	1.66	2.36	29.7	0.42
182	1134	A	7	H	5	68.0	70.0	58.68	13.5	15.6	1.93	1.67	2.24	25.4	0.34
182	1134	A	7	H	5	127.0	129.0	59.27	18.0	22.0	1.91	1.57	2.37	33.7	0.51
182	1134	A	7	H	7	51.0	53.0	61.51	15.1	17.8	1.93	1.64	2.29	28.5	0.40
182	1134	A	8	H	1	98.0	100.0	62.48	19.6	24.4	1.94	1.56	2.48	37.1	0.59
182	1134	A	8	H	2	8.0	10.0	63.08	18.9	23.3	1.93	1.57	2.43	35.6	0.55
182	1134	A	8	H	2	108.0	110.0	64.08	19.2	23.8	1.97	1.59	2.52	36.9	0.59
182	1134	A	8	H	3	108.0	110.0	65.58	21.5	27.4	1.89	1.48	2.45	39.6	0.66
182	1134	A	8	H	4	108.0	110.0	67.08	25.3	33.8	1.86	1.39	2.56	45.8	0.85
182	1134	A	8	H	5	108.0	110.0	68.58	21.7	27.7	1.86	1.45	2.39	39.3	0.65
182	1134	A	8	H	6	48.0	50.0	69.48	24.1	31.7	1.85	1.40	2.48	43.4	0.77
182	1134	A	8	H	7	48.0	50.0	70.48	26.3	35.7	1.81	1.33	2.49	46.5	0.87
182	1134	A	9	H	1	108.0	110.0	72.08	29.0	40.8	1.80	1.28	2.60	50.9	1.04
182	1134	A	9	H	2	108.0	110.0	73.58	23.1	30.0	1.83	1.41	2.40	41.3	0.70
182	1134	A	9	H	3	108.0	110.0	75.08	24.5	32.5	1.80	1.36	2.38	43.0	0.76
182	1134	A	9	H	4	108.0	110.0	76.58	24.9	33.2	1.79	1.34	2.37	43.5	0.77
182	1134	A	9	H	5	108.0	110.0	78.08	25.5	34.3	1.82	1.36	2.48	45.4	0.83
182	1134	A	9	H	6	108.0	110.0	79.58	25.6	34.4	1.85	1.37	2.55	46.2	0.86
182	1134	A	9	H	7	50.0	52.0	80.50	23.2	30.1	1.82	1.40	2.38	41.2	0.70
182	1134	A	10	H	1	108.0	110.0	81.58	22.1	28.4	1.82	1.41	2.33	39.2	0.65
182	1134	A	10	H	2	108.0	110.0	83.08	23.4	30.6	1.82	1.40	2.40	41.7	0.72
182	1134	A	10	H	3	108.0	110.0	84.58	22.6	29.3	1.81	1.40	2.34	40.0	0.67
182	1134	A	10	H	4	108.0	110.0	86.08	23.2	30.3	1.83	1.41	2.40	41.5	0.71
182	1134	A	10	H	5	108.0	110.0	87.58	21.3	27.1	1.87	1.47	2.40	38.9	0.64
182	1134	A	11	H	1	108.0	110.0	91.08	22.9	29.7	1.84	1.42	2.41	41.1	0.70
182	1134	A	11	H	2	108.0	110.0	92.58	22.9	29.8	1.84	1.41	2.40	41.1	0.70

Note: Only a portion of this table appears here. The complete table is available in **ASCII format.**

Table T16. Undrained shear strength measurements, Site 1134.

Leg	Site	Hole	Core	Type	Section	Interval (cm)	Depth (mbsf)	Maximum shear strength (kPa)	Peak (kPa)
182	1134	A	1	H	2	121.3	2.71	9.81	11.97
182	1134	A	1	H	3	124.2	4.24	16.83	20.53
182	1134	A	2	H	1	128.0	5.78	8.64	10.54
182	1134	A	2	H	2	110.2	7.10	15.66	19.10
182	1134	A	2	H	3	115.8	8.66	16.11	19.65
182	1134	A	2	H	4	100.1	10.00	7.65	9.33
182	1134	A	2	H	5	133.2	11.83	11.70	14.27
182	1134	A	2	H	6	112.4	13.12	13.23	16.14
182	1134	A	2	H	7	34.8	13.85	8.01	9.77
182	1134	A	3	H	1	119.1	15.19	9.36	11.42
182	1134	A	3	H	2	130.4	16.80	5.58	6.81
182	1134	A	3	H	3	100.2	18.00	5.85	7.14
182	1134	A	3	H	4	97.7	19.48	8.37	10.21
182	1134	A	3	H	5	113.9	21.14	11.16	13.61
182	1134	A	3	H	6	115.7	22.66	15.21	18.55
182	1134	A	3	H	7	7.5	23.08	14.94	18.22
182	1134	A	4	H	1	102.8	24.53	9.81	11.97
182	1134	A	4	H	2	124.9	26.25	5.94	7.25
182	1134	A	4	H	3	111.0	27.61	8.55	10.43
182	1134	A	4	H	4	122.1	29.22	10.26	12.51
182	1134	A	4	H	5	125.9	30.76	3.33	4.06
182	1134	A	4	H	6	115.1	32.15	17.91	21.84
182	1134	A	4	H	7	19.6	32.70	27.72	33.81
182	1134	A	5	H	1	119.6	34.20	10.62	12.95
182	1134	A	5	H	2	133.3	35.83	5.76	7.03
182	1134	A	5	H	3	105.6	37.06	14.49	17.67
182	1134	A	5	H	4	135.9	38.86	9.99	12.18
182	1134	A	5	H	5	120.3	40.20	31.59	38.53
182	1134	A	5	H	6	129.2	41.79	21.24	25.91
182	1134	A	5	H	7	67.5	42.67	61.20	74.64
182	1134	A	6	H	1	119.7	43.70	28.44	34.69
182	1134	A	6	H	2	106.0	45.06	17.01	20.75
182	1134	A	6	H	3	110.7	46.61	13.77	16.79
182	1134	A	6	H	4	132.3	48.32	18.18	22.17
182	1134	A	6	H	5	113.3	49.63	9.36	11.42
182	1134	A	6	H	6	134.5	51.35	16.11	19.65
182	1134	A	6	H	7	27.5	51.78	13.41	16.36
182	1134	A	7	H	1	130.6	53.31	17.10	20.86
182	1134	A	7	H	2	116.7	54.67	15.03	18.33
182	1134	A	7	H	3	121.6	56.22	18.99	23.16
182	1134	A	7	H	3	121.6	56.22	18.99	23.16
182	1134	A	7	H	4	116.6	57.67	21.15	25.80
182	1134	A	7	H	5	135.3	59.35	17.46	21.30
182	1134	A	7	H	6	94.2	60.44	18.72	22.83
182	1134	A	7	H	7	64.2	61.64	48.78	59.49

Note: This table is also available in **ASCII format.**

Table T17. Summary of tool strings, intervals logged, and logging speeds, Hole 1134A.

	Tool strings	
First pass:	Triple combo	FMS/sonic
Logging speed (m/hr)	275	275
Total interval (mbsf)	386-296	386-118
Open hole interval (mbsf)	386-296	386-118
Calipers closed (mbsf)	296	158
Second pass:	Triple combo	FMS/sonic
Logging speed (m/hr)	275	275
Total interval (mbsf)	386-0	386-74
Open hole interval	386-105	386-95
Calipers closed (mbsf)	127	129

Note: Triple combo = triple combination logging tool, FMS = Formation MicroScanner.

Table T18. Differences between depths to key horizons and corrected depths.

Seismic horizons	Predicted intersection (mbsf)	Check-shot corrected depth (mbsf)	Difference (m)
Base of Sequence 2	39	~46	
Intra-Sequence 3 Horizon	103	113	+10
Base of Sequence 3	147	158	+11
Top of Sequence 6A	205	213	+8
Top of Sequence 6A, Lobe 2	264	272	+8
Base of Cenozoic	361	370	+9
Intra-Cenomanian Horizon	432		

Notes: Predicted intersection depths were derived using high-resolution site-survey seismic data stacking velocities. Corrected depths were based on check-shot data and interval transit-time (ITT) data.